Sustainable Energy & Fuels

ROYAL SOCIETY OF CHEMISTRY

REVIEW

View Article Online
View Journal | View Issue



Cite this: *Sustainable Energy Fuels*, 2026, **10**, 728

# Development of core–shell nanofibers in magnetoelectric sensors, fuel cells, and drug-delivery applications: a review

Sandeep Kumar Yadav, *[a] Vishwa Prakash Jha,[b] Durga Prasad Pabba[c] and Arun Thirumurugan[d]

Core–shell nanofibers have emerged as a versatile class of nanostructured materials due to their unique ability to integrate multiple functionalities within a single architecture. Their coaxial geometry, which combines core and shell domains, allows for precise control over composition, interfacial interactions, and surface characteristics, making them highly attractive for advanced electronic and biomedical applications. This review highlights recent advancements in the design, synthesis, and application of core–shell nanofibers, with a focus on their roles in magnetoelectric devices and drug delivery systems. For magnetoelectric devices, core–shell nanofibers provide efficient coupling between magnetic and electric order parameters, enabling the development of miniaturized, flexible, high-sensitivity sensors, energy harvesters, and transducers. Their high aspect ratio, tunable interfacial stress transfer, and enhanced magnetoelectric coupling provide new opportunities for next-generation spintronic and wearable technologies. In parallel, the unique core–shell morphology offers distinct advantages in drug delivery, such as high loading efficiency, sequential or sustained release, and protection of bioactive agents, which are crucial for wound healing, tissue engineering, and targeted therapies. Also, this review highlights recent progress in core–shell nanofiber-based electrodes for HT-PEMFCs, DEFCs, and IT-SOFCs, emphasizing their role in enhancing catalytic activity, stability, and ionic conductivity. These advancements pave the way for high-efficiency and durable fuel cell technologies for next-generation, efficient, and sustainable fuel cell systems. We further summarize the progress in electrospinning and other fabrication techniques that enables scalable production of uniform core–shell nanofibers, along with critical insights into structure–property relationships, challenges, and future perspectives. This review highlights the multifunctional potential of core–shell nanofibers as a transformative platform for next-generation devices and healthcare solutions, bridging developments in the electronic and biomedical domains.

Received 18th October 2025
Accepted 14th December 2025

DOI: 10.1039/d5se01377a

rsc.li/sustainable-energy



## 1. Introduction

### 1.1 Nanotechnology and nanofibers

The fundamental principle of nanotechnology is reducing the size of materials to nanometer dimensions, which alters their physicochemical properties due to quantum confinement, increased surface-to-volume ratios, and modified electronic and interfacial behaviors. In semiconductors, size confinement can induce quantum effects that significantly change their opto-electronic characteristics, while magnetic materials transition to superparamagnetic behavior below a critical size. In catalytic metal nanoparticles, decreasing the particle diameter to a few nanometers can alter the crystal structure, surface topology, and electronic properties, including shifts in the Fermi level and reduction, which can potentially influence adsorption behavior and catalytic activity.[1–4] These nanoscale phenomena underpin the broad utility of nanostructured systems in various applications, including nanoelectromechanical system (NEMS) sensors, targeted drug delivery, tissue engineering, implant surface modification, and wound healing.[5–8] One-dimensional (1D) nanofibers are fiber structures characterized by diameters in the nanometer range. Recent advancements have broadened the definition of nanofibers; according to Horne *et al.*,[9] fibers with diameters ranging from 0 to 500 nm are nanofibers. Prabu *et al.*[10] extended this definition, reporting that fibers with diameters between 50 and 1000 nm are also categorized as nanofibers, while their lengths can extend to several centimeters. 1D nanofibers exhibit a high surface area-to-volume ratio,

[a]*Department of Physics and Electronics, Christ (Deemed to be University), Bangalore, 560029, Karnataka, India. E-mail: sandeeplumar.yadav@christuniversity.in*
[b]*School of Computer Science and Engineering, IILM University, Gurugram, 122011, Haryana, India*
[c]*Departamento de Electricidad, Facultad de Ingenieria, Universidad Tecnologica Metropolitana, Santiago, Chile*
[d]*Sede Vallenar, Universidad de Atacama, Costanera #105, 1612178, Vallenar, Chile*

tunable surface functionalities, and enhanced mechanical properties as the polymer fiber diameter decreases to submicron or nanometer scales. For instance, a nanofiber is 2 cm long and 400 nm in diameter, corresponding to an aspect ratio of approximately 5000, which significantly increases the available surface area for interactions while maintaining a low total volume.[11,12]

The nanoscale holds particular significance for biological systems, as the characteristic dimensions of viruses, bacteria, biomolecules, carbon nanotubes (CNTs), and other nanostructures fall within this range. A comparison with these objects reveals that electrospun fibers can exhibit diameters across a relatively broad spectrum, as shown in Fig. 1(a). The principal motivation for utilizing nanofiber-based systems is that materials at the micro- and nano-scale exhibit unique physical and chemical properties not observed in their bulk forms. Likewise, tailoring materials at the nanoscale can drastically alter thermal transport, for example, reducing lattice thermal conductivity in nanostructured thermoelectrics, thereby improving their energy conversion efficiency. Electrospinning is a versatile technique for fabricating continuous nanofibers by applying a high-voltage electric field to a polymer solution, inducing jet formation. In a standard laboratory electrospinning setup, a polymer solution or melt is fed through a spinneret nozzle with an inner diameter of approximately 10–100 μm (Fig. 1(b)). This nozzle also acts as an electrode, across which a high electric field of 50–500 kV $m^{-1}$ is applied, while the counter electrode is positioned 10–25 cm away. The fibers are usually collected on a substrate connected to the counter electrode. Electrospun fibers exhibit superior porosity, surface area, and application versatility, rendering them highly suitable for biomedical and filtration applications. CNTs excel in strength, and hair has the largest diameter, but limited surface functionality, as illustrated in Fig. 1(c). Electrospun fibers provide a balanced combination of biocompatibility, porosity, and practical applicability. Nanofibers, in particular, can achieve

**Sandeep Kumar Yadav**

*Sandeep Kumar Yadav received his BSc in Physics from the University of Allahabad, India (2014), and his MSc in Physics from the National Institute of Technology, Durgapur, India (2017). He completed his PhD at the National Institute of Technology, Tiruchirappalli, India (2024). He is currently working as a postdoctoral fellow at Christ (Deemed to be University), Bangalore, India. His research interests include the synthesis, characterization, and applications of multiferroics, magnetic nanoparticles, and two-dimensional (2D) materials for energy harvesting and energy storage.*

**Vishwa Prakash Jha**

*Vishwa Prakash Jha is an Assistant Professor at IILM University, Gurugram, in the School of Computer Science and Engineering, with a strong interdisciplinary research background spanning mathematical statistics, computational mathematics, and data-driven modelling for materials science applications. He earned his PhD in Mathematical Statistics from the National Institute of Technology, Tiruchirappalli, where he developed Teissier-related probability distributions and applied them to complex real-world datasets.*

**Durga Prasad Pabba**

*Durga Prasad Pabba obtained his MSc in Physics from Andhra University in Visakhapatnam, India, in 2013. He completed his PhD at the National Institute of Technology in Tiruchirappalli, India, in 2021. Currently, he is working as an Assistant Professor at the Universidad Tecnológica Metropolitana (UTEM) in Chile. His research interests include polymer-based magnetoelectric nanocomposites, multifunctional polymer structures, piezoelectric nanogenerators, triboelectric nanogenerators, magnetoelectric energy-harvesting devices, and magnetic and pressure sensors using multifunctional nanocomposites.*

**Arun Thirumurugan**

*Arun Thirumurugan is an Assistant Professor at the University of Atacama, Sede Vallenar, Chile. He earned his PhD from the National Institute of Technology Tiruchirappalli, India, and completed postdoctoral research at the Institute of Physics (India) and the University of Chile, Santiago. His research focuses on the synthesis and surface engineering of nanomaterials for energy conversion, environmental remediation, and sustainable technological applications. He currently serves as the Director of a central Regional Fund for the Productivity and Development (FRPD) project in the Atacama Region, Chile.*

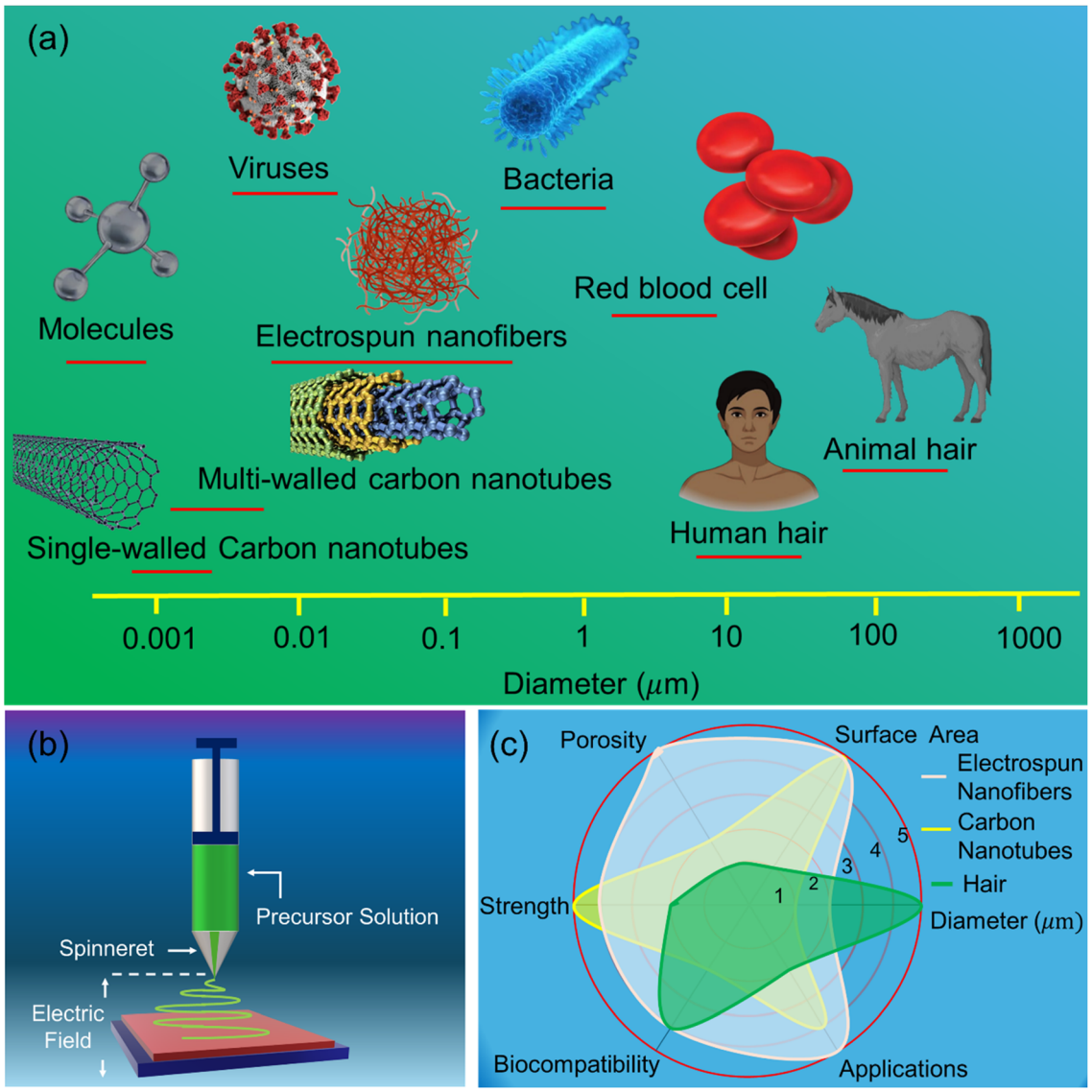


Fig. 1 (a) Comparison of the diameters of nanofibers with biological and technological objects, (b) illustration of the electrospinning setup for preparation of nanofibers, and (c) comparison of biocompatibility, strength, porosity, surface area, diameter, and potential applications of electrospun nanofibers with CNTs and human hairs.

pronounced ME coupling by eliminating substrate clamping effects commonly encountered in thin film bilayers or nanopillars deposited on substrates.[13–15] Furthermore, the application of nanofibers in the medical and aerospace industries has been broadened. For example, nanofibers are being explored in the medical sector for their utility in tissue engineering scaffolds, wound dressing materials, drug delivery systems, and biosensors due to their high surface area and tunable physicochemical properties.[16,17] In the aerospace and space industries, nanofiber composites contribute to the development of lightweight, high-strength structural components and radiation shielding, thereby further enhancing the performance and safety of spacecraft.[18,19] The food industry benefits from utilizing nanofibers in areas such as active packaging and filtration, as well as for the controlled release of nutraceuticals and preservatives.[20–22] Overall, the multifunctional nature of nanofiber-based materials continues to expand their application landscape across various domains, including medical, space, food, environmental, and other advanced technological fields.

### 1.2 Core–shell nanofibers

Core–shell nanofibers are one-dimensional nanostructures characterized by an inner core material enveloped by an outer shell, typically fabricated through coaxial electrospinning or emulsion methods. This architecture enables the independent tuning of core and shell compositions, allowing for multifunctional properties and precise control over released profiles or surface functionalities. Core–shell nanofibers are widely recognized for their enhanced stability, tunable mechanical and electrical properties, and efficacy in drug delivery, catalysis, and

 

sensor applications. Their structure offers protective encapsulation for sensitive molecules while maintaining nanofiber flexibility and high surface area.[23] Furthermore, with the progression of nanofiber technology, core–shell nanofibers have emerged as an advanced architecture in which a core material is encapsulated within a surrounding shell, enabling tunable physicochemical properties and multifunctionality. This configuration simplifies fabrication compared to more complex nanofiber assemblies while offering superior performance in targeted applications. In drug delivery, core–shell nanofibers facilitate controlled release kinetics and site-specific transport of therapeutics. As catalytic supports, their high surface-to-volume ratio and dual-compartment design enhance reaction efficiency and stability. The distinct core–shell interface improves coupling efficiency and sensitivity in ME sensing. Additionally, they have been employed in the food industry for active preservation and innovative packaging, in tissue engineering as biocompatible scaffolds promoting cell adhesion and proliferation, and in water purification systems for efficient adsorption and removal of contaminants. A schematic illustrating the applications of core–shell nanofibers in drug delivery, catalysis, sensors, the food industry, tissue engineering, and water purification is presented in Fig. 2.

### 1.3 Development in core–shell nanofibers

Core–shell nanofibers offer distinct advantages over traditional and bulk composites due to their high surface-to-volume ratio, enabling enhanced functionality and efficiency. Their unique structure allows precise control over core and shell material properties, facilitating tailored applications such as ME coupling and drug delivery. Unlike bulk composites, they offer flexibility, a lightweight design, and enhanced interfacial interactions, which are crucial for advanced devices. Scalable fabrication methods, such as coaxial electrospinning, surpass traditional composites in producing uniform, multifunctional nanostructures. These features make core–shell nanofibers ideal for next-generation biomedical, energy, and environmental technologies. However, the roots of core–shell nanofibers lie in the development of electrospinning, a technique pioneered in the 1990s for producing micro- and nanofibers using electrostatic forces.[24] Early studies by Reneker and Doshi (1995) laid the groundwork for electrospinning, demonstrating the ability to develop ultrafine fibers from polymer solutions.[14] Initial electrospinning focused on monolithic (single-component) nanofibers; however, researchers soon recognized the potential for more complex structures to enhance functionality. Core–shell nanofibers were introduced with the advent of coaxial electrospinning, which occurred around 2002–2003. Loscertales *et al.* (2002) and others demonstrated the use of a coaxial nozzle to simultaneously spin two different materials, forming a core–shell structure.[25] This allowed for the encapsulation of one material (the core) within another (the shell), enabling the tailoring of properties.[26–28] Early studies, such as those by Zhang *et al.* (2004), investigated core–shell nanofibers composed of polymers like PCL and gelatin, highlighting their potential in biomedical applications.[29] By the late 2000s, coaxial electrospinning was refined to improve control over fiber morphology, diameter, and composition. Innovations included emulsion electrospinning and modified coaxial/triaxial electrospinning, which enabled the use of unspinnable core materials (*e.g.*, drug solutions or lipids) by leveraging spinnable shell polymers. Alternative methods, such as self-assembly and

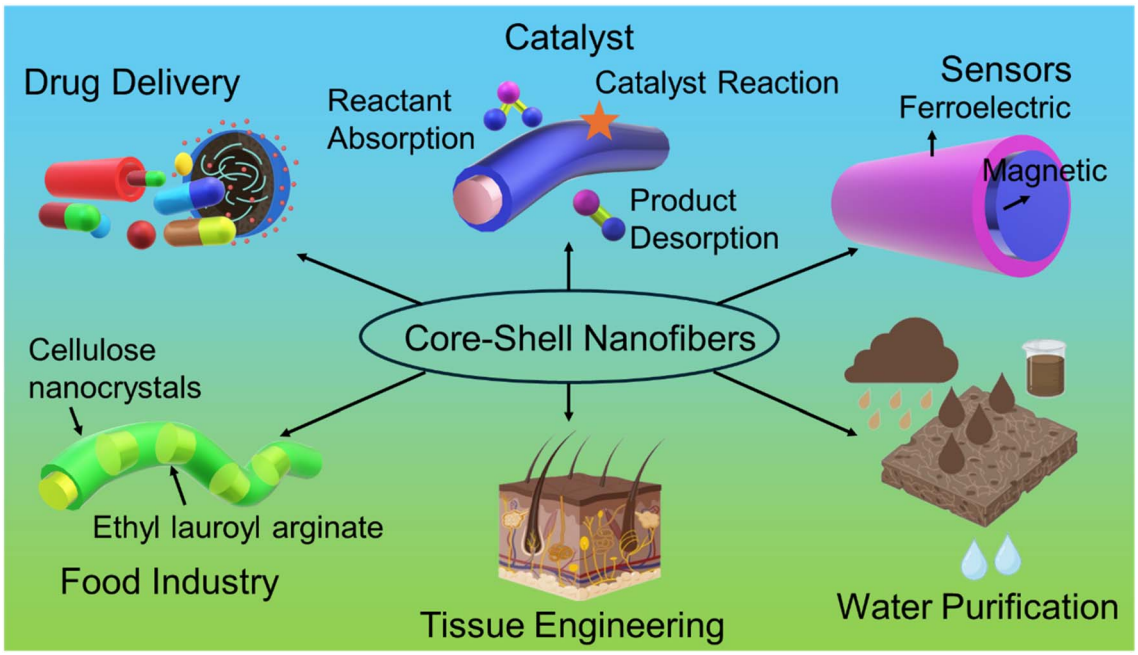


Fig. 2 Schematic representation of core–shell nanofiber applications, including in drug delivery, catalysis, sensors, the food industry, tissue engineering, and water purification.

phase-separation electrospinning, have emerged for producing core–shell-like structures without the need for coaxial setups.[30] For instance, Jiang *et al.* (2013) utilized vapor-induced phase separation to create core–shell nanofibers, thereby expanding the versatility of fabrication.[31] The period also saw the integration of non-polymeric materials, such as ceramics and metal oxides, into core–shell nanofibers, broadening their applications beyond biomedicine.[32]

Since the 2010s, core–shell nanofibers have gained traction due to their improved scalability and functionalization capabilities. Techniques like coaxial centrifugal spinning address the limitations of coaxial electrospinning, such as low production rates and high energy consumption, thereby enabling commercialization potential. Recent advancements include multiaxial electrospinning for producing multi-layered fibers and needleless electrospinning for achieving higher yields, particularly for chitosan-based nanofibers.[33–35] Furthermore, coaxial electrospinning remains the cornerstone for fabricating ME core–shell nanofibers due to its ability to precisely control the composition of both the core and shell. By 2015–2025, researchers had optimized parameters such as solution viscosity, flow rates, and electric field strength to achieve uniform fiber diameters (50–500 nm) and enhance interfacial strain transfer, which is crucial for ME coupling. ME-based core–shell nanofibers have evolved from niche research to a versatile platform for advanced devices, driven by innovations in coaxial, multiaxial, and needleless electrospinning, as well as novel material combinations.

Although several reviews have discussed ME composites, electrospun nanofibers, or polymer–ceramic multifunctional systems, these studies have primarily focused on bulk laminates, thin films, or general fiber fabrication techniques, without examining core–shell nanofibers as an integrated materials platform. Furthermore, recent advances from 2022 to 2025—including coaxial electrospinning optimization, self-assembled core–shell structures, and newly reported ME fiber systems such as $CoFe_2O_4$–$Ba_{0.95}Ca_{0.05}Ti_{0.89}Sn_{0.11}O_3$, $Ba_2Zn_2Fe_{12}O_{22}$–PZT, and $NdFeO_3$–PZT—have not been consolidated in any existing review. To the best of our knowledge, no comprehensive article has simultaneously examined (i) the structure–property relationships of core–shell nanofibers, (ii) their strain-mediated ME coupling mechanisms, and (iii) their emerging roles in fuel cells and drug-delivery technologies. This review uniquely integrates these interdisciplinary developments, highlighting material design principles, fabrication strategies, and application-specific performance metrics. Likewise, recent progress in core–shell nanofiber-based drug carriers—including dual-drug systems, stimuli-responsive release, and coaxial fibers for tissue regeneration—remains fragmented in the literature. In addition to their roles in magnetoelectric sensing and biomedical delivery systems, core–shell nanofibers have recently emerged as promising materials for fuel cell technologies due to their tunable nanoarchitecture, enhanced surface area, and ability to integrate multifunctional components within a single fiber. By integrating recent findings from these domains and identifying key knowledge gaps, this work offers a timely and distinctive perspective that complements and extends existing reviews.

## 2. Materials and application

### 2.1 Magnetoelectrics

In recent years, there has been increased scientific focus on multiferroic materials exhibiting magnetoelectric (ME) phenomena, which are characterized by the correlation between the applied magnetic field and the corresponding electric voltage.[36–41] The intrinsic coupling between electric and magnetic orders in ME materials enables wirelessly induced electric charge generation, facilitating the less-invasive incorporation of these materials into next-generation electronic devices. Recent literature[42–49] reports the notable progress in the fundamental understanding and development of advanced ME materials. These innovations have established ME materials as a promising candidate for applications in microelectronics and engineering, such as high-speed memory devices,[50,51] advanced ME antennas,[52–54] and ME sensors,[55–57] among others. Additionally, ME materials enable the detection of low-intensity magnetic fields in MEMS sensor technologies for navigation and automotive applications, operating effectively at room temperature (RT). In contrast, highly complex SQUIDs need low-temperature environments.[58–60] Furthermore, ME materials enable the harvesting of energy from ambient magnetic fields for Internet of Things (IoT) applications, the realization of non-volatile ME random-access memory (ME-RAM) for data storage devices, and the development of highly compact, tunable antennas for radio-frequency communication in space, demonstrating enhanced efficiency relative to conventional materials.[61–63]

In ME composites, coupling occurs through mechanical strain that is generated in the magnetostrictive (ferromagnetic) phase, which is transferred to the piezoelectric (ferroelectric) phase, resulting in an electrical response.[64–66] In the direct ME effect, an in-plane magnetic field ($H$) induces strain in the magnetic component through a phenomenon known as magnetostriction. This strain is mechanically transferred to the ferroelectric component, generating dielectric polarization *via* the piezoelectric effect, as illustrated in Fig. 3(a). In contrast, the converse ME effect involves an out-of-plane electric field ($E$) that creates strain in the ferroelectric component through the inverse piezoelectric effect. This strain is mechanically linked to the magnetic element, resulting in changes in magnetization ($\Delta M$) or domain reorientation due to the piezomagnetic impact, as shown in Fig. 3(b).

As a result, extensive research has focused on exploring the micro- and nanoscale structures of heterogeneous materials and their configurations, which include: (i) 0–3 type structures,[67–69] where magnetostrictive nanoparticles are dispersed within a piezoelectric matrix as shown in Fig. 2(a); (ii) 2–2 type structures,[70–74] characterized by alternating layers of magnetostrictive and piezoelectric phases as shown in Fig. 4(b); (iii) 1–3 type structures,[75–78] consisting of piezoelectric fibers or rods embedded in a magnetostriction matrix or fiber network, as illustrated in Fig. 4(c).

 

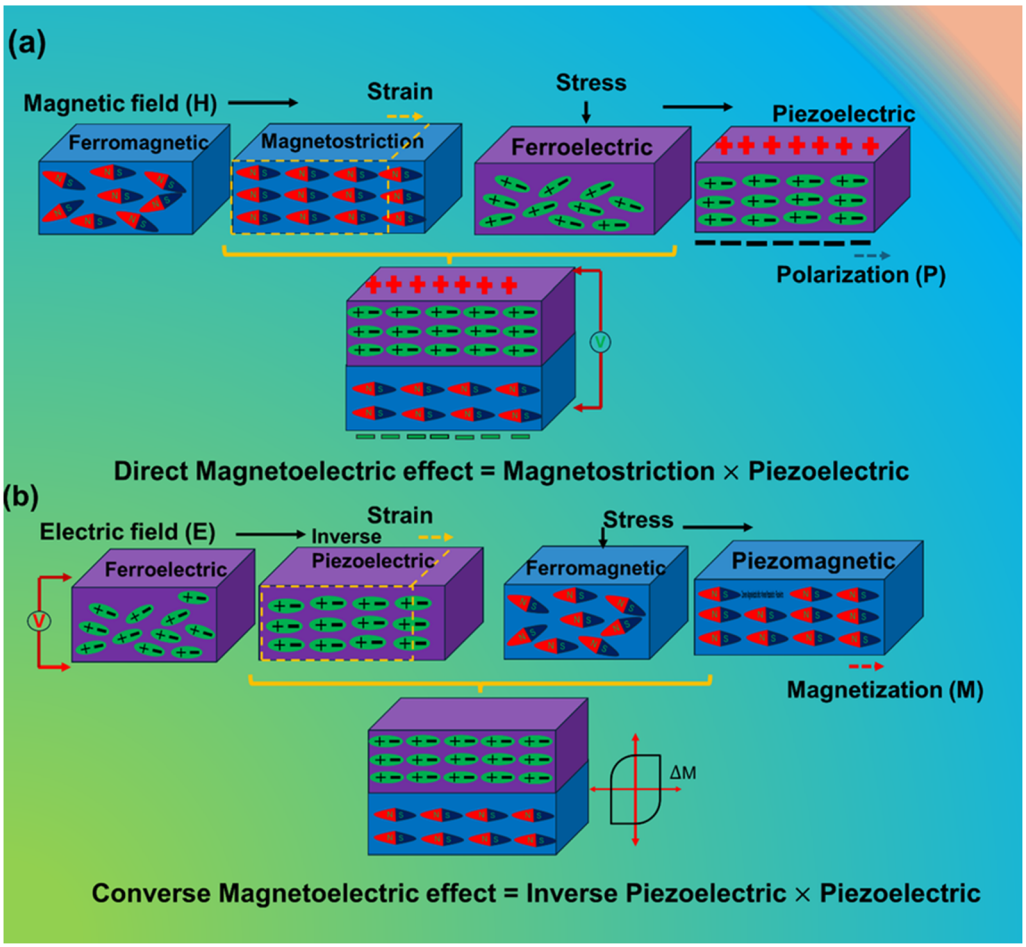


Fig. 3 Schematic illustration of the strain-mediated ME effect in a composite system: the (a) direct ME effect and (b) converse ME effect.

Efficient higher-order interfaces in composite heterostructures are critical for achieving strain transfer across phase boundaries. This maximizes ME coupling, which governs the interaction between magnetic and electric order parameters. Therefore, there is significant potential to enhance ME coupling by tailoring surface interactions in these heterostructures to optimize strain transfer, ultimately facilitating ME performance.[79] The phase architectures of 0–3 and 2–2 type structures exhibit irregular spatial distributions of ferroelectric/ferromagnetic phases, which impede efficient strain transfer and consequently result in relatively weak ME coupling. In particular, 2–2 type composites, characterized by alternating layered structures of magnetostrictive and piezoelectric phases, often suffer from limited interfacial contact area and possible mechanical mismatch between layers, thereby restricting effective mechanical coupling. These factors hinder robust

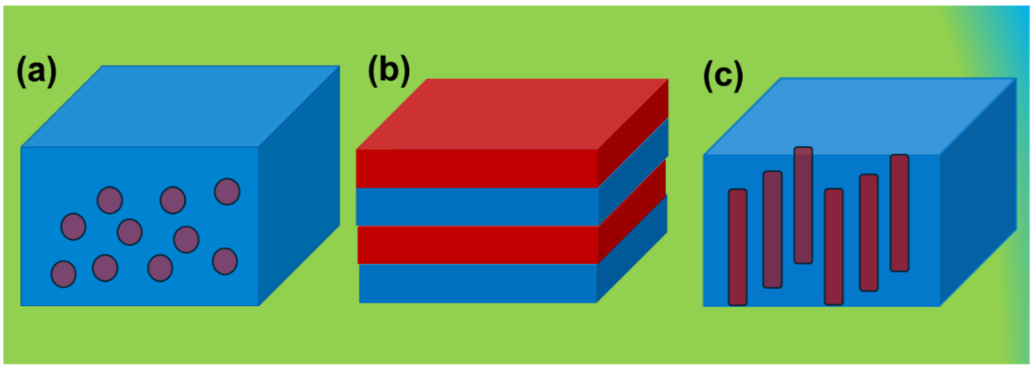


Fig. 4 Composite ME materials with different types of structure, (a) 0–3, (b) 2–2, (c) 1–3 type structures.

interactions between magnetic and electric order parameters, limiting the overall ME response.

In contrast, the 1–3 type composite structure, nanofibers or core–shell nanofibers, particularly those incorporating nanofibers as the magnetostrictive phase embedded within a piezoelectric matrix, provides a more continuous and anisotropic pathway for strain-mediated coupling. Furthermore, core–shell nanofibers are sometimes described as hybrid or variant 1–3 type structures, and both constituent phases are continuous along the length of the fiber. They are co-located within the same one-dimensional structure. This configuration facilitates higher mechanical strain transfer across the interfaces, significantly enhancing the ME coupling strength compared to other composite structures. Most importantly, the nanoscale dimensions and high aspect ratio of the fibers contribute to an increased interfacial area and improved load transfer efficiency, further enhancing the ME performance.[80,81]

The first intrinsic ME effect was experimentally demonstrated in antiferromagnetic (chromic oxide) $Cr_2O_3$ single crystals in 1961 by Folen at RT.[82] Over the past century, considering both material composition and dimensionality, ME materials have progressed from single-phase to particulate, laminated, and, more recently, micro- and nano-scale nanofibers and thin films. To date, more than ten distinct families of single-phase compounds have been extensively investigated as ME materials, including $BiFeO_3$,[83,84] $RMnO_5$ (R = Eu, Gd, Er, Y),[85,86] and $RMnO_3$ (R = Gd, Tb, Dy).[87,88] Such studies have been driven by potential applications, including metallic memories,[89] universal memory,[90] Bennett clocking,[91] and resistive switching.[92] However, achieving strong intrinsic ME coupling at or above RT remains challenging, as most single-phase multiferroics possess relatively low Curie temperatures.[93,94] In general, for multiferroic crystals, the polarization ($P$) and magnetization ($M$) are coupled to the electric ($E$) and magnetic ($H$) fields through the following relations:[47] Landau theory describes the ME effect in a single-phase material through the expansion of the free energy expression as

$$F(\mathrm{E},\mathrm{H}) = F_0 - P_\mathrm{i}^\mathrm{S}E_\mathrm{i} - M_\mathrm{i}^\mathrm{S}H_\mathrm{i} - \frac{1}{2}\varepsilon_0\varepsilon_{\mathrm{ij}}E_\mathrm{i}E_\mathrm{j} - \frac{1}{2}\mu_0\mu_{\mathrm{ij}}H_\mathrm{i}H_\mathrm{j} - \alpha_{\mathrm{ij}}E_\mathrm{i}E_\mathrm{j} + \frac{\beta_{\mathrm{ijk}}}{2}E_\mathrm{i}H_\mathrm{j}H_\mathrm{k} + \frac{\gamma_{\mathrm{ijk}}}{2}H_\mathrm{i}E_\mathrm{j}E_\mathrm{k} \quad (1)$$

Here, $\varepsilon_0$ and $\mu_0$ denote the dielectric permittivity and magnetic permeability of the medium, respectively, while $\varepsilon_{\mathrm{ij}}$ and $\mu_{\mathrm{ij}}$ represent the relative dielectric permittivity and magnetic permeability of the material. The second and third terms in eqn (1) correspond to the temperature-dependent spontaneous polarization ($P_\mathrm{i}^\mathrm{S}$) and spontaneous magnetization ($M_\mathrm{i}^\mathrm{S}$). The fourth and fifth terms describe the influence of electric and magnetic fields on the electrical and magnetic responses, respectively. The sixth term, containing $\alpha_{\mathrm{ij}}$, represents the linear ME coupling. The subsequent two terms, involving $\beta_{\mathrm{ijk}}$and $\gamma_{\mathrm{ijk}}$, are third-rank tensors that account for higher-order coupling effects.

Differentiation of eqn (1) concerning electric and magnetic fields, respectively, leads to polarization and magnetization, which are as follows:

$$P_\mathrm{i} = -\frac{\partial F(\mathrm{E},\mathrm{H})}{\partial E_\mathrm{i}} = P_\mathrm{i}^\mathrm{S} + \varepsilon_0\varepsilon_{\mathrm{ij}}E_\mathrm{j} + \alpha_{\mathrm{ij}}H_\mathrm{j} + \frac{1}{2}\beta_{\mathrm{ijk}}H_\mathrm{j}H_\mathrm{k} + \gamma_{\mathrm{ijk}}H_\mathrm{j}E_\mathrm{k} \quad (2)$$

$$M_\mathrm{i} = -\frac{\partial F(\mathrm{E},\mathrm{H})}{\partial H_\mathrm{i}} = M_\mathrm{i}^\mathrm{S} + \mu_0\mu_{\mathrm{ij}}H_\mathrm{j} + \alpha_{\mathrm{ij}}E_\mathrm{j} + \frac{1}{2}\beta_{\mathrm{ijk}}E_\mathrm{j}E_\mathrm{k} + \gamma_{\mathrm{ijk}}E_\mathrm{j}H_\mathrm{k} \quad (3)$$

In practice, to eliminate the influence of material electrical conductivity, ME effects are investigated dynamically by applying an alternating magnetic or electric field to the samples. The magnitude of dynamic effects is characterized by using ME coefficients:

$$\alpha_E = \frac{\delta E}{\delta H}(\mathrm{V/Oe.cm}) \text{ for the direct ME effect,}$$

$$\alpha_B = \frac{\delta B}{\delta H}(\mathrm{Oe.cm/V}) \text{ for converse ME effect}$$

where $\delta_\mathrm{E}$ and $\delta_\mathrm{B}$ are the amplitudes of the ac electric field and magnetic induction in the substance, caused by a change in the magnetic $\delta_\mathrm{H}$ and electric $\delta_\mathrm{E}$ fields, respectively. However, in ME crystals, the effects are small in magnitude $\alpha_\mathrm{E} \sim$ 1–20 mV ($\mathrm{Oe}^{-1}$ $\mathrm{cm}^{-1}$) and are observed in single phase materials such as $BiFeO_3$, $Y_3Fe_5O_{12}$, and $SrCo_2Ti_2Fe_8O_{19}$ at low temperatures ($T \approx$ 4–20 K)[95,96] or under high magnetic fields ($H \approx$ 10–50 kOe) in $BaFe_{12}O_{19}$ and $Ba_2Co_2Fe_{12}O_{22}$ (ref. 97 and 98) which poses challenges for their practical applications.

In composite ME, the ME coupling is primarily strain-mediated, occurring at the interface between the magnetostrictive and piezoelectric phases. This coupling arises from the interaction between magnetic and electric fields *via* mechanical strain transfer across the interface. To quantitatively describe this phenomenon, a mathematical formulation based on continuum mechanics and electromagnetism, incorporating key physical quantities such as strain ($S$), displacement ($D$), electric field ($E$), magnetic field ($H$), permittivity ($\varepsilon$), and permeability ($\mu$) is used. For general composites, the tensor notation accounts for anisotropic material properties and complex microstructures.[99–101] For the magnetostrictive and piezoelectric phases, the constitutive relations can be expressed as:

$$S_\mathrm{i} = s_{\mathrm{ij}}T_\mathrm{J} + d_{\mathrm{ki}}E_\mathrm{k} + q_{\mathrm{ki}}H_\mathrm{k} \quad (4)$$

$$D_\mathrm{k} = d_{\mathrm{ki}}T_\mathrm{i} + \varepsilon_{\mathrm{kn}}E_\mathrm{n} + \alpha_{\mathrm{kn}}H_\mathrm{n} \quad (5)$$

$$B_\mathrm{k} = q_{\mathrm{ki}}T_\mathrm{i} + \alpha_{\mathrm{kn}}E_\mathrm{n} + \mu_{\mathrm{kn}}H_\mathrm{n} \quad (6)$$

where $S_\mathrm{i}$ and $T_\mathrm{J}$ are strain and stress tensor components, respectively; $E_\mathrm{k}$, $D_\mathrm{k}$, $H_\mathrm{k}$, and $B_\mathrm{k}$ are the components of the electric field, electric displacement, magnetic field, and magnetic induction, respectively; $s_{\mathrm{ij}}$, $d_{\mathrm{ki}}$, and $q_{\mathrm{ki}}$ denote the effective elastic compliance, and piezoelectric, and piezomagnetic constants, respectively, while $\varepsilon_{\mathrm{kn}}$, $\mu_{\mathrm{kn}}$, and $\alpha_{\mathrm{kn}}$ correspond to the effective permittivity, permeability, and linear ME coupling tensor.[102–104] The ME coefficient can be written by solving eqn (4)–(6).

 

$$\alpha_{\mathrm{ME,\,ij}} = \frac{\delta E_{\mathrm{i}}}{\delta H_{\mathrm{i}}} \approx s_{\mathrm{ij}} \cdot d_{\mathrm{ki}} \cdot q_{\mathrm{ki}} \quad (7)$$

This formulation combines the sequential coupling pathway in which an applied magnetic field induces strain in the magnetostrictive phase ($q_{\mathrm{ki}}$), the strain is elastically transferred across the interface ($s_{\mathrm{ij}}$), and the piezoelectric phase converts the strain into an electric polarization ($d_{\mathrm{ki}}$). Under the assumptions of linear constitutive behavior, ideal interfacial strain transfer, and negligible intrinsic ME effects, this product–property relationship quantitatively explains the enhanced ME coefficients observed in engineered composites relative to single-phase materials, particularly at RT.

From eqn (7), it is evident that the characteristics of ME effects in composites can be tuned by H and E fields and by the interfacial interaction between constituent phases. Particularly attractive for practical applications are coaxial nanofiber architectures integrating ferromagnetic and ferroelectric phases, which can be fabricated relatively easily *via* electrospinning. Recent advances have yielded a range of composite materials exhibiting high ME conversion efficiency. Furthermore, as indicated by eqn (3), enhancing the ME effect in composites requires the selection of ferromagnetic components with significant piezomagnetic coefficients; $q_{\mathrm{ki}}$ such as metals (Ni and Co), and alloys such as FeCo,[105–107] FeGa,[108,109] Metglas,[110–112] Terfenol-D ($Tb_xDy_{1-x}Fe_2$),[113–115] and ferrites ($NiFe_2O_4$[116–118] and $CoFe_2O_4$ (ref. 119–121)-combined with piezoelectric materials possessing high piezoelectric constants, $d_{\mathrm{ki}}$. Examples include ceramics like $PbZr_{0.52}Ti_{0.48}O_3$ (PZT),[122–124], $(1-x)Pb(Mg_{1/3}Nb_{2/3})O_3$-$xPbTiO_3$ (PMN–PT),[125–127] $LaNiO_3$,[128–130] $BaTiO_3$,[131,132] and aluminum nitride (AlN) crystals,[133–135] and polymers such as polyvinylidene fluoride (PVDF),[136–138] which are highly promising for device applications. The $\alpha_{\mathrm{E}}$ typically ranges from ~1–100 mV ($Oe^{-1}$ $cm^{-1}$) for bulk composites, whereas for planar structures it is about 1–50 V ($Oe^{-1}$ $cm^{-1}$), increasing up to 100 V ($Oe^{-1}$ $cm^{-1}$) at acoustic resonance frequencies. The capability to interconvert magnetic and electric fields enables the application of the ME effect in multiferroic materials across diverse areas of science and technology. The direct ME effect serves as the foundation for devices such as sensors for detecting static and low-frequency alternating magnetic fields with sensitivities approaching $\sim 10^{-11}$ T at RT,[139] solid-state inductors and transformers tunable *via* electric fields,[131] and energy harvesters capable of converting alternating-current (AC) magnetic fields into direct-current (DC) voltage,[140] among others. The literature highlights several advanced ME composite sensors for detecting magnetic fields. Dong *et al.*[141] achieved the sensing of low-frequency ($10^2$ Hz) AC fields down to $10^{-12}$ T using a Terfenol-D/PMN–PT laminate. Zhai *et al.*[142] achieved pico-tesla-level (10–12 T) detection across a broad $10^{-2}$–10^3 Hz range using a Terfenol-D/PZT composite. Li *et al.*[143] demonstrated nano-electromechanical ME sensing using FeGaB/AlN, achieving 800 pT DC detection at 3.19 MHz. Duc *et al.*[144] developed a $(Fe_{80}Co_{20})_{78}Si_{12}B_{10}$/PZT laminate sensitive to micro-tesla fields at 5 kHz, while Chu *et al.*[145] reported PMN-PT/FeBSi composites capable of detecting ultra-low AC fields of $10^{-13}$ T at 23.3 kHz. Together, these examples highlight the remarkable dynamic range of ME sensors—from femto-tesla and pico-Tesla AC detection to nano-tesla DC measurements. The converse ME effect finds applications in electrically tunable resonators, microwave filters, and electric field-controlled data storage devices.[146–149] Several significant demonstrations of converse ME composites have been reported. Yinan *et al.*[150] developed a dual-drive DC magnetic sensor utilizing a Metglas/PZT composite, achieving a remarkably low detection limit of 1 nT. Chen *et al.*[151] explored the converse ME effect in a Metglas/PMN-PT composite structure, while Jia *et al.*[152] investigated a PMN-PT/Terfenol-D composite, reporting a notable electric-field-induced magnetization coefficient ($\alpha_{\mathrm{E}}$) of 150 mG $V^{-1}$ at RT.

### 2.2 Fuel cells and drug delivery

In fuel-cell architectures, core–shell nanofibers serve multiple roles simultaneously — as catalyst supports that improve catalyst dispersion and stability, as gas-diffusion or microporous layers that regulate water management and oxygen transport, and as reinforced membrane scaffolds that maintain proton conduction under low-humidity conditions. Several recent studies demonstrate the heterogeneous ways core–shell or closely related coaxial nanofiber designs improve electrochemical performance. For example, electrospun porous carbon nanofibers bearing $TiO_2$ hollow structures or $TiO_2$–derived cores coated with conductive carbon shells provide a high-surface-area, corrosion-resilient support that enhances methanol oxidation and oxygen-reduction activity while resisting particle agglomeration. Tailoring the core composition (*e.g.*, metal oxide or ceramic) and the conductivity/porosity of the carbon shell enables independent control of catalytic anchoring and mass-transport pathways, a design freedom that is difficult to achieve with particulate supports.[153,154] Similarly, nitrogen-doped carbon nanofiber composites with embedded $TiO_2$ or other metal-oxide cores have been shown to act as robust anode/cathode scaffolds with improved durability and enhanced ORR/oxidation kinetics, particularly when thermal treatment and heteroatom-doping are used to tailor the electronic structure and surface chemistry. Taken together, these advances suggest that core–shell nanofiber designs offer a materials-by-architecture route to decouple catalytic, ionic, and mass-transport functions, a critical capability for next-generation, low-Pt or Pt-free electrodes.[155,156] For example, oxide–metal core–shell structures (such as $CoO_x$@Pt supported on carbon) promote strong metal–oxide interactions that suppress Pt dissolution, regulate the local electronic environment, and improve the durability of oxygen-reduction catalysts—all essential for high-performance and long-lived fuel-cell electrodes as shown in Fig. 5(a). Such engineered interfaces enable the decoupling of catalytic activity (dominated by the noble-metal shell) from structural stability (provided by the metal-oxide core), allowing for improved mass transport and enhanced long-term operational resilience.

In drug-delivery and wound-healing contexts, coaxial and core–shell electrospun fibers provide decisive advantages for controlled release, multi-drug dosing, and local

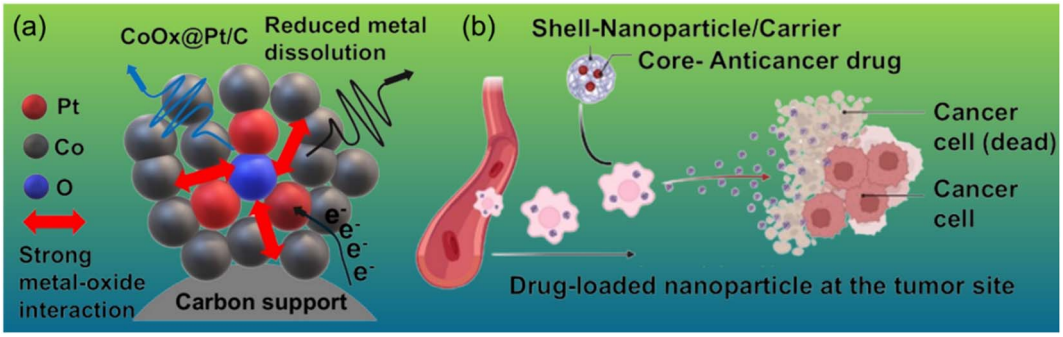


Fig. 5 Schematic illustration of the core–shell nanostructure functionality in (a) fuel-cell catalysis and (b) drug-delivery systems.

bioactivity.[157–159] The enclosed core enables high loading of fragile payloads (proteins, growth factors, or hydrophobic anticancer drugs) with reduced burst release, while the shell can be engineered for stimuli-responsiveness (pH, temperature, and enzymatic degradation) or surface bioactivity (adhesion and antimicrobial coatings). Recent comprehensive reviews and studies demonstrate progress in both the fundamentals and applications of core–shell fibers for therapeutics: from design rules for coaxial electrospinning and core–shell morphology control to application-specific demonstrations such as wound dressings with separate antimicrobial and healing-promoting compartments. Notably, hybrid fabrication strategies that combine self-emulsifying cores with coaxial spinning enhance the encapsulation of poorly soluble drugs (*e.g.*, paclitaxel) and accelerate dissolution without compromising sustained release properties.[160]

Beyond performance, recent work has also emphasized translational considerations. For fuel cells, research explores how electrospun networks can be integrated into electrode laminates and how process conditions (fiber diameter, shell porosity, and post-treatment) influence both short-term activity and long-term stability under realistic operating cycles. In drug delivery, the literature emphasizes the importance of standardized release testing, cytotoxicity, and biocompatibility assays for core–shell systems, as well as strategies for scale-up, such as needleless or multi-jet electrospinning, to enhance throughput without compromising core–shell morphology.[161]

Core–shell designs also provide unique advantages in biomedical and therapeutic applications, where controlled release, protection of bioactive molecules, and spatially selective drug delivery are essential. Coaxial fibers or nanoparticles with drug-loaded cores and protective or stimuli-responsive shells can transport therapeutic agents through the bloodstream, shield them from premature degradation, and release them in a controlled manner at the target site, as shown in Fig. 5(b). By tuning shell composition, porosity, and degradation kinetics, these systems can achieve sustained or on-demand release profiles, improved drug localization, and reduced systemic toxicity. Such multifunctional platforms have been explored for anticancer therapies, antimicrobial delivery, wound healing, and regenerative medicine, demonstrating the broader utility of core–shell architectures beyond purely physical or electrochemical applications.

## 3. Core–shell nanofibers: advantages for magnetoelectric devices, fuel cells, and drug delivery

Core–shell nanofibers represent a cutting-edge class of 1D nanostructures with unique morphological and functional characteristics. The core–shell design can spatially separate different functional materials within a single fiber geometry, leading to tunable physicochemical properties and enhanced performance in various applications, including sensors, catalysis, drug delivery, energy harvesting, and wearable electronics. Core–shell nanofibers feature a core material completely encapsulated by a concentric shell, allowing for distinct functionalities in each layer. Fabricated primarily through coaxial electrospinning, this method utilizes dual nozzles to deliver core and shell solutions simultaneously, thereby enabling precise control over fiber morphology.[162] The core typically serves as the primary functional component, while the shell provides protection, biocompatibility, or controlled environmental interaction. Coaxial nanofibers are widely used in drug delivery, where a core containing a drug (polycaprolactone-clindamycin) is encapsulated by a biodegradable shell (silk fibroin (SF)) for sustained release.[163] In catalysis, coaxial nanofibers with a catalytic core (*e.g.*, metal nanoparticles) and a porous shell enhance reaction efficiency by improving the accessibility of active sites.[164] The active pharmaceutical ingredient is loaded in the core, while the shell controls the release kinetics in a drug delivery system. Coaxial fibers enable the precise spatial separation of functional domains, making them ideal for applications that require encapsulation, sustained release, or stimuli-responsive behaviour.

Moradipour *et al.*[165] fabricated core–shell nanofibers based on polycaprolactone/polyvinyl alcohol (PCL/PVA) and PCL/Col) for biomedical applications such as drug delivery and wound healing. A notable application of coaxial nanofibers is in ME materials, where the core and shell are designed to couple magnetic and electric properties. ME core–shell nanofibers typically consist of a magnetic core, such as $CoFe_2O_4$ and

 

$Ba_2Zn_2Fe_{12}O_{22}$, and a piezoelectric or ferroelectric shell, such as PVDF and $BaTiO_3$. This configuration enables the nanofibers to generate electric polarization under magnetic fields or *vice versa*, making them promising for applications in sensors, actuators, and energy harvesting devices. For example, coaxial nanofibers with a $BaTiO_3$ core and $Ba_2Zn_2Fe_{12}O_{22}$ shell have been shown to exhibit strong ME coupling, suitable for flexible electronics.[166] Fabricating ME nanofibers involves carefully optimizing electrospinning parameters to achieve uniform core–shell interfaces and ensure compatibility between the magnetic and electrical phases. For instance, coaxial nanofibers with a PLA-$CoFe_2O_4$ core and a PVDF-TrFE shell have demonstrated significant ME coupling, which can be utilized for energy harvesting. Therefore, continuous research and development of core–shell nanofibers are essential to fully utilize their multifunctional potential and tailor their structural and interfacial properties for advanced applications. Core–shell nanofibers are designed to optimize interfacial interactions and enable controlled transport of charge, ions, or energy across the core–shell interface.[167–170] They combine distinct core and shell materials to achieve multifunctionality, precise surface control, and superior performance unattainable in traditional nanofibers or bulk composites. This architecture enables efficient encapsulation and controlled release of sensitive agents, while also providing enhanced mechanical strength and structural versatility. Moreover, scalable fabrication methods, such as coaxial or emulsion electrospinning, ensure energy-efficient production for applications in drug delivery, fuel cells, energy harvesting, and environmental remediation.[171–173]

# 4. Fabrication methods for core–shell nanofibers

Core–shell nanofibers are fabricated using various techniques that allow precise control over their morphology, composition, and functionality. These methods enable the creation of nanofibers with tailored core and shell materials, making them suitable for applications in biomedical engineering, energy storage, catalysis, and ME systems. The primary fabrication methods include coaxial electrospinning, emulsion electrospinning, and self-assembly or coating. Each method offers unique advantages and challenges, with the choice of technique depending on the desired fiber properties, material compatibility, and application requirements.

## 4.1 Coaxial electrospinning

The coaxial electrospinning technique has emerged as a highly versatile and efficient method for fabricating core–shell nanofibers with tunable morphology and functionality. Unlike traditional single-fluid electrospinning, coaxial electrospinning employs a concentric spinneret (also known as a nozzle spinneret) composed of two coaxial needles that allow the simultaneous flow of two different polymer solutions: one designated as the core material and the other as the shell material. When subjected to a high electric field, the combined jet undergoes stretching (Taylor cone), elongation, and solidification, ultimately forming nanofibers with a distinct core–shell structure as shown in the schematic in Fig. 6(a).[174–176] The successful preparation of core–shell nanofibers *via* coaxial electrospinning requires careful optimization of several process parameters, including the concentration and viscosity of the polymer solutions, the applied voltage, the distance between the spinneret and the collector, and the flow rates of both the core and shell solutions.[177] Each of these factors influences the morphology, diameter, and uniformity of the resulting nanofibers, as well as the stability of the Taylor cone during electrospinning.[178] The digital image of the Taylor cone during coaxial electrospinning and the SEM image of the PVDF-PC core–shell nanofiber are shown in Fig. 6(b) and (c).[162]

**4.1.1 Concentration and properties of polymer solution.** The concentration and viscosity of the polymer solutions play a pivotal role in determining the spinnability and morphology of the coaxial fibers. For the shell solution, sufficient chain entanglement is necessary to provide mechanical stability to the jet and to prevent jet breakup during electrospinning.[179] A solution that is too dilute tends to form beads or droplets, while an excessively viscous solution may hinder the electrospinning process due to difficulties in pumping and jet elongation. Similarly, the core solution must be optimized depending on whether it is a solid polymer, a liquid, or an active agent dispersed in a carrier. For instance, the core fluid may be a bioactive compound dissolved in a biocompatible polymer, as seen in drug delivery applications. In contrast, the shell fluid provides structural support and controlled release properties. Proper miscibility between core and shell solutions is not essential; however, interfacial tension and flow stability must be managed to maintain a distinct core–shell configuration. Fiber formation requires a polymer concentration above a critical value to ensure sufficient chain entanglement.[180] Below this threshold, beads form due to Rayleigh instability; above it, viscosity increases sharply, enabling smooth jet formation.[181] For example, in SF–based core–shell fibers, SF concentrations below 6% led to bead-like fibers, whereas at 8%, the viscosity reached ~2308 cP. Similarly, increasing the PVA concentration from 3% to 9% increased the viscosity from ~92.7 cP to ~165.1 cP. Higher polymer concentrations generally enlarge fiber

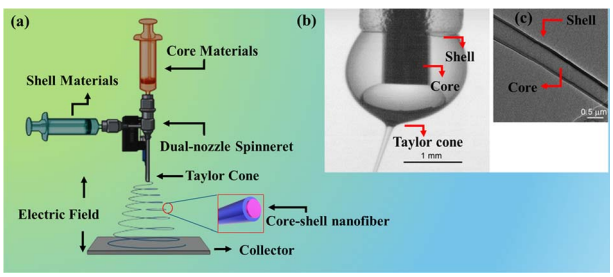


Fig. 6 (a) Schematic of the electrospinning setup for preparation of core–shell nanofibers. (b) Optical image of core–shell droplets on the nozzles of an apparatus for coaxial electrospinning. (c) SEM image of core–shell fibers of PVDF (core) and PC (shell) produced by coaxial electrospinning. (b and c) adopted from ref. 162. Copyright© 2007 WILEY-VCH Verlag GmbH & Co. KGaA, Weinheim.

diameters. In SF/PVA systems, increasing the SF in the shell from 6% to 8% resulted in thicker core–shell fibers. Changing PVA in the core had a lesser effect; however, at high shell/core concentrations, the core concentration also influenced the diameter.[182] In PVDF fibers, increasing the concentration from 25 wt% % (yielding ~473 nm) to 30 wt% % increased the average diameter to ~644 nm.[183] With PAN solutions, an increasing concentration also led to an increase in fiber diameter and electrical conductivity.[184] Higher solution conductivity enables more vigorous jet stretching, resulting in smaller fiber diameters. For instance, embedding cellulose nanocrystals (CNCs) into a PMMA shell significantly increased solution conductivity, yielding finer and more uniform PMMA-CNCs/PAN core–shell fibers.[185]

**4.1.2 Applied voltage.** The applied voltage is a critical parameter that governs the initiation of the Taylor cone, jet formation, and subsequent fiber elongation.[186] In coaxial electrospinning, the voltage must be sufficiently high to overcome the surface tension of both core and shell solutions simultaneously. Typically, the required voltage ranges from 5 to 50 kV, although the exact value depends on the conductivity and viscosity of the polymer solutions. A lower voltage may result in intermittent jet formation or bead-like structures, while excessively high voltage can cause whipping instabilities, irregular fiber diameter, or even fiber breakage. Moreover, the shell solution usually dominates the jet stability in the coaxial configuration. Therefore, the applied voltage should be tuned to balance the electrostatic force acting on the shell while ensuring the smooth encapsulation of the core fluid.[187] High voltage is necessary to overcome surface tension and form a stable Taylor cone. Fiber diameter typically decreases as voltage increases due to enhanced elongation, but jet instability may ensue above a critical voltage. Empirically, for PCL/PVA/Thyme core–shell fibers, increasing the voltage from 8 kV to 15 kV decreased the average diameter from ~750 nm to ~201 nm and promoted stable compound Taylor cone formation.[188] However, excessive voltage disrupts the coaxial structure, causing separate jets and loss of core–shell morphology.

**4.1.3 Distance between the spinneret and collector.** The distance between the coaxial spinneret tip and the collector strongly affects the flight time and solidification of the jet. The typical range is 10–20 cm, though it varies with solution volatility, applied voltage, and ambient conditions. Fibers may not have sufficient time to solidify if the distance is too short, resulting in ribbon-like or fused structures on the collector. Conversely, excessively long distances may reduce the electric field strength, weakening the stretching force on the jet and resulting in thicker, less uniform fibers.[189] The optimal distance ensures that the solvent in both core and shell solutions evaporates adequately, maintaining distinct core–shell morphology without collapsing or mixing the two phases. Additionally, the type of collector (stationary plate, rotating drum, or patterned collector) also influences fiber alignment and surface morphology.[190] The distance between the coaxial spinneret tip and the collector, typically 10–20 cm, significantly influences jet flight time and solidification in coaxial electrospinning, with optimal distances (*e.g.*, 15 cm for polycaprolactone in chloroform) ensuring complete solvent evaporation to form stable fibers, as noted by Dosunmu *et al.*[191] and Subbiah *et al.*[192] This range varies with solution volatility, applied voltage (10–20 kV for polyethylene oxide), and ambient conditions, such as 50% humidity, as reported by Huang *et al.*[193] Short distances (*e.g.*, 5 cm) result in insufficient evaporation, leading to ribbon-like or fused structures (2–3 μm wide for PLA). In contrast, long distances (25 cm) reduce electric field strength (from 0.67 kV $cm^{-1}$ to 0.4 kV $cm^{-1}$), resulting in thicker, less uniform fibers (400 nm for PVDF), as reported by Reneker and Yarin *et al.*[194] and Li and Xia *et al.*[195] The optimal distance (12–15 cm for PCL/gelatin) ensures solvent evaporation from both the core and shell, maintaining distinct core–shell morphology (100 nm core; 200 nm shell) without phase mixing.[179] Additionally, the collector type affects alignment; rotating drums at 1000 rpm produces highly aligned fibres (within 10° of the axis), whereas stationary plates yield random fibres, as shown by Teo *et al.*[196]

**4.1.4 Flow rates of core and shell solutions.** Flow rates are a critical parameter in coaxial electrospinning, significantly influencing jet stability and fiber morphology, requiring precise adjustment of core and shell flow rates to maintain a stable coaxial jet, as noted by Khalf and Madihally,[197] discussing core flow rates of 0.1–0.5 mL $h^{-1}$ and shell flow rates of 0.8–2 mL $h^{-1}$ for PLGA/Col fibers. The shell flow rate is typically higher than that of the core to ensure robust encapsulation; for instance, Mickova *et al.*[198] reported that a shell flow rate of 1.5 mL $h^{-1}$ with a core flow rate of 0.3 mL $h^{-1}$ for PVA-core/PCL-shell nanofibers produced uniform core–shell structures with core diameters of ~150 nm and total fiber diameters of ~500 nm. Excessive core flow disrupts the coaxial configuration, causing jet breakup or core exposure, as observed by Lu *et al.*,[199] where increasing the core flow from 0.2 mL $h^{-1}$ to 0.6 mL $h^{-1}$ (shell at 1.2 mL $h^{-1}$) in a PEO/PVA system led to irregular fibers with diameters up to 600 nm and partial core leakage.

### 4.2 Emulsion electrospinning

Emulsion electrospinning is a versatile technique used to fabricate ultrafine core–shell nanofibers by electrospinning an emulsion, typically composed of two immiscible phases, such as oil-in-water (O/W) or water-in-oil (W/O).[200,201] In this process, the internal dispersed phase (*e.g.*, drugs, proteins, or functional materials) is encapsulated within the continuous polymer solution phase. Under the influence of a high-voltage electric field, the emulsion is stretched into a fine jet. As the solvent evaporates during jet flight, the fibers are deposited onto a collector, with the dispersed droplets entrapped inside the polymer matrix, forming a core–shell structure as shown in Fig. 7(a).[202,203] This method enables the encapsulation and protection of sensitive biomolecules while allowing for controlled release, making it particularly useful in drug delivery, tissue engineering, and the development of advanced functional materials.[204] The preparation of core–shell nanofibers by emulsion electrospinning depends on multiple factors, including the nature of the emulsion (type, stability, and droplet size), polymer concentration, surfactant selection, applied voltage, solution conductivity, tip–collector distance,

 

and flow rate.[205] Each parameter plays a crucial role in ensuring successful fiber formation and achieving a well-defined core–shell morphology. Confocal laser scanning microscopy (CLSM) images of core-sheath structured nanofibers prepared from a W/O emulsion of PEO-FTIC as the core and PEG-PLA as the shell nanofibers are shown in Fig. 7(b).[201]

**4.2.1 Emulsion characteristics and stability.** The success of emulsion electrospinning relies heavily on the stability of the emulsion. Typically, a hydrophilic polymer is dissolved in the aqueous phase, while a hydrophobic polymer is dissolved in the organic solvent phase. Surfactants such as PVA, PEG, or Pluronic F-127 are often added to reduce interfacial tension and stabilize droplet size. Stable emulsions with small, uniformly distributed droplets favour the formation of continuous core channels within nanofibers. If the emulsion is unstable, phase separation may occur before spinning, leading to heterogeneous fibers without a clear core–shell structure.[206] The type of emulsion (O/W *vs.* W/O) dictates the location of the core; for example, encapsulating hydrophilic drugs requires a W/O emulsion, whereas hydrophobic compounds are better suited for O/W systems. Double emulsions are particularly useful for encapsulating sensitive biomolecules such as proteins or growth factors, as the multiple interfaces protect them from organic solvents.[207]

**4.2.2 Polymer concentration and viscosity.** Polymer concentration determines the spinnability of the emulsion. At low concentrations, insufficient chain entanglement results in bead formation or droplet spray, rather than the formation of fibers. At excessively high concentrations, viscosity increases, making it difficult to eject a stable jet. An optimal concentration ensures smooth jet elongation, continuous fiber formation, and proper encapsulation of the dispersed phase. In emulsion electrospinning, shell-forming and core-forming polymers must be optimized.[201] For instance, PCL dissolved in chloroform/DMF mixtures is widely used as a shell polymer due to its hydrophobicity and mechanical strength. In contrast, hydrophilic polymers such as gelatin or PEO are often placed in the dispersed aqueous phase. Proper viscosity matching between the phases helps avoid droplet coalescence and irregular fiber morphologies.[208]

**4.2.3 Surfactant and solvent selection, and evaporation rate.** Surfactants are indispensable for stabilizing emulsions. The choice of surfactant depends on the emulsion type; hydrophilic surfactants stabilize O/W emulsions, whereas hydrophobic surfactants stabilize W/O emulsions. Surfactant concentration must be carefully tuned: too little surfactant leads to phase separation, while excessive surfactant can migrate to the fiber surface during spinning, affecting fiber smoothness and surface chemistry.[209] Moreover, residual surfactants may influence the biocompatibility of fibers in biomedical applications. Solvent volatility critically affects emulsion stability and fiber morphology. A fast-evaporating solvent (chloroform) promotes rapid solidification of the shell polymer, which traps the dispersed phase inside, thus favouring core–shell structures. If the solvent evaporates too slowly, phase separation can occur during flight, resulting in uneven fiber formation. Often, solvent mixtures are used to balance volatility and polymer solubility.[210,211]

### 4.3 Self-assembly methods

Core–shell nanofibers formed by self-assembly represent an elegant bottom-up fabrication route that leverages material properties, such as phase separation, block copolymer architecture, and intermolecular interactions, thereby avoiding the need for complex spinneret setups. This section reviews key self-assembly strategies, parameters influencing morphology, and practical implementations.

**4.3.1 Phase separation *via* spontaneous self-assembly in single-nozzle electrospinning.** Another versatile route is the spontaneous phase separation during electrospinning from blended solutions. Liu *et al.*[212] produced organic core–shell nanofibers *via* single-nozzle electrospinning of a PQT-12 and PEO blend. PQT-12 migrated to the fiber surface (forming the shell) during solvent evaporation while PEO formed the core. The shell thickness and overall fiber morphology could be tuned simply by adjusting the PQT-12/PEO mass ratio, as shown

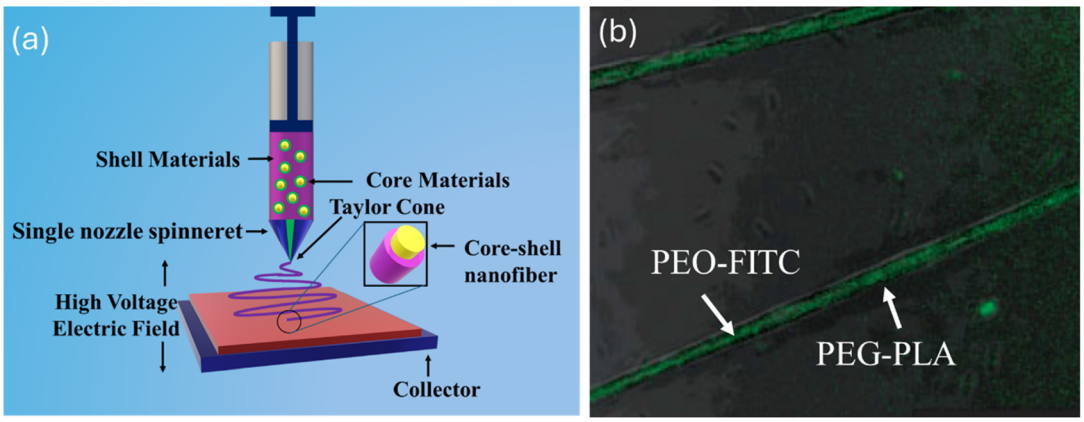


Fig. 7 (a) Schematic of preparation of core–shell nanofibers by the emulsion technique and (b) CLSM images of core-sheath structured nanofibers prepared from the W/O emulsion of PEO-FTIC as the core, and PEG-PLA as shell nanofibers. (b) adopted from ref. 201. Copyright© 2006 WILEY-VCH Verlag GmbH & Co. KGaA, Weinheim.

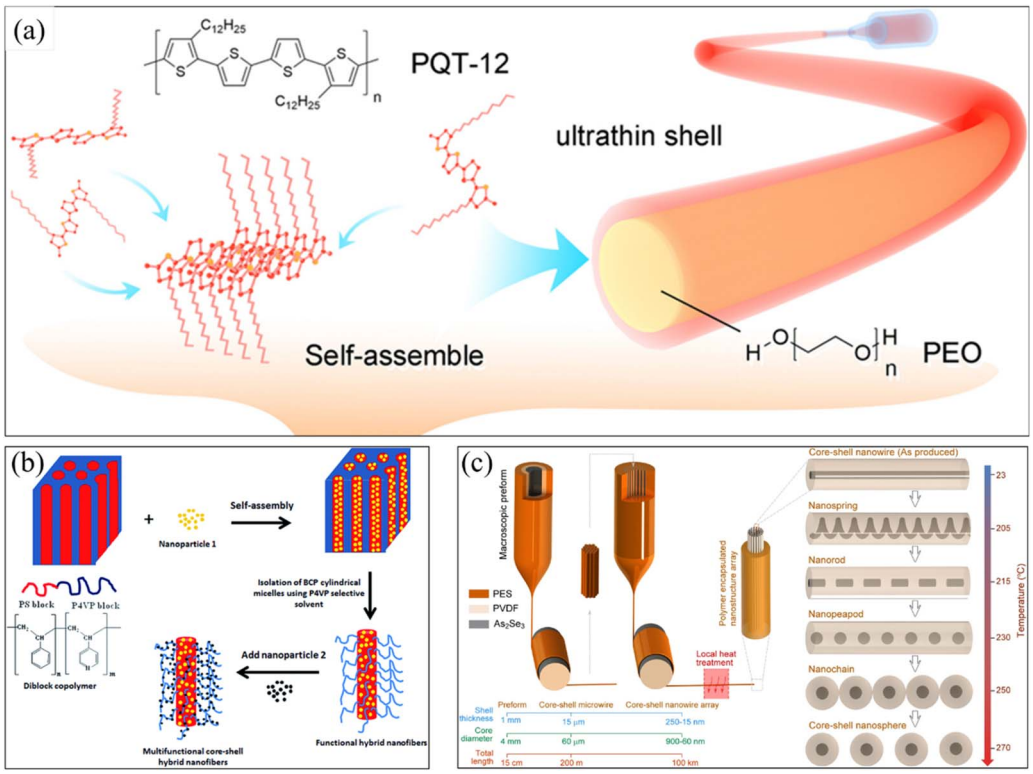


Fig. 8 (a) Chemical structure of PQT-12 and PEO and the formation of a core–shell structure by self-assembling induced phase separation, adopted from ref. 212, (b) schematic illustration for the preparation of multifunctional core–shell nanofibers functionalized with two different types of nanoparticles loaded in the core and in the shell from a self-assembled block copolymer template *via* a selective solvent approach, adopted from ref. 213, Copyright© The Royal Society of Chemistry 2015, and (c) low temperature, multimaterial fiber drawing method used for the iterative size reduction of a macroscopic layered rod down to core–shell nanowires, adopted from ref. 214, Copyright© Springer Nature 2014.

in Fig. 8(a). Optimized parameters include the composition ratio (semiconductor *vs.* matrix polymer), solvent evaporation rate, polymer miscibility, and dynamics within the jet for homogeneous core–shell nanofibers.

**4.3.2 Block copolymer–directed self-assembly.** One compelling method utilizes block copolymer self-assembly. Sanwaria *et al.*[213] demonstrated a strategy to prepare core–shell polymer–inorganic hybrid nanofibers using a PS-b-P4VP diblock copolymer. Silver nanoparticles (with PS ligands) selectively reside in PS domains, forming the core, while the P4VP matrix remains as the shell. Subsequent selective solvent swelling isolates cylindrical PS core fibers, which can be functionalized with additional nanoparticles (Au and CdS) on the P4VP shell as shown in Fig. 8(b). Key parameters include block copolymer composition (block lengths and volume fraction), nanoparticle functionalization and affinity to specific blocks, and solvent selectivity—swelling P4VP without dissolving PS to form ultrafine core–shell nanofibers.

**4.3.3 Thermal self-organization from preforms.** Although not electrospinning, a notable self-assembly approach has emerged from the thermal drawing of layered preforms. Thermally drawing a composite rod composed of core and shell materials (an $As_2Se_3$ core wrapped with a PVDF sheath) produced kilometre-long core–shell nanowires as shown in Fig. 8(c).[214] Post-thermal treatment induces transformations to structures such as nano-springs, peapods, and core–shell nanospheres, governed by parameters including diameter, temperature, and heat duration. Control factors include the preform layer structure and compatibility, drawing ratios (scale reduction), and treatment temperature and duration.

## 5. Core–shell nanofibers for magnetoelectric sensors

ME materials, which couple magnetic and electric order parameters through strain mediation, are at the forefront of research in sensors, energy harvesters, and spintronic devices. In conventional bulk composites or thin films, substrate clamping, poor interfacial bonding, and dimensional constraints often limit the ME coefficient. The core–shell nanofiber geometry provides an exceptionally high surface area, reduced mechanical clamping, and excellent stress transfer across core–shell interfaces, favouring stronger ME interactions than bulk or thin-film counterparts. In these fibers, the magnetostrictive phase (commonly spinel ferrites, hexaferrites, or orthoferrites) forms the core, while the piezoelectric phase (such as PZT, $BaTiO_3$, or lead-free perovskites) forms the shell, or *vice versa*. The concentric architecture ensures that strain

generated in one phase under a magnetic or electric field is efficiently transferred to the other, enabling direct and converse ME effects.[215]

The first experimental demonstration of ME interactions in electrospun core–shell nanofibers was reported by Xie *et al.* (2011), who fabricated $CoFe_2O_4$–PZT fibers using coaxial electrospinning followed by annealing at 600 °C, as shown in the schematic in Fig. 9(a). The resulting fibers had diameters of ~200–400 nm, with a uniform concentric architecture confirmed by the TEM micrograph in Fig. 9(b). Piezo-response force microscopy under applied magnetic fields revealed strain-mediated ME coupling at the single-fiber level, establishing electrospinning as a viable route to 1D ME nanostructures, as shown in Fig. 9(c).[216] Building on this, Sreenivasulu *et al.* (2018) synthesized $NiFe_2O_4$–$BaTiO_3$ core–shell fibers *via* coaxial spinning of sol–gel precursors in PVP, followed by calcination at 700 °C. The nanofibers, with diameters in the 150–300 nm range, exhibited a ME voltage coefficient of ~0.4 mV $cm^{-1}$ $Oe^{-1}$ at low frequency and demonstrated magnetodielectric effects in mat assemblies.[217]

A significant theoretical advance was made by Petrov *et al.* (2018), who developed a continuum model for ME coupling in coaxial nanofibers. The theory predicted direct ME coefficients of tens to hundreds of mV $cm^{-1}$ $Oe^{-1}$ and converse ME shifts at ferromagnetic resonance, depending on the core–shell diameter ratio, elastic constants, and magnetostrictive/piezoelectric coefficients of the chosen phases.[218] Experimentally, Liu *et al.* (2020) validated converse ME coupling in $NiFe_2O_4$–PZT fibers (diameters 200–500 nm) using NSMM as shown in Fig. 9(d), observing an electric-field-induced resonance shift with a CME coefficient of −24 Oe cm $V^{-1}$.[219] Shahzad *et al.* [2024] fabricated a core–shell nanofiber of $CoFe_2O_4$–$BaTiO_3$ nanofibers for magnetic-field-triggered release of doxorubicin, achieving 95% drug release in 30 minutes under a 4 mT field, and demonstrating ~90% cytotoxicity against SK-MEL-28 melanoma cells while remaining biocompatible in homolysis assays.[220] After that, Ge *et al.* (2024) reported hexaferrite–BTO core–shell fibers (average diameter ~300 nm) as shown in Fig. 9(e), confirmed by MFM analysis, and prepared by coaxial spinning and high-temperature annealing, which exhibited robust ME voltage responses by measuring the polarization under an external magnetic field as shown in Fig. 9(f), in aligned mats suitable for device-level integration.[221]

Beyond spinel and hexaferrite systems, Yadav *et al.* (2022) demonstrated ME properties in electrospun $NdFeO_3$-PZT fibers, with diameters ~128 nm, as confirmed by TEM analysis (Fig. 10(a)), showing ME coupling by recording polarization under an external magnetic field as shown in Fig. 10(b and c) at RT.[222] Furthermore, Yadav *et al.* (2022) developed a hexaferrite-PZT ME-enabled core–shell nanofiber as shown in a TEM micrograph (Fig. 9(d)). They demonstrated direct ME coupling as depicted in Fig. 10(e and f).[223] A notable step toward environmentally benign systems came from Hadouch *et al.* (2023), who synthesized lead-free CFO-BCTSn fibers (core and shell ~100–250 nm) by coaxial electrospinning as shown in the schematic in Fig. 10(g) followed by the core–shell configuration (Fig. 10(h)), achieving a high ME voltage coefficient of ~346 mV $cm^{-1}$ $Oe^{-1}$ as depicted in Fig. 10(i).[224] Later, Yadav *et al.* (2024) demonstrated sensor-grade $Ba_2Zn_2Fe_{12}O_{22}$-PZT core–shell nanofiber ME responses (650–730 V/T at ~8.3 kHz) suitable for

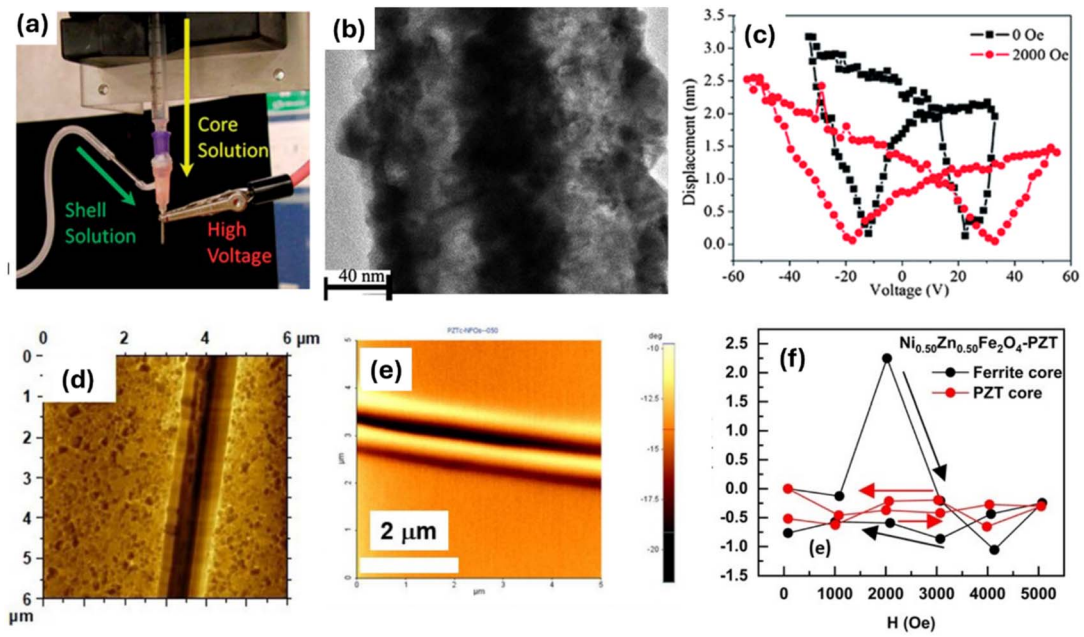


Fig. 9 (a) Digital photo of an actual coaxial spinneret in the electrospinning setup, (b) TEM micrograph of CFO-PZT core–shell nanofibers, (c) the switching characteristics of piezo response in a CFO-PZT core–shell nanofiber before and after the application of an external magnetic field by using the variable field module (VFM), (a–c) adopted from ref. 216, Copyright©-The Royal Society of Chemistry 2011, (d) NSMM image of NFO-PZT core–shell nanofibers, adopted from ref. 219, (e) MFM for a fiber of NFO shell–PZT core nanofibers, adopted from ref. 221, and (f) fractional change in the remnant polarization ($P_r$) as a function of magnetic field ($H$), adopted from ref. 221.

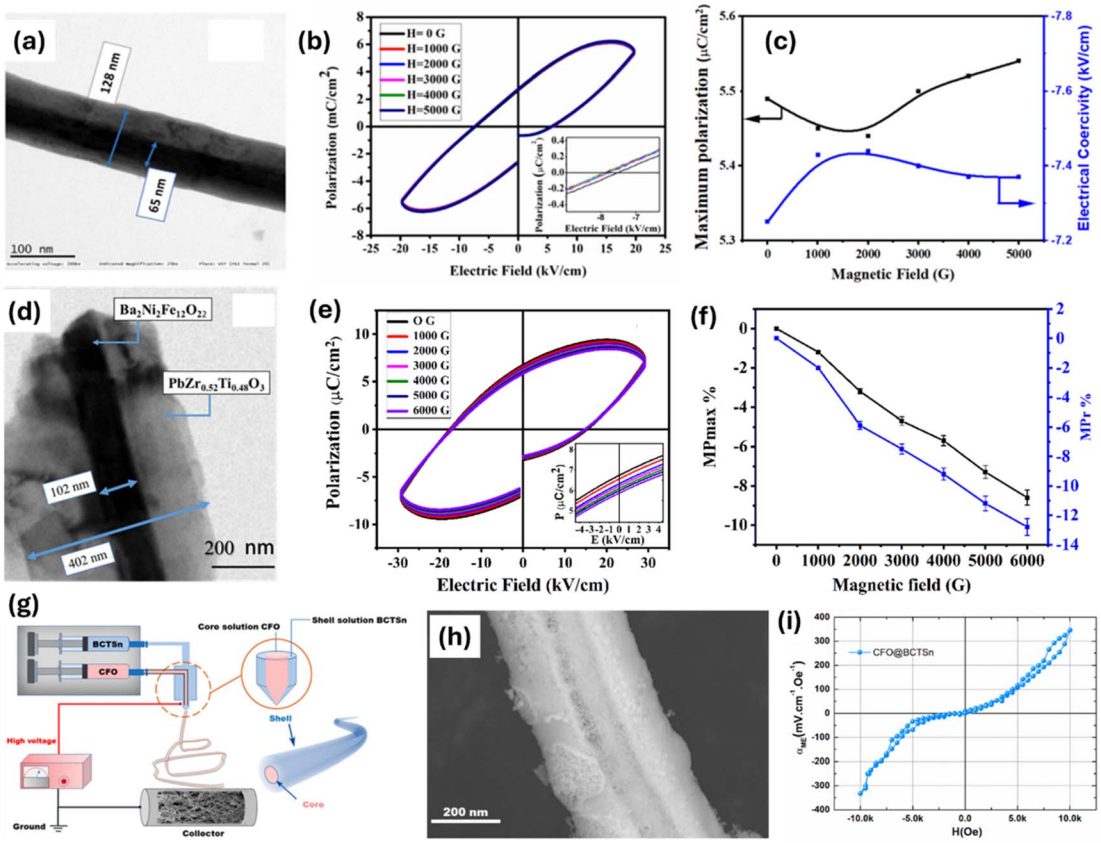


Fig. 10 (a) TEM images of the core–shell $NdFeO_3$–$PbZr_{0.52}Ti_{0.48}O_3$ nanofibers, (b) *P*–*E* loops of the core–shell NF–PZT nanofibers under various magnetic fields, (c) variations in maximum polarization and electric coercivity with respect to the applied magnetic field, (a–c) adopted from ref. 222, Copyright© Elsevier-(2022), (d) TEM micrograph, (e) variations in the *P*–*E* loop, (f) variations in MPmax% and MPr% with respect to magnetic field, (d–f) adopted from ref. 223, Copyright© Elsevier-(2022), (g) coaxial electrospinning of core–shell nanofibers: setup schematics, (h) annealed CFO-BCTSn core–shell nanofibers, and (i) dependence of the magnetoelectric coefficient of CFO-BCTSn NFs on the DC magnetic field at RT; (g–i) adopted from ref. 224, Copyright© 2023 American Chemical Society.

AC/DC field detection.[225] Most recently, Saha *et al.* (2025) summarized these developments, emphasizing that optimization of electrospinning parameters (solution concentration, applied voltage 10–25 kV, flow rates 0.2–1 mL $h^{-1}$, and post-annealing at 500–700 °C) is crucial to achieve uniform diameters, strong interfaces, and enhanced ME coefficients for sensor and harvester applications.[215] Despite these critical milestones, it is clear that research on ME core–shell nanofibers remains very limited compared to bulk composites, thin films, or 2D heterostructures. Fewer than a dozen detailed experimental studies have been reported, and only a handful of material systems—primarily CFO–PZT, NFO–BTO, hexaferrite–BTO, and rare-earth orthoferrites—have been explored. This narrow materials base and the lack of systematic studies on factors such as the core–shell ratio, fiber alignment, interfacial strain engineering, and device integration leave significant scope for further research. Exploring lead-free ferroelectrics, integrating flexible polymers with oxide cores, and developing aligned fiber arrays for magnetic sensing or spintronic devices could yield breakthroughs in ME performance. Thus, ME core–shell nanofibers represent a highly promising but underexplored frontier with ample opportunities for innovation. The compilation of ME core–shell nanofiber structures, including the diameter, ME coefficients/sensitivities, and application-specific features, is summarized in Table 1.

## 6. Core–shell nanofibers for fuel cell applications

Recent progress in fuel-cell engineering has highlighted the effectiveness of core–shell nanofibers in addressing long-standing challenges related to catalyst stability, mass-transport limitations, and fuel crossover. Compared with traditional carbon blacks or granular ceramic catalysts, 1D nanofibers and core–shell nanofibers enable a continuous conductive framework with high porosity, improved catalyst anchoring, and enhanced electron/ion mobility. Iskandarani *et al.*[226] demonstrated that P(VDF-TrFE)/Pt/C/S–$SiO_2$ nanofiber cathodes maintain high performance and exceptional durability under low-humidity PEMFC operation due to their interconnected fiber network and enhanced Pt–ionomer interfacial contact. Complementary mechanistic insights from Kabir *et al.*[227] and Khandavalli *et al.*[228] demonstrate that optimized polymer–

 

Table 1 Compilation of ME core–shell nanofiber structures, including the diameter, ME coefficients/sensitivities, and application-specific characteristics

| Core–Shell system | Fiber diameter | Core diameter | Shell thickness | ME coefficient/response | Notes | Ref. no. |
|---|---|---|---|---|---|---|
| $CoFe_2O_4$/PZT | 200–400 nm | 120–260 nm | 40–140 nm | Demonstrated strain-mediated ME coupling *via* PFM | First experimental demonstration of electrospun ME core–shell fibers | 216 |
| $NiFe_2O_4$/$BaTiO_3$ | 150–300 nm | 90–200 nm | 40–100 nm | $\alpha$ME = 0.4 mV cm$^{-1}$ Oe$^{-1}$; magnetodielectric response | Prepared *via* coaxial sol–gel electrospinning | 217 |
| $NiFe_2O_4$/PZT | 200–500 nm | 150–350 nm | 50–150 nm | CME coefficient = −24 Oe· cm V$^{-1}$ (electric-field-induced FMR shift) | Validated the converse ME effect *via* NSMM | 219 |
| Hexaferrite/$BaTiO_3$ | 300 nm | 200–240 nm | 40–80 nm | Strong ME voltage response under a magnetic field | Aligned mats exhibit device-scale ME coupling | 221 |
| $NdFeO_3$/PZT | 128 nm | 80–100 nm | 20–40 nm | Direct ME coupling shown *via* a *P–E* loop shift | Ultra-thin orthoferrite–PZT fibers | 222 |
| $CoFe_2O_4$/$BaTiO_3$ | 180–320 nm | 120–220 nm | 40–100 nm | $\alpha$ME = 346 mV cm$^{-1}$ Oe$^{-1}$ | Lead-free system; strong ME voltage peak | 224 |
| Hexaferrite ($Ba_2Zn_2Fe_{12}O_{22}$)/PZT | 300 nm | 200–260 nm | 40–80 nm | ME sensitivity 650–730 V T$^{-1}$ at ∼8.3 kHz | Sensor-grade ME fibers; strong AC/DC ME response | 225 |

particle interactions and controlled ionomer distribution within nanofibers significantly enhance Pt accessibility, oxygen-reduction kinetics, and catalyst utilization, underscoring the critical role of the ink microstructure and spinnability in producing high-quality nanofiber catalyst layers. Beyond electrodes, Liu *et al.*[229] reported that electrospun nanofiber-reinforced polymer electrolyte membranes offer superior mechanical stability, proton-transport pathways, and humidification tolerance, indicating that nanofiber engineering can also enhance membrane function. In parallel, Kallina *et al.*[230] demonstrated that humidity-robust nanofiber cathode layers can be realized through the use of tailored ionomer content and multilayer designs, thereby mitigating mass-transport resistance during PEMFC operation. This section provides a brief review and discussion of prominent research studies on fuel cells employing 1D nanofibers and core–shell nanofiber structures, highlighting their design strategies, functional advantages, and performance enhancements in energy conversion applications. Li *et al.*[231] developed core–shell $TiO_2$/C nanofibers as catalyst supports for fuel cells, where uniformly dispersed Pt nanoparticles (∼2 nm) enhanced methanol oxidation activity and stability. SEM and TEM micrographs of $TiO_2$/C are shown in Fig. 11(a and b), respectively. The system exhibited 7 times higher current density and a 2.5 times boost under UV light, highlighting a synergistic photo-electrocatalytic effect that is beneficial for fuel cell efficiency. Singh and Dempsey *et al.*[232] synthesized Pt-decorated functionalized carbon nanofibers (fCNFs) for fuel cell applications, achieving uniform Pt dispersion inside and outside the fibers as shown in Fig. 11(c). This design improved Pt utilization, CO tolerance, and long-term durability, outperforming commercial Pt/C catalysts and offering a cost-effective route for high-performance fuel cells, as shown in Fig. 11(d).

Karuppannan *et al.*[233] presented a highly durable Pt–C core–shell catalyst supported on carbon nanofibers (CNFs) for a proton exchange membrane fuel cell, as shown in the TEM image in Fig. 11(e). The core–shell structure refers to individual Pt nanoparticles, each consisting of a Pt core encapsulated by a thin (∼1 nm) nitrogen-doped carbon shell, which are uniformly dispersed on the CNF surface, serving as a stable and conductive support. Using a simple Pt–aniline complex coating followed by heat treatment, the researchers obtained 3–4 nm Pt nanoparticles with excellent uniformity and strong protection against aggregation or dissolution. The optimized catalyst (heat-treated at 900 °C) exhibited superior oxygen reduction reaction (ORR) activity and exceptional durability, maintaining nearly constant performance for 30 000 accelerated stress test cycles with negligible voltage loss at 0.8 A cm$^{-2}$, as displayed in Fig. 11(f). Its performance exceeded the U.S. DOE 2020 stability targets, demonstrating strong potential for ultra-low Pt loading and long-lasting PEM fuel cells. Senthilkumar *et al.*[234] reported the direct growth of hierarchical $Co_3O_4$@NiO and $Co_3O_4$@-$MnO_2$ core–shell nanostructures on carbon fibers for bifunctional catalysis in direct urea fuel cells (DUFCs). SEM and TEM micrographs of $Co_3O_4$@NiO nanofibers are shown in Fig. 12(a) and (b), respectively. The engineered architecture enhances both urea oxidation and oxygen reduction kinetics while

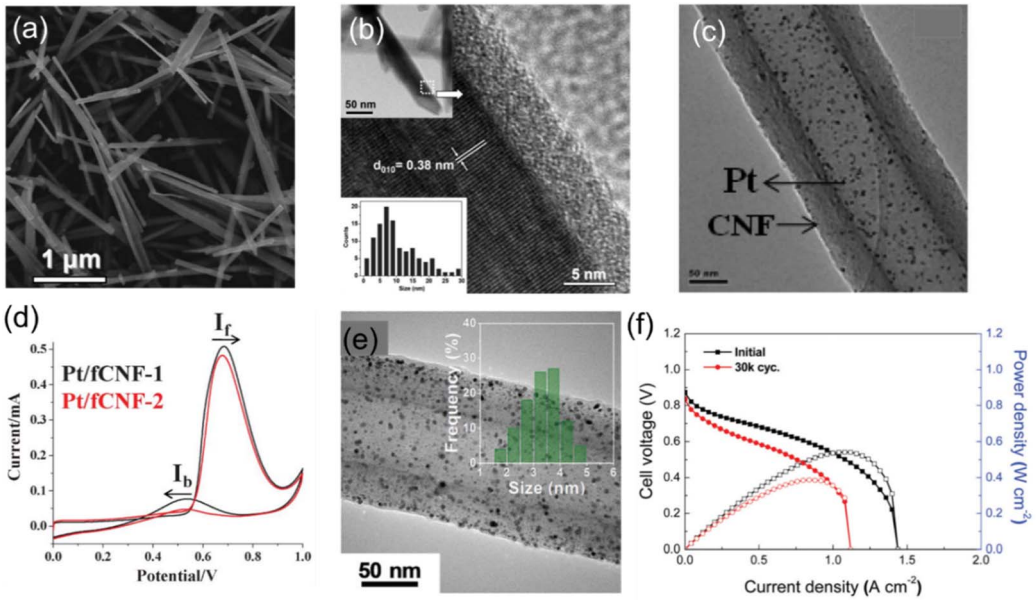


Fig. 11 (a) SEM image of $TiO_2$ nanofibers and (b) TEM images of $TiO_2$/C. Upper inset: low-magnification TEM image of several fibers; lower inset: distribution of carbon thickness over different regions and fibers, (a and b) adopted from ref. 231, Copyright© Royal Society of Chemistry-(2012), (c) TEM image of Pt/fCNF-1 core–shell nanofibers, and (d) cyclic voltametric responses for methanol electro-oxidation by Pt/fCNF-1 (response after 60 min) and Pt/fCNF-2 (response after 63 min) modified electrodes (labelled) under acidic conditions (1 M methanol + 0.5 M $H_2SO_4$) at a scan rate of 0.01 V *vs.* Ag/AgCl. (c and d) adopted from ref. 232, Copyright© Royal Society of Chemistry-(2013). (e) TEM images of Pt@CS/CNF600 core–shell nanofibers. (f) Polarization curves of (a) Pt/C, before and after 30 k AST cycles. Solid and open symbols represent the cell voltage and power density, respectively. (e and f) adopted from ref. 233, Copyright© Royal Society of Chemistry-(2019).

reducing charge-transfer resistance. The DUFC achieved a high-power density of 33.8 mW cm$^{-2}$ using urea and 23.2 mW cm$^{-2}$ with human urine, maintaining stable performance over 120 hours, as depicted in Fig. 12(c). The robust 3D structure offers superior durability, efficient electron/ion pathways, and potential for wastewater-to-energy conversion. Lee *et al.*[235] developed a novel $SiO_2$@C core–shell nanofiber *via* coaxial electrospinning for use as a microporous layer (MPL) in PEM fuel cells. SEM and TEM micrographs of $SiO_2$@C core–shell nanofibers are shown in Fig. 12(d) and (e), respectively. The hydrophilic silica core regulates water retention, while the hydrophobic conductive carbon shell ensures efficient electron transport and prevents flooding. The composite exhibits a higher surface area, strength, and conductivity than pure carbon fibers. When used in PEMFCs, it enhanced power density by 66–302% under varied humidity and temperature conditions, offering an effective strategy for improved water management and stable fuel cell operation, as displayed in Fig. 12(f). In solid oxide fuel cells (SOFCs), Choi *et al.*[236] developed $La_{0.75}Sr_{0.25}Cr_{0.5}Mn_{0.5}O_3$@-$Sm_{0.2}Ce_{0.8}O_{1.9}$ (LSCM@SDC) core–shell nanofiber anodes *via* a simple electrospinning route, achieving outstanding coking resistance and ultra-low polarization resistance (~0.11 Ω cm$^2$ at 800 °C) under methane fuel, owing to the SDC shell that improved oxygen-ion transport and prevented carbon buildup.

Similarly, Yang *et al.*[237] fabricated $YCo_{0.5}Fe_{0.5}O_3$–$Gd_{0.1}Ce_{0.9}O_{1.95}$ core–shell cathodes for intermediate-temperature SOFCs (IT-SOFCs), where the GDC shell facilitated oxygen-ion diffusion and charge transfer, yielding a low area-specific resistance of 0.66 Ω.cm$^2$ and a peak power density of 426.5 mW cm$^{-2}$ at 550 °C. Extending the concept to direct methanol fuel cells (DMFCs), Lee *et al.*[238] synthesized Pt–C core–shell catalysts supported on carbon nanofibers (Pt@CS/CNF), in which a graphitized carbon shell selectively blocked methanol while allowing $O_2$ access to Pt sites. The optimised Pt@CS/CNF900 catalyst demonstrated superior methanol tolerance, oxygen reduction reaction (ORR) activity, and stability over 30 000 cycles, outperforming commercial Pt/C catalysts. Collectively, these studies highlight the versatility of core–shell nanofiber designs as a unifying strategy for developing high-efficiency, durable, and fuel-flexible fuel cell electrodes. Delikaya *et al.*[239] developed a porous electrospun carbon nanofiber network that acts as an integrated electrode and gas diffusion layer (GDE@GDL) for high-temperature polymer electrolyte membrane fuel cells (HT-PEMFCs). This design enhanced oxygen transport, reduced mass-transport resistance, and achieved a 21% higher Pt-normalised power density compared to conventional GDL-based cells. Symillidis *et al.*[240] fabricated conductive PANI–based core–shell polymer nanofibers supporting Pd and Pd–M (Ag, Bi, Cu) catalysts for direct ethanol fuel cells (DEFCs). The PANI shell improved conductivity, CO tolerance, and catalyst stability, while Pd–Ag and Pd–Bi combinations showed the highest ethanol oxidation activity with lower activation energies than monometallic Pd. Sanna *et al.*[241] studied $Ce_{0.9}Gd_{0.1}O_{1.95}$–core/Cu-doped $La_{0.6}Sr_{0.4}MnO_3$–shell nanofiber cathodes for intermediate-temperature solid oxide fuel cells (IT-SOFCs). Electrochemical impedance spectroscopy revealed polarisation resistances as low as 1.7 Ω cm$^2$ at 650 °C, significantly lower than those of conventional composite

 

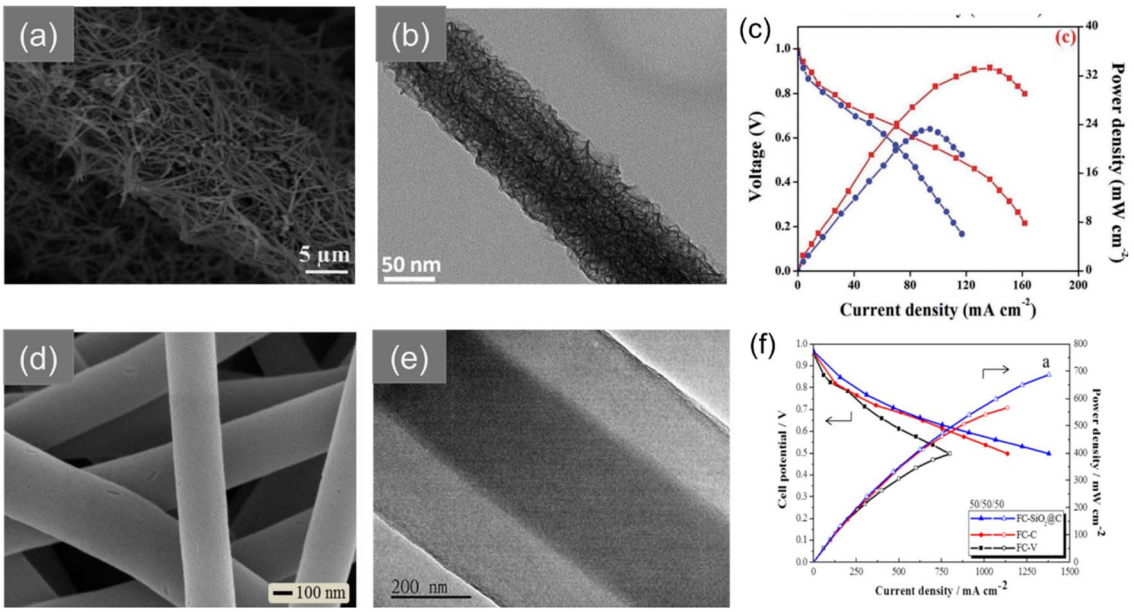


Fig. 12 (a) SEM and (b) TEM images of $Co_3O_4$@NiO nanofibers. (c) Polarization of the DUFCs with $50 \times 10^{-3}$ m urea at RT. (a–c) adopted from ref. 234, Copyright© John Wiley and Sons- (2018). (d) SEM and (e) TEM images of SiO2@C core–shell nanofibers. (f) Polarization curves (I–V curves) and power density curves (I–P curves) of FC-V, FC-C, and FC-$SiO_2$@C under different operating cells at 50 °C. (d–f) adopted from ref. 235, Copyright© Springer- (2018).

cathodes, with a stable nanofiber morphology after testing. Collectively, these results confirm that core–shell nanofiber engineering enhances mass transport, electrocatalytic activity, and long-term durability across multiple fuel cell technologies, from HT-PEMFCs to DEFCs and SOFCs. An overview of reported core–shell nanofiber systems for fuel cell applications, highlighting structural parameters (fiber diameter, core diameter, and shell thickness), device type, and key electrochemical performance metrics, is provided in Table 2.

## 7. Core–shell nanofibers for drug delivery applications

Controlled drug delivery has long been a challenge in biomedicine, where achieving precise dosage, sustained release, and protection of fragile biomolecules is crucial. Electrospun core–shell nanofibers offer a unique solution by providing a high surface-to-volume ratio, tunable porosity, and the ability to encapsulate drugs within the fiber core while protecting them with a polymer shell. This architecture not only prolongs release kinetics but also prevents premature degradation of sensitive molecules such as proteins, peptides, and nucleic acids. Therefore, core–shell nanofibers prepared by coaxial or emulsion electrospinning have emerged as promising carriers for drug delivery, tissue engineering, and wound healing.

### 7.1 Establishing encapsulation and release control

The concept of drug-loaded core–shell fibers was first rigorously demonstrated by Jiang *et al.* (2006), who fabricated BSA-dextran as the core and PCL (with PEG modification) as the shell *via* coaxial electrospinning, as shown in Fig. 13(a). The resulting fibers had diameters of approximately 200–500 nm, as shown in Fig. 13(b). They demonstrated tunable release rates by modifying the inner feed rates and PEG concentration in the shell, allowing BSA to be released gradually over periods ranging from one week to more than one month, with markedly reduced burst release compared to blend spinning.[242] Maleki *et al.* (2013) fabricated a PLGA/PLA shell and a TCH core using the coaxial electrospinning method, with a nanofiber diameter of ~200–800 nm, as confirmed by TEM analysis (Fig. 13(c)). This analysis demonstrates that the shell thickness can be precisely controlled to regulate the release duration.[243]

### 7.2 Biopolymers and protein stability

After 2016, the literature broadened: Kalwar *et al.* [2016] used chitosan–PCL and Ovideo *et al.* [2021] used core–shell nanofiber systems, which were explicitly fabricated by coaxial electrospinning, confirming that PCL core/chitosan shell geometries are practicable for biomedical cargo, as illustrated in Fig. 13(d) (ref. 244) and wound-care uses,[245] respectively. Emulsion and aqueous coaxial methods improved compatibility with biologics, allowing for the loading of growth factors, enzymes, and peptides with reduced burst release from 2017 to 2024. Recent reviews[246–248] highlight advances in electrospun systems, such as triaxial structures, responsive shells, nanoparticle-hybrid cores, and solvent strategies that preserve protein activity. Yet, protein loaded core–shell fibers still represent a small fraction of studies, leaving a broad scope for quantitative bioactivity metrics, systematic stabilization research, and translation-oriented efforts in sterilization, scale-up, and regulatory pathways.

Table 2 Overview of reported core–shell nanofiber systems for fuel-cell applications, highlighting structural parameters (fiber diameter, core diameter, and shell thickness), device type, and key electrochemical performance metrics

| Core–shell system | Fiber diameter | Core diameter | Shell thickness | Fuel-cell type | Key performance highlights | Ref. no. |
|---|---|---|---|---|---|---|
| $TiO_2$ core – carbon shell ($TiO_2$@C) | 200–400 nm | ~150–300 nm | ~20–80 nm | DMFC/methanol oxidation | 7× higher oxidation current; strong photo-electrocatalytic enhancement | 231 |
| Functionalized CNF core – Pt shell nanoparticles (Pt/f-CNF) | 250–400 nm | CNF core with uniformly anchored Pt | Thin f-C shell around CNF | DMFC | High CO tolerance; enhanced durability *vs.* Pt/C | 232 |
| Pt core – *N*-doped carbon shell on a CNF support (Pt@C/CNF600) | Pt particles 3–4 nm; shell ~1 nm | 3–4 nm Pt | 1 nm *N*-doped carbon | PEMFC (cathode) | Excellent stability (30 000 AST); surpasses DOE targets; improved ORR | 233 |
| $Co_3O_4$ core – NiO shell ($Co_3O_4$@NiO) | 100–250 nm | 80–150 nm | 20–60 nm | Direct urea fuel cell (DUFC) | Power density: 33.8 mW $cm^{-2}$ (urea), 23.2 mW $cm^{-2}$ (urine); 120 h stability | 234 |
| $Co_3O_4$ core – $MnO_2$ shell ($Co_3O_4$@$MnO_2$) | 120–260 nm | 90–160 nm | ~30–100 nm | DUFC | Enhanced bifunctional activity (OER/ORR); strong chemical stability | 234 |
| $SiO_2$ core – carbon shell ($SiO_2$@C) | 300–600 nm | 200–350 nm | 80–150 nm | PEMFC (microporous layer, MPL) | Strong hydrophilicity; improved water management; better conductivity | 235 |
| $Ce_{0.9}Gd_{0.1}O_{1.95}$ core – Cu-doped LSM shell (CGO@LSM) | 150–300 nm (from SOFC cathode NF synthesis) | 100–200 nm | 30–80 nm | SOFC (cathode) | Very low polarization resistance (1.7 $\Omega cm^2$ @ 650 °C) | 241 |
| PANI core – Pd/Pd–Ag/Pd–Bi catalyst shell polymer nanofibers | 200–450 nm (PANI NF) | Conductive PANI | Pd, Pd–Ag, Pd–Bi nanoparticle shells | DEFC | Highest ethanol oxidation with Pd–Ag & Pd–Bi; high CO tolerance | 240 |
| Porous carbon network (GDE@GDL) with core–shell-like graded layers | Micro–nano hybrid | — | — | HT-PEMFC | 21% higher Pt-normalized power density; improved $O_2$ diffusion | 239 |

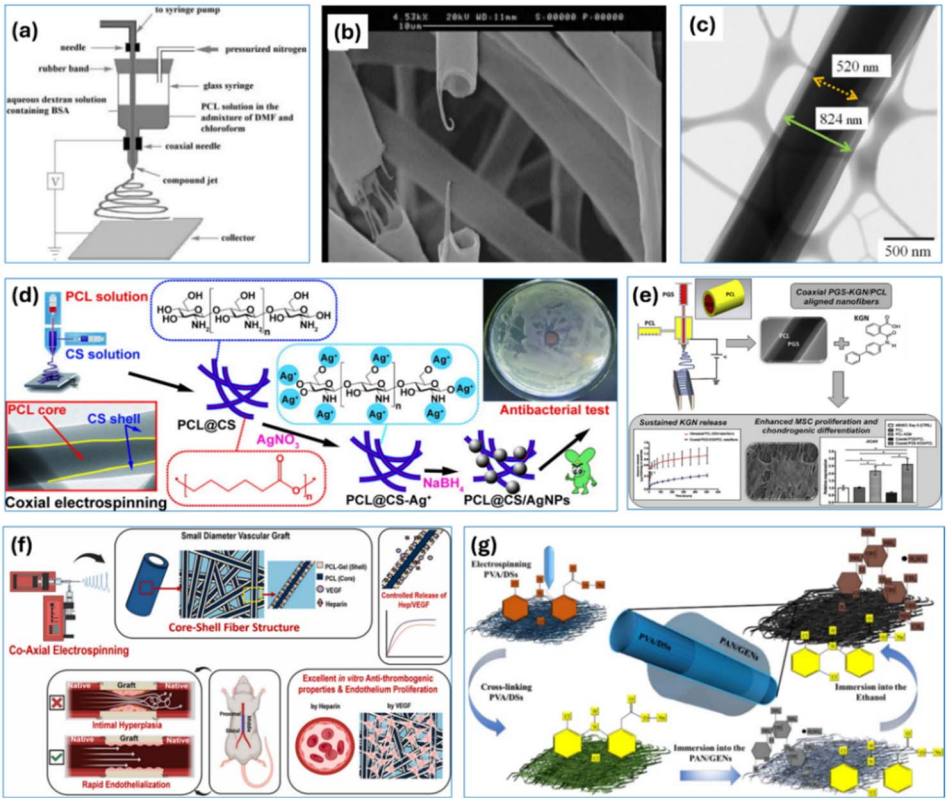


Fig. 13 (a) Configuration of the coaxial electrospinning setup used for preparing core–shell structured fibers composed of PCL as the shell and dextran containing BSA as the core. (b) The morphology changes in the core–shell structured fibers during BSA release after 21 days. (a and b) adopted from ref. 242, Copyright© 2006 Wiley Periodicals, Inc., (c) TEM images of dual nanofibers (scale bar was 500 nm), core solution: [PLGA, 0.5 wt%, chloroform (8): DMF (2)] (67%) + [TCH 5.94 wt%, methanol] (33%), 0.3 mL $h^{-1}$, shell solution: [PLGA, 2 wt%, chloroform (8): DMF (2)], 3 mL $h^{-1}$, 10 kV, 15 cm, adopted from ref. 243, Copyright© Society of Plastics Engineers-2013, (d) coaxial electrospinning of polycaprolactone-chitosan for antibacterial activity, adopted from ref. 244, Copyright© 2016 Elsevier B.V. All rights reserved, and (e) Kartogenin-loaded coaxial PGS/PCL aligned nanofibers for cartilage tissue engineering, adopted from ref. 250, Copyright© 2019 Elsevier B.V. All rights reserved. (f) Small-diameter vascular graft composed of core–shell structured micro-nanofibers for neointimal hyperplasia, adopted from ref. 251, Copyright© 2024 Elsevier Ltd All rights reserved. (g) Illustration skims of core–shell nanofibers for dual simultaneous drug delivery, adopted from ref. 252.

### 7.3 Tissue engineering and wound healing

Hou *et al.* (2017) fabricated biodegradable, bioactive core–shell fibrous mats *via* coaxial electrospinning using a PCL shell and PGS core system with surface-immobilized heparin, yielding scaffolds with favorable chemical, mechanical, and biological characteristics for broad tissue-engineering applications.[249] Silva *et al.* [2020] reported the development of aligned core–shell nanofibers composed of a PGS (core) and a PCL (shell), engineered to mimic the anisotropic architecture of articular cartilage while enhancing mechanical strength as illustrated in Fig. 13(e).[250] Kartogenin, a small chondrogenic molecule, was encapsulated within the PGS core, allowing for sustained release over a period of up to 21 days. This controlled delivery promoted proliferation and chondrogenic differentiation of human mesenchymal stem/stromal cells without the need for exogenous growth factors such as TGF-β3, highlighting the potential of KGN-loaded coaxial nanofibers as promising scaffolds for cartilage tissue engineering. Al Fahad *et al.* (2024) developed a small-diameter vascular graft using coaxial electrospun micro-nanofibers with a PCL/gelatin shell loaded with heparin and VEGF and a PCL core—demonstrating sustained release (~79% heparin; ~86% VEGF over 25 days), as shown in Fig. 13(f) with excellent mechanical performance, full endothelialization, smooth muscle regeneration, and 100% patency in rat aorta implants.[251] Kharaghani *et al.* (2019) designed core–shell PVA/PAN nanofibers *via* coaxial electrospinning for dual-drug delivery as depicted in Fig. 13(g), enabling the simultaneous release of water- and organic-solvent–soluble drugs for tailored therapeutic applications.[252] Li *et al.* (2021) reported a core–shell GelMA-PDLLA nanofiber-hydrogel composite scaffold with enhanced porosity, water retention, and angiogenic activity, which accelerates chronic diabetic wound healing *in vivo*, as shown in Fig. 14(a).[253] Guo *et al.* (2022) developed a core–shell coaxial fiber membrane loaded with CTG in the core and CIP in the shell, achieving controlled release, antibacterial performance, and improved fibroblast proliferation, as well as enhanced scald wound repair in rats,[254] as illustrated in Fig. 14(b).

Abadi *et al.* (2025) engineered core–shell PCL–CS/PVA nanofibers *via* coaxial electrospinning to co-deliver PIO-NEs and GEM over 14 days as shown in the schematic in Fig. 14(c), achieving sustained and controlled release (~80% of PIO;

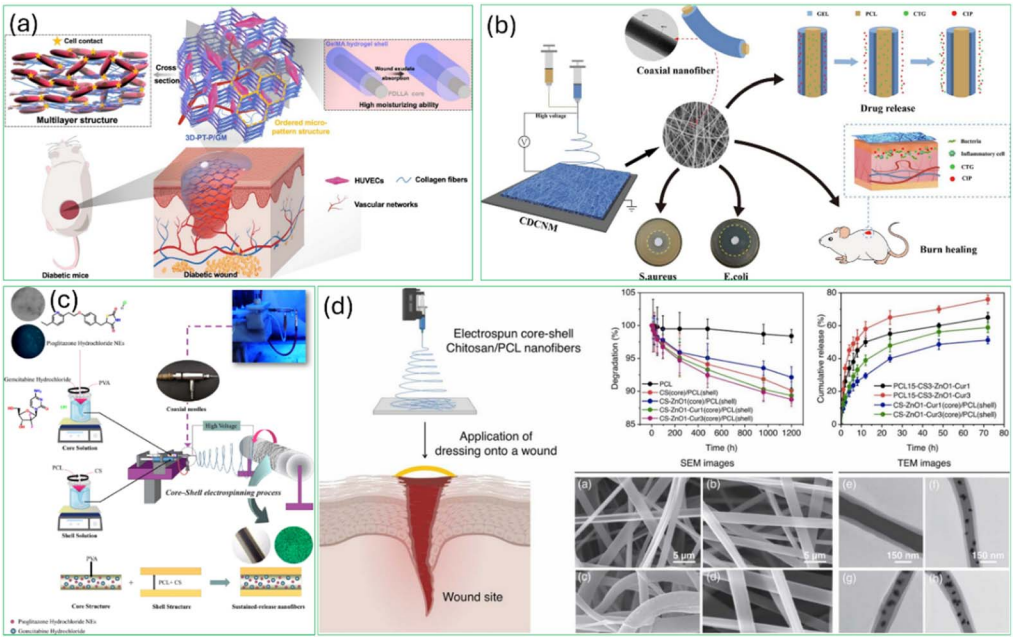


Fig. 14 (a) Nanofiber/hydrogel core–shell scaffolds with a three-dimensional multilayer patterned structure for accelerating diabetic wound healing, adapted from ref. 231. (b) Dual drug-loaded nanofiber membranes based on coaxial electrostatic spinning technology adopted from ref. 254, Copyright© 2022 Elsevier B. V. All rights reserved. (c) The schematic of nanofiber preparation for localized melanoma therapy delivering Pioglitazone nano-emulsions and a gemcitabine dual-loaded system, adopted from ref. 255, Copyright © 2025, Springer Nature. (d) Core–shell chitosan-polycaprolactone nanofibers for controlled curcumin release, adopted from ref. 256, Copyright© 2025 Elsevier B. V. All rights are reserved.

Table 3 Summary of core–shell nanofiber systems used in drug-delivery applications, including fiber diameters, core and shell dimensions, therapeutic payloads, and corresponding release behaviours

| Core–shell system | Fiber diameter | Core diameter | Shell thickness | Drug/payload | Release behavior | Ref. |
|---|---|---|---|---|---|---|
| PCL core – SF shell | 200–450 nm | 120–250 nm | 50–150 nm | Clindamycin | Sustained release for wound healing | 163 |
| PCL/PVA or PCL/Col core–shell | 200–600 nm | 120–350 nm | 80–150 nm | Biomedical drugs | Controlled/sustained | 165 |
| BSA–dextran core – PCL-PEG shell | 200–500 nm | 120–300 nm | 50–200 nm | BSA protein | Release adjustable (1 week – 1 month) | 242 |
| TCH core – PLGA/PLA shell | 200–600 nm | 150–350 nm | 50–200 nm | Tetracycline | Sustained antibiotic release | 243 |
| CTG core – CIP shell | 300–700 nm | 200–450 nm | 80–200 nm | Ceftazidime + ciprofloxacin | Controlled dual-drug release; improved wound healing | 254 |
| PCL–CS/PVA core–shell | 250–550 nm | 150–300 nm | 50–150 nm | PIO + GEM | Sustained (14 days) | 255 |
| Chitosan-PCL core–shell | 250–600 nm | 150–350 nm | 50–200 nm | Curcumin | Antimicrobial; wound healing | 256 |

~77% of GEM), which significantly inhibited proliferation and induced apoptosis in A375 melanoma cells *via* P53 and PPARγ pathways.[255] Furthermore, Mosallanezhad *et al.* (2025) developed core–shell chitosan-PCL nanofibers loaded with curcumin for controlled wound therapy. These fibers demonstrated a favorable morphology, enhanced structural and release properties, and strong antimicrobial performance, indicating their promise for infection-resistant wound dressings, as shown in Fig. 14(d).[256] Together, these studies emphasize the versatility of core–shell architectures in controlled drug delivery, tissue regeneration, and wound management. A summary of core–shell nanofiber systems used in drug-delivery applications, including fiber diameters, core and shell dimensions, therapeutic payloads, and corresponding release behaviours, is provided in Table 3. Furthermore, Table 4 summarizes details of parameters involved in the preparation of core–shell nanofiber fabrication techniques.

## 8. Challenges, limitations, and future directions of core–shell nanofibers

Despite significant progress, the development and deployment of core–shell nanofibers in magnetoelectric sensors, fuel-cell systems, and drug-delivery platforms still encounter several critical challenges that prevent their transition from laboratory research to practical use. One major issue is scalability. Although coaxial and emulsion electrospinning are excellent for producing uniform fibers on a laboratory scale, they suffer from

Table 4 Comparison of core–shell nanofiber fabrication techniques and their parameters

| | | | Self-assembly methods | | |
|---|---|---|---|---|---|
| Parameters | Coaxial electrospinning | Emulsion electrospinning | Single-nozzle phase-separation | Block copolymer self-assembly | Thermal self-organization |
| Material loading | Core/shell-8–20 wt% each (independent solutions; need viscosity matching) | Total polymer -8–20 wt% (continuous phase); dispersed phase fraction 5–30% depending on core | 8–20 wt% (polymer solution for ES) | 0.5–5 wt% (micelles); up to 10–20 wt% (gels) | Bulk preforms (100% solids) |
| Blend/block design | Independent choice of core (magnetostrictive, drug, and NPs) and shell (piezo/structural polymer) | Core encapsulated *via* immiscible emulsion droplets; surfactant stabilizes phase boundaries | 30–70% minor phase viscosity for shell/core $\gtrsim$ 1–2 | Volume fraction of the minority block = 0.2–0.35 $\chi N \gtrsim 10$–15 | Pre-stacked core/shell glass or polymer with viscosity-matched layers |
| Operating field/force | Dual nozzle high-voltage (HV)- 10–25 kV; tip–collector 10–20 cm; flow rate balance 0.2–1.0 mL $h^{-1}$ | Single-nozzle HV (10–25 kV); 10–20 cm; flow rate 0.2–1.0 mL $h^{-1}$ (continuous phase dominates) | HV- 10–30 kV; tip–collector 10–20 cm; 0.2–1.0 mL $h^{-1}$ | Ambient assembly; selective swelling; RT–80 °C | Thermal draw above softening/glass-*T*; ~180–230 °C (PVDF shell); higher for silica cores |
| Evaporation/consolidation | Solvent evaporation for both streams; annealing removes the porosity and improves crystallinity | Solvent evaporation fixes the shell first; dispersed droplets lock in; annealing may remove the surfactant | Fast-evaporating solvent favours shell localization; anneal at 60–500 °C (inorganics) | Solvent selectivity + drying drives segregation; optional NP incorporation | No solvent; thermal relaxation after draw sets nano-geometry |
| Output geometry | Continuous fibers, typically 150–800 nm in diameter, with transparent concentric shells | Continuous mats; diameter. 100–700 nm; core domain size follows droplet size | Random mats; diameter. 100–800 nm typical nanofibers | Extracted nanofibers (discrete); morphology depends on $\chi N$ | Kilometre-long arrays, 50 nm to 1 μm diameter |
| Best for | Precise core–shell alignment, tunable diameter ratio, and multifunctional innovative fibers for sensors | Encapsulation of bioactive proteins, or drugs, in scalable mats with phase-separation-driven shells for medical | Thin reactive shells, sensing, and simple tooling for biomedicals | Functional shells/cores; multi-NP hybrids and biomedical | Ultrahigh uniformity, photonics, and scalable optical/electrical arrays for industry |

low throughput and high sensitivity to process variations, making it difficult to produce large-area, industrial-scale fibers with consistent core–shell structures. Ensuring reproducibility—especially uniform core diameters, shell thicknesses, and concentricity—requires precise control over solution viscosity, voltage, flow rates, humidity, and solvent evaporation. These factors become more difficult to regulate during scale-up, often leading to structural inconsistencies and batch-to-batch differences. Furthermore, many high-performance materials involve costly precursors or require multiple steps of annealing and calcination, which increase fabrication costs, especially for metal oxides, perovskites, and noble-metal catalysts used in fuel cells.

Another key concern is toxicity and environmental safety, particularly for lead-based piezoelectric systems, such as PZT and PMN-PT. While these materials offer strong magnetoelectric coupling, their inherent lead content limits their use in biomedical devices, wearable technology, and environmentally regulated commercial products. Restrictions from standards such as RoHS and REACH greatly limit their real-world application, highlighting the need for lead-free options like BCTSn, $BaTiO_3$, KNN, and zinc- or barium-based hexaferrites. However, matching the magnetoelectric performance of lead-based systems while maintaining processability and long-term stability remains an ongoing research challenge.

Device integration and long-term stability are also critical issues. Arranging core–shell nanofibers into ordered arrays and incorporating them into multilayer device architectures require advanced assembly methods that are not yet standardized. In magnetoelectric sensors, defects at the core–shell interface, inadequate strain transfer, or microcracking from repeated magnetic and electric cycling can reduce coupling efficiency. In fuel cells, durability issues such as catalyst detachment, carbon corrosion, ionomer redistribution, or shell degradation in humid, acidic, or high-temperature environments can compromise performance. Drug-delivery fibers must also sustain structural integrity during storage and implantation, prevent uncontrolled burst release, and ensure the biocompatibility of both organic and inorganic elements. These challenges emphasize the importance of robust interfacial engineering, better encapsulation techniques, and stronger mechanical reinforcement of core–shell structures.

Looking ahead, several opportunities can help advance core–shell nanofiber technologies. New fabrication methods—like real-time controlled coaxial electrospinning, 3D-assisted fiber patterning, and hybrid printing-electrospinning platforms—offer promising paths for scalable and precise structural control. Innovations in interface engineering, defect reduction, and domain alignment can further improve coupling efficiency and stability. For biomedical use, creating stimuli-responsive shells that react to pH, temperature, or magnetic/electric fields will be essential for enabling personalized or on-demand therapies. For fuel cells, enhancing ionomer distribution, controlling shell porosity, and stabilizing catalyst–support interactions are crucial for high performance under low-humidity conditions. Using computational tools such as AI-based material design and multiphysics simulations can speed up optimization and predict long-term behavior *in vivo* or under operational stresses. Ultimately, collaboration across disciplines—materials science, chemical engineering, electronics, and biomedicine—is vital to transforming core–shell nanofibers from laboratory prototypes into reliable, scalable, and commercially viable solution technologies.

# 9. Conclusion

Core–shell nanofibers represent a transformative class of one-dimensional architectures, whose tunable interfaces, high aspect ratios, and multifunctional compositions enable superior performance in magnetoelectric sensing, fuel cell catalysis, and drug delivery applications. Despite significant progress, several critical research gaps must be addressed before these systems can advance toward technologically relevant devices and scalable commercialization. First, optimizing interfacial coupling remains a major challenge across all areas. In magnetoelectric systems, inadequate strain transfer, interfacial defects, and uncontrolled core–shell ratios greatly limit ME coefficients and device sensitivity. Similarly, fuel-cell nanofibers need improved catalyst–support interactions and controlled ionomer distribution to achieve durable and efficient electrochemical performance. For drug-delivery fibers, ensuring long-term shell stability and preventing burst release are key obstacles. Second, there is an urgent need for reliable, lead-free alternatives to traditional high-performance piezoelectric materials, such as PZT and PMN-PT. Although promising candidates—such as BCTSn, $BaTiO_3$, KNN, and Zn- or Ba-based hexaferrites—have been developed, their electromechanical response and long-term reliability still fall short of lead-based systems. Bridging this gap is crucial for enabling sustainable, biocompatible magnetoelectric devices, particularly in biomedical and wearable applications that require strict regulatory standards. Third, flexible and integrated device architectures are a promising yet underdeveloped area. For magnetoelectric sensing, integrating aligned or woven coaxial nanofibers into soft substrates could support wearable or implantable devices. In fuel cells, multilayer nanofiber electrodes and microporous layers need to be engineered for mechanical durability under varying humidity and temperature conditions. For biomedical uses, seamless integration with hydrogels, scaffolds, and tissue-mimicking platforms will be vital for clinical translation. Lastly, commercialization challenges persist throughout the field. Coaxial electrospinning faces issues with low throughput and batch variability. Maintaining uniform core–shell morphology at an industrial scale is difficult due to sensitivities to viscosity, flow rate, voltage, and humidity. Material costs—especially for noble metals, rare-earth ferrites, and high-purity polymers—further limit scalability. Moreover, the lack of standardized testing protocols for ME performance, drug release kinetics, mechanical stability, and long-term degradation complicates cross-study comparisons. Overall, while core–shell nanofibers offer exceptional multifunctionality and potential, realizing their broader use depends on overcoming these challenges through interdisciplinary advances in interface engineering, scalable

 

manufacturing, predictive modeling, and device integration. With ongoing innovation, core–shell nanofibers are positioned to drive the next generation of sensing, energy, and biomedical technologies.

## Author contributions

Sandeep Kumar Yadav: visualization, resources, methodology, investigation, formal analysis, conceptualization, writing – original draft. Vishwa Prakash Jha: theoretical analysis, conceptualization, writing – review & editing. Durga Prasad Pabba and Arun Thirumurugan: supervision, resources, project administration, methodology.

## Conflicts of interest

The authors declare that they have no known competing financial interests or personal relationships that could have appeared to influence the work reported in this paper.

## Abbreviations

| | |
|---|---|
| ME | Magnetoelectric |
| 1D | One-dimensional |
| CNTs | Carbon nanotubes |
| nT | Nano-tesla |
| PZT | $PbZr_{0.52}Ti_{0.48}O_3$ |
| PMN–PT | $(1-x)Pb(Mg_{1/3}Nb_{2/3})O_3$–$xPbTiO_3$ |
| AIN | Aluminum nitride |
| Terfenol-D | $Tb_xDy_{1-x}Fe_2$ |
| PCL | Polycaprolactone |
| PVA | Polyvinyl alcohol |
| PCL | Polycaprolactone |
| Col | Collagen |
| PVDF | Polyvinylidene fluoride |
| DOX | Doxorubicin |
| *N*-CMCS | *N*-carboxymethyl chitosan |
| SF | Silk fibroin |
| cP | Centipoise |
| CNCs | Cellulose nanocrystals |
| PMMA | poly(methyl methacrylate) |
| PAN | Polyacrylonitrile |
| PLA | Poly(lactic acid) |
| PLGA | Poly(lactic-*co*-glycolic acid) |
| PEG | Polyethylene glycol |
| PEO | polyethylene oxide |
| nm | Nanometer |
| μm | Micrometer |
| FITC | Fluorescein isothiocyanate |
| PGS | Poly(glycerol sebacate) |
| GelMA | Gelatin methacryloyl |
| PDLLA | Poly(d, l-lactic acid) |
| CTG | Centella total glucoside |
| CIP | Ciprofloxacin |
| PIO-Nes | Pioglitazone nanoemulsions |
| GEM | Gemcitabine |
| PQT-12 | Poly(3,3‴-didodecyl quarter thiophene) |
| NSMM | Near field scanning microwave microscope |
| MFM | Magnetic force microscope |

## Data availability

No data were used for the research described in the article.

## References

1 B. A. Grzybowski and W. T. S. Huck, The nanotechnology of life-inspired systems, The nanotechnology of life-inspired systems, *Nat. Nanotechnol.*, 2016, **11**, 585–592, DOI: 10.1038/nnano.2016.116.
2 M. T. Bohr, Nanotechnology goals and challenges for electronic applications, *IEEE Trans. Nanotechnol.*, 2002, **1**, 56–62, DOI: 10.1109/TNANO.2002.1005426.
3 M.-C. Daniel and D. Astruc, Gold Nanoparticles: Assembly, Supramolecular Chemistry, Quantum-Size-Related Properties, and Applications toward Biology, Catalysis, and Nanotechnology, *Chem. Rev.*, 2004, **104**(1), 293–346, DOI: 10.1021/cr030698+.
4 C. P. Bean and J. D. Livingston, Superparamagnetism, *J. Appl. Phys.*, 1959, **30**, S120–S129, DOI: 10.1063/1.2185850.
5 B. Bhushan, Nanotribology and nanomechanics of MEMS/NEMS and BioMEMS/BioNEMS materials and devices, *Microelectron. Eng.*, 2007, **84**(3), 387–412, DOI: 10.1016/j.mee.2006.10.059.
6 U. Boudriot, R. Dersch, A. Greiner and J. H. Wendorff, Electrospinning Approaches Toward Scaffold Engineering—A Brief Overview, *Artif. Organs*, 2006, **30**(10), 785–792, DOI: 10.1111/j.1525-1594.2006.00301.x.
7 D. S. Katti, K. W. Robinson, F. K. Ko and C. T. Laurencin, Bioresorbable nanofiber-based systems for wound healing and drug delivery: optimization of fabrication parameters, *J. Biomed. Mater. Res., Part B*, 2004, **70B**(2), 286–296, DOI: 10.1002/jbm.b.30041.
8 F. Mustafa and S. Andreescu, Nanotechnology-based approaches for food sensing and packaging applications, *RSC Adv.*, 2020, **10**, 19309–19336, DOI: 10.1039/D0RA01084G.
9 J. Horne, L. McLoughlin, B. Bridgers and E. K. Wujcik, Recent developments in nanofiber-based sensors for disease detection, immunosensing, and monitoring, *Sens. Acutators Rep.*, 2020, **2**, 100005, DOI: 10.1016/j.snr.2020.100005.
10 G. T. V. Prabu and B. Dhurai, A Novel Profiled Multi-Pin Electrospinning System for Nanofiber Production and Encapsulation of Nanoparticles into Nanofibers, *Sci. Rep.*, 2020, **10**, 4302, DOI: 10.1038/s41598-020-60752-6.
11 J. A. Nairn, Aspect ratio requirements for nanotube-reinforced, polymer–matrix composites, *Composites, Part A*, 2011, **42**, 1850–1855, DOI: 10.1016/j.compositesa.2011.08.012.
12 S. Iwamoto, S. Lee and T. Endo, Relationship between aspect ratio and suspension viscosity of wood cellulose

nanofibers, *Polym. J.*, 2014, **46**, 73–76, DOI: 10.1038/pj.2013.64.
13 A. Frenot and I. S. Chronakis, Polymer nanofibers assembled by electrospinning, *Curr. Opin. Colloid Interface Sci.*, 2003, **8**, 64–75, DOI: 10.1016/S1359-0294(03)00004-9.
14 J. Doshi and D. H. Reneker, Electrospinning process and applications of electrospun fibers, *J. Electrost.*, 1995, **35**, 151–160, DOI: 10.1016/0304-3886(95)00041-8.
15 N. Bhardwaj and S. C. Kundu, Electrospinning: A fascinating fiber fabrication technique, *Biotechnol. Adv.*, 2010, **28**, 325–347, DOI: 10.1016/j.biotechadv.2010.01.004.
16 Y. Sun, S. Cheng, W. Lu, Y. Wang, P. Zhang and Q. Yao, Electrospun fibers and their application in drug-controlled release, biological dressings, tissue repair, and enzyme immobilization, *RSC Adv.*, 2019, **9**, 25712–25729, DOI: 10.1039/C9RA05012D.
17 M. K. Gaydhane, C. S. Sharma and S. Majum, Electrospun nanofibres in drug delivery: advances in controlled release strategies, *RSC Adv.*, 2023, **13**, 7312–7328, DOI: 10.1039/D2RA06023J.
18 B. G. DJ and G. J. J. Wessley, A study on EMI shielding in aircraft: introduction, methods and significance of using electrospun nanocomposites, *J. Space Saf. Eng*, 2024, **11**, 150–160, DOI: 10.1016/j.jsse.2024.01.001.
19 M. S. Nisha and D. Singh, Manufacturing of Smart Nanomaterials for Structural Health Monitoring (SHM) in Aerospace Application Using CNT and CNF, *J. Nano Res.*, 2015, **37**, 42–50, DOI: 10.4028/www.scientific.net/JNanoR.37.42.
20 M. Jurić, G. Goksen, F. Donsì and S. Jurić, Innovative Applications of Electrospun Nanofibers Loaded with Bacterial Cells Towards Sustainable Agri-Food Systems and Regulatory Compliance, *Food Eng. Rev.*, 2024, **16**, 270–303, DOI: 10.1007/s12393-024-09369-3.
21 D. Martins, V. P. Scagion, R. Schneider, A. C. C. Lemos, J. Oliveira, and D. S. Correa, Biodegradable Polymer Nanofibers Applied in Slow Release Systems for Agri-Food Applications, in *Polymers for Agri-Food Applications*, ed. T., Gutiérrez, Springer, Cham, 2019, DOI: 10.1007/978-3-030-19416-1_15.
22 J. B. Moreira, S. G. Kuntzler, B. P. Vargas, A. A. Comitre, J. A. V. Costa, and M. G. de Morais, Nanofiber-Reinforced Bionanocomposites in Agriculture Applications. in *Polymer Based Bio-Nanocomposites. Composites Science and Technology*, ed. C., Muthukumar, S. M. K., Thiagamani, S., Krishnasamy, R., Nagarajan, and S., Siengchin, Springer, Singapore, 2022, DOI: 10.1007/978-981-16-8578-1_17.
23 T. Wang, Z. Chen, W. Gong, F. Xu, X. Song, X. He and M. Fan, Electrospun Carbon Nanofibers and Their Applications in Several Areas, *ACS Omega*, 2023, **8**(25), 22316–22330, DOI: 10.1021/acsomega.3c01114.
24 J. Xue, T. Wu, Y. Dai and Y. Xia, Electrospinning and Electrospun Nanofibers: Methods, Materials, and Applications, *Chem. Rev.*, 2019, **119**(8), 5298–5415, DOI: 10.1021/acs.chemrev.8b00593.
25 I. G. Loscertales, A. Barrero, I. Guerrero, R. Cortijo, M. Marquez and A. M. Ganan-Calvo, Micro/Nano Encapsulation *via* Electrified Coaxial Liquid Jets, *Science*, 2002, **295**(5560), 1695–1698, DOI: 10.1126/science.1067595.
26 M. Yousefzadeh and F. Ghasemkhah, in *Design of Porous, Core–Shell, and Hollow Nanofibers*, ed. A. Barhoum, M. Bechelany and A. Makhlouf, Springer, Cham, 2019, DOI: 10.1007/978-3-319-42789-8_9-2.
27 M. Yousefzadeh, S. Ramakrishna, Modeling performance of electrospun nanofibers and nanofibrous assembles, in *Electrospun Nanofibers*, ed. M. Ashanti, Woodhwad Publishing, Cambridge, 2017, 303–337, DOI: 10.1016/B978-0-08-100907-9.00013-1.
28 S. Ramakrishna, K. Fujihara, W.-E. Teo, T. Yong, Z. Ma and R. Ramaseshan, Electrospun nanofibers: solving global issues, Mater, *Today*, 2006, **9**(3), 40–50, DOI: 10.1016/S1369-7021(06)71389-X.
29 Y. Zhang, Z. Huang, X. Xu, C. T. Lim and S. Ramakrishna, Preparation of Core–Shell Structured PCL-r-Gelatin Bi-Component Nanofibers by Coaxial Electrospinning, *Chem. Mater.*, 2004, **16**(18), 3406–3409, DOI: 10.1021/cm049580f.
30 Y. Liu, X. Chen, Y. Gao, Y. Liu, D. Yu and P. Liu, Electrospun Core–Sheath Nanofibers with Variable Shell Thickness for Modifying Curcumin Release to Achieve a Better Antibacterial Performance, *Biomolecules*, 2022, **12**, 1057, DOI: 10.3390/biom12081057.
31 Y. Jiang, D. Fang, G. Song, J. Nie, B. Chen and G. Ma, Fabrication of core–shell nanofibers by single capillary electrospinning combined with vapor induced phase separation, *New J. Chem.*, 2013, **37**, 2917, DOI: 10.1039/c3nj00654a.
32 D. Ponnamma, M. M. Chamakh, A. M. Alahzm, N. Salim, N. Hameed and M. Maadeed, Core-Shell Nanofibers of Polyvinylidene Fluoride-based Nanocomposites as Piezoelectric Nanogenerators, *Polymers*, 2020, **12**, 2344, DOI: 10.3390/polym12102344.
33 S. Taokaew and T. Chuenkaek, Developments of Core/Shell Chitosan-Based Nanofibers by Electrospinning Techniques: A Review, *Fibers*, 2024, **12**, 26, DOI: 10.3390/fib12030026.
34 L. Zhu, Y. Zheng, J. Fan, Y. Yao, Z. Ahmad and M.-W. Chang, A novel core-shell nanofiber drug delivery system intended for the synergistic treatment of melanoma, *Eur. J. Pharm. Sci.*, 2019, **137**, 105002, DOI: 10.1016/j.ejps.2019.105002.
35 S. Mallick, K. R. B Singh, V. Nayak, J. Singh and R. P. Singh, Potentialities of core@shell nanomaterials for biosensor technologies, *Mater. Lett.*, 2022, **306**, 130912, DOI: 10.1016/j.matlet.2021.130912.
36 D. Khomskii, Classifying multiferroics: mechanisms and effects, *Physics*, 2009, **2**, 20, DOI: 10.1103/physics.2.20.
37 H. Palneedi, V. Annapureddy, S. Priya and J. Ryu, Status and perspectives of multiferroic magnetoelectric composite materials and applications, *Actuators*, 2016, **5**, 9, DOI: 10.3390/act5010009.
38 J. Mundy, C. Brooks, M. Holtz and D. G. Schlom, Atomically engineered ferroic layers yield a room-temperature magnetoelectric multiferroic, *Nature*, 2016, **537**, 523–527, DOI: 10.1038/nature19343.

 

39 Y. Wang, J. Li and D. Viehland, Magnetoelectrics for magnetic sensor applications: status, challenges and perspectives, *Mater. Today*, 2014, **17**, 269–275, DOI: 10.1016/j.mattod.2014.05.004.
40 D. I. Khomskii, Multiferroics: different ways to combine magnetism and ferroelectricity, *J. Magn. Magn. Mater.*, 2006, **306**, 1–8, DOI: 10.1016/j.jmmm.2006.01.238.
41 L. W. Martin, S. P. Crane, Y. H. Chu, M. B. Holcomb, M. Gajek, M. Huijben, C. H. Yang, N. Balke and R. Ramesh, Multiferroics and magnetoelectrics: thin films and nanostructures, *J. Phys.:Condens. Matter*, 2008, **20**, 434220, DOI: 10.1088/0953-8984/20/43/434220.
42 H. Liu and X. Yang, A brief review on perovskite multiferroics, *Ferroelectrics*, 2017, **507**, 69–85, DOI: 10.1080/00150193.2017.1283171.
43 W. Prellier, M. P. Singh and P. Murugavel, The single-phase multiferroic oxides: from bulk to thin film, *J. Phys.:Condens. Matter*, 2005, **17**, R803, DOI: 10.1088/0953-8984/17/30/R01.
44 J. Zhang, W. Xue, T. Su, H. Ji, G. Zhou, F. Jiang, Z. Quan and X. Xu, Nanoscale magnetization reversal by magnetoelectric coupling effect in Ga 0.6 Fe 1.4 O 3 multiferroic thin films, *ACS Appl. Mater. Interfaces*, 2021, **13**, 18194–18201, DOI: 10.1021/acsami.0c21659.
45 M. Niu, H. Zhu, Y. Wang, J. Yan, N. Chen, P. Yan and J. Ouyang, Integration-friendly, chemically stoichiometric BiFeO3 films with a piezoelectric performance challenging that of PZT, *ACS Appl. Mater. Interfaces*, 2020, **12**, 33899–33907, DOI: 10.1021/acsami.0c07155.
46 C. Lu, M. Wu, L. Lin and J. M. Liu, Single-phase multiferroics: new materials, phenomena, and physics, *Natl. Sci. Rev.*, 2019, **6**, 653–668, DOI: 10.1093/nsr/nwz091.
47 H. Schmid, Some symmetry aspects of ferroics and single phase multiferroics, *J. Phys.:Condens. Matter*, 2008, **20**, 434201, DOI: 10.1088/0953-8984/20/43/434201z.
48 Y. Cheng, B. Peng, Z. Hu, Z. Zhou and M. Liu, Recent development and status of magnetoelectric materials and devices, *Phys. Lett.*, 2018, **382**, 3018–3025, DOI: 10.1016/j.physleta.2018.07.014.
49 X. Liang, H. Chen and N. X. Sun, Magnetoelectric materials and devices, *Appl. Mater.*, 2021, **9**, 41114, DOI: 10.1063/5.0044532.
50 A. Jaiswal, I. Chakraborty and K. Roy, Energy-Efficient Memory Using Magneto-Electric Switching of Ferromagnets, *IEEE Magn. Lett.*, 2017, **8**, 4306905, DOI: 10.1109/LMAG.2017.2712685.
51 K. L. Wang, H. Lee and P. K. Amiri, Magnetoelectric Random Access Memory-Based Circuit Design by Using Voltage-Controlled Magnetic Anisotropy in Magnetic Tunnel Junctions, *IEEE Trans. Nanotechnol.*, 2015, **14**, 992–997, DOI: 10.1109/TNANO.2015.2462337.
52 Z. Fang, J. Jiao, H. Wu, T. Jiang, S. Fu, J. Cheng, O. Sokolov, S. Ivanov, M. Bichurin, F. Li and Y. Wang, Crafting very low frequency magnetoelectric antenna *via* piezoelectric and electromechanical synergic optimization strategy, *J. Materiomics*, 2025, **11**(3), 100900, DOI: 10.1016/j.jmat.2024.05.010.
53 T. Nan, H. Lin, Y. Gao, A. Matyushov, G. Yu, H. Chen, N. Sun, S. Wei, Z. Wang, M. Li, X. Wang, A. Belkessam, R. Guo, B. Chen, J. Zhou, Z. Qian, Y. Hui, M. Rinaldi, M. E. McConney, B. M. Howe, Z. Hu, J. G. Jones, G. J. Brown and N. X. Sun, Acoustically actuated ultra-compact NEMS magnetoelectric antennas, *Nat. Commun.*, 2017, **8**, 296, DOI: 10.1038/s41467-017-00343-8.
54 C. Dong, C. Sun, L. Chen, Y. He, Y. Liu, B. Luo and N. X. Sun, Ultra-compact magnetoelectric sensor for femto-Tesla VLF signal reception, *Mater. Today Electron.*, 2025, **11**, 100135, DOI: 10.1016/j.mtelec.2025.100135.
55 X. Hu, L. Zhang, Z. Wang, Y. Xiang, X. Chen and Z. Xue, Wireless driven and self-sensing flexible gripper based on piezoelectric elastomer/high-entropy alloy magnetoelectric composite, *Chem. Eng. J.*, 2024, **498**, 155415, DOI: 10.1016/j.cej.2024.155415.
56 P. Yang, X. Hu, R. Li, Z. Zhou, Y. Gui, R. Sun, D. Wu, X. Wang and X. Bian, Flexible magnetoelectric sensors with enhanced output performance and response time for parking spaces detection systems, *Sens. Actuators, A*, 2025, **382**, 116161, DOI: 10.1016/j.sna.2024.116161.
57 E. Spetzler, B. Spetzler, D. Seidler, J. Arbustini, L. Thormählen, E. Elzenheimer, M. Höft, A. Bahr, D. Meyners and J. McCord, On the Origin of Signal and Bandwidth of Converse Magnetoelectric Magnetic Field Sensors, *Adv. Sens. Res.*, 2025, **4**, 2400109, DOI: 10.1002/adsr.202400109.
58 L. Zimoch, S. Schröder, E. Elzenheimer, S. Kaps, T. Strunskus, F. Faupe, M. Höft and R. Adelung, Electret integrated magnetic field sensor based on magnetostrictive polymer composite with nT resolution, *Sci. Rep.*, 2025, **15**, 1561, DOI: 10.1038/s41598-024-85069-6.
59 Y. Qiu, Q. Zhong, Y. Zhou, J. An, Y. Li, A. Song, J. Wang, G. Yu, M. Zhu, Y. Wu and H. Zhou, A Low Conductivity Medium Detection Module Based on Magnetoelectric Sensors, *IEEE Trans. Instrum. Meas.*, 2025, **4**, 6007509, DOI: 10.1109/TIM.2025.3561443.
60 X. Xu, W. Wu, T. Zhu, M. Pei, X. Zhang and Q. Han, High-performance magnetoelectric composite with low DC bias magnetic field for detecting ultra-weak magnetic field, *Compos. Commun.*, 2025, **56**, 102371, DOI: 10.1016/j.coco.2025.102371.
61 J. Shen, J. Cong, D. Shang, Y. Chai, S. Shen, K. Zhai and Y. Sun, A multilevel nonvolatile magnetoelectric memory, *Sci. Rep.*, 2016, **6**, 34473, DOI: 10.1038/srep34473.
62 N. Rangarajan, S. Patnaik, J. Knechtel, O. Sinanoglu and S. Rakheja, SMART: A Secure Magnetoelectric Antiferromagnet-Based Tamper-Proof Non-Volatile Memory, *IEEE Access*, 2020, **8**, 76130–76142, DOI: 10.1109/ACCESS.2020.2988889.
63 M. Müller, Y. -Lin Huang, S. Vélez, R. Ramesh, M. Fiebig and M. Trassin, Training the Polarization in Integrated La0.15Bi0.85FeO3-Based Devices, *Adv. Mater.*, 2021, **33**, 2104688, DOI: 10.1002/adma.202104688.
64 J. Ma, J. Hu, Z. Li and C.-W. Nan, Recent Progress in Multiferroic Magnetoelectric Composites: from Bulk to

Thin Films, *Adv. Mater.*, 2011, **23**, 1035–1165, DOI: 10.1002/adma.201003636.

65 N. A. Spaldin and R. Ramesh, Advances in magnetoelectric multiferroics, Advances in magnetoelectric multiferroics, *Nat. Mater.*, 2019, **18**, 203–212, DOI: 10.1038/s41563-018-0275-2.

66 C. A. F. Vaz, J. Hoffman, C. H. Ahn and R. Ramesh, Magnetoelectric Coupling Effects in Multiferroic Complex Oxide, *Compos. Struct.*, 2010, **22**, 2900–2918, DOI: 10.1002/adma.200904326.

67 C. -hong Lin and Y. -Chuan Lin, Magnetoelectric coupling in nonlinear three-phase composites: A micromechanical study, *Int. J. Mech. Sci.*, 2025, **299**, 110425, DOI: 10.1016/j.ijmecsci.2025.110425.

68 Y. Li, Z. Wang, J. Yao, T. Yang, Z. Wang, J. Mian Hu, C. Chen, R. Sun, Z. Tian, J. Li, L. Qing Chen and D. Viehland, Magnetoelectric quasi-(0-3) nanocomposite heterostructures, *Nat. Commun.*, 2015, **6**, 6680, DOI: 10.1038/ncomms7680.

69 A. Kumar and D. Kaur, Magnetoelectric heterostructures for next-generation MEMS magnetic field sensing applications, *J. Alloys Compd.*, 2022, **897**, 163091, DOI: 10.1016/j.jallcom.2021.163091.

70 D. K. Pradhan, S. Kumari, R. K. Vasudevan, E. Strelcov, V. S. Puli, D. K. Pradha, A. Kumar, J. M. Gregg, A. K. Pradhan, S. V. Kalinin and R. S. Katiyar, Exploring the Magnetoelectric Coupling at the Composite Interfaces of FE/FM/FE Heterostructures, *Sci. Rep.*, 2018, **8**, 17381, DOI: 10.1038/s41598-018-35648-1.

71 S. Ryu, J. H. Park and H. M. Jang, Magnetoelectric coupling of [00l]-oriented $Pb(Zr_{0.4}Ti_{0.6})O_3$-$Ni_{0.8}Zn_{0.2}Fe_2O_4$ multilayered thin films, *Appl. Phys. Lett.*, 2007, **91**, 142910, DOI: 10.1063/1.2798054.

72 G. -Liang Yu, H. Wu Zhang, F. -Ming Bai, Y. -Xun Li and J. Li, Theoretical investigation of magnetoelectric effect in multilayer magnetoelectric composites, *Compos. Struct.*, 2015, **119**, 738–748, DOI: 10.1016/j.compstruct.2014.09.049.

73 A. C. Lima, N. Pereira, R. Policia, C. Ribeiro, V. Correia, S. Lanceros-Mendez and P. Martins, All-printed multilayer materials with improved magnetoelectric response, *J. Mater. Chem. C*, 2019, **7**, 5394–5400, DOI: 10.1039/C9TC01428D.

74 G. Srinivasan, E. T. Rasmussen, J. Gallegos, R. Srinivasan, Yu. I. Bokhan and V. M. Laletin, Magnetoelectric bilayer and multilayer structures of magnetostrictive and piezoelectric oxides, *Phys. Rev. B:Condens. Matter Mater. Phys.*, 2001, **64**, 2144080, DOI: 10.1103/PhysRevB.64.214408.

75 Y. Wang, J. Xu, Y. Shen, C. -ai Wang, Z. Zhang, F. Li, J. Cheng, Y. Ye and R. Shen, Fabrication of energetic aluminum core/hydrophobic shell nanofibers *via* coaxial electrospinning, *Chem. Eng. J.*, 2022, **427**, 132001, DOI: 10.1016/j.cej.2021.132001.

76 J. Hu, Y. Liu, S. Zhang and B. Tang, Novel designed core–shell nanofibers constituted by single element-doped BaTiO3 for high-energy–density polymer nanocomposites, *Chem. Eng. J.*, 2022, **428**, 131046, DOI: 10.1016/j.cej.2021.131046.

77 A. Almasian, M. Giahi, G. C. Fard, S. A. Dehdast and L. Maleknia, Removal of heavy metal ions by modified PAN/PANI-nylon core-shell nanofibers membrane: Filtration performance, antifouling and regeneration behavior, *Chem. Eng. J.*, 2018, **351**, 1166–1178, DOI: 10.1016/j.cej.2018.06.127.

78 J. Zhang, S. Li, D.-D. Ju, X. Li, J.-C. Zhang, X. Yan, Y.-Z. Long and F. Song, Flexible inorganic core-shell nanofibers endowed with tunable multicolor upconversion fluorescence for simultaneous monitoring dual drug delivery, *Chem. Eng. J.*, 2018, **349**, 554–561, DOI: 10.1016/j.cej.2018.05.112.

79 Y. Liu, G. Sreenivasulu, P. Zhou, J. Fu, D. Filippov, W. Zhang, T. Zhou, T. Zhang, P. Shah, M. R. Page, G. Srinivasan, S. Berweger, T. M. Wallis and P. Kabos, Converse magneto-electric effects in a core–shell multiferroic nanofiber by electric field tuning of ferromagnetic resonance, *Sci. Rep.*, 2020, **10**, 20170, DOI: 10.1038/s41598-020-77041-x.

80 L. F. Henrichs, X. Mu, T. Scherer, U. Gerhards, S. Schuppler, P. Nagel, M. Merz, C. Kübel, M. H. Fawey, T. C. Hansen and H. Hahn, First-time synthesis of a magnetoelectric core–shell composite *via* conventional solid-state reaction, *Nanoscale*, 2020, **12**, 15677, DOI: 10.1039/d0nr02475a.

81 G. Schileo, Recent developments in ceramic multiferroic composites based on core/shell and other heterostructures obtained by sol-gel routes, *Prog. Solid State Chem.*, 2013, **41**, 87–98, DOI: 10.1016/j.progsolidstchem.2013.09.001.

82 V. J. Folen, G. T. Rado and E. W. Stalder, Anisotropy of the Magnetoelectric Effect in $Cr_2O_3$, *Phys. Rev. Lett.*, 1961, **6**, 607, DOI: 10.1103/PhysRevLett.6.607.

83 J. Wang, J. B. Neaton, H. Zheng, V. Nagarajan, S. B. Ogale, B. Liu, D. Viehland, V. Vaithyanathan, D. G. Schlom, U. V. Waghmare, N. A. Spaldin, K. M. Rabe, M. Wuttig and R. Ramesh, Epitaxial BiFeO3 Multiferroic Thin Film Heterostructures, *Science*, 2003, **299**, 1719–1722, DOI: 10.1126/science.1080615.

84 C.-Y. Kuo, Z. Hu, J. C. Yang, S.-C. Liao, Y. L. Huang, R. K. Vasudevan, M. B. Okatan, S. Jesse, S. V. Kalinin, L. Li, H. J. Liu, C.-H. Lai, T. W. Pi, S. Agrestini, K. Chen, P. Ohresser, A. Tanaka, L. H. Tjeng and Y. H. Chu, Single-domain multiferroic $BiFeO_3$ films, *Nat. Commun.*, 2016, **7**, 12712, DOI: 10.1038/ncomms12712.

85 A. M. Kadomtseva, S. S. Krotov, Yu. F. Popov and G. P. Vorob'ev, Features of the magnetoelectric behavior of the family of multiferroics $RMn_2O_5$ at high magnetic fields, *Low Temp. Phys.*, 2006, **32**, 709–724, DOI: 10.1063/1.2219494.

86 B. Kh. Khannanov, V. A. Sanina, E. I. Golovenchits and M. P. Scheglov, Electric polarization induced by phase separation in magnetically ordered and paramagnetic states of $RMn_2O_5$ (R=Gd, Bi), *J. Magn. Magn. Mater.*, 2017, **421**, 326–335, DOI: 10.1016/j.jmmm.2016.08.040.

 

87 T. Kimura, G. Lawes, T. Goto, Y. Tokura and A. P. Ramirez, Magnetoelectric phase diagrams of orthorhombic $RMnO_3$ (R=Gd, Tb, and Dy), *Phys. Rev. B:Condens. Matter Mater. Phys.*, 2005, **71**, 224425, DOI: 10.1103/PhysRevB.71.224425.

88 G. E. Tongue Magne, R. M. Keumo Tsiaze, A. J. Fotué, N. M. Hounkonnou and L. C. Fai, Cumulative effects of fluctuations and magnetoelectric coupling in two-dimensional $RMnO_3$ (R = Tb, Lu and Y) multiferroics, *Phys. Lett. A*, 2021, **400**, 127305, DOI: 10.1016/j.physleta.2021.127305.

89 R. Ramesh, Making metallic memories, *Nat. Nanotechnol.*, 2010, **5**, 761–762, DOI: 10.1038/nnano.2010.218.

90 S. A. Wolf, J. Lu, M. R. Stan, E. Chen and D. M. Treger, The Promise of Nanomagnetics and Spintronics for Future Logic and Universal Memory, *Proc. IEEE*, 2010, **98**, 2155–2168, DOI: 10.1109/JPROC.2010.2064150.

91 J. Atulasimha and S. Bandyopadhyay, Bennett clocking of nanomagnetic logic using multiferroic single-domain nanomagnets, *Appl. Phys. Lett.*, 2010, **97**, 173105, DOI: 10.1063/1.3506690.

92 N. A. Pertsev and H. Kohlstedt, Resistive switching *via* the converse magnetoelectric effect in ferromagnetic multilayers on ferroelectric substrates, *Nanotechnology*, 2010, **21**, 475202, DOI: 10.1088/0957-4484/21/47/475202.

93 C. Nan, M. I. Bichurin, S. Dong, D. Viehland and G. Srinivasan, Multiferroic magnetoelectric composites: Historical perspective, status, and future directions, *J. Appl. Phys.*, 2008, **103**, 031101, DOI: 10.1063/1.2836410.

94 J. Ma, J. Hu, Z. Li and C. Nan, Recent Progress in Multiferroic Magnetoelectric Composites: from Bulk to Thin Films, *Adv. Mater.*, 2011, **23**, 1062–1087, DOI: 10.1002/adma.201003636.

95 Y. F. Popov, A. M. Kadomtseva, G. P. Vorob'ev and A. K. Zvezdin, Discovery of the linear magnetoelectric effect in magnetic ferroelectric $BiFeO_3$ in a strong magnetic field, *Ferroelectrics*, 1994, **162**(1), 135–140, DOI: 10.1080/00150199408245098.

96 W. Eerenstein, N. D. Mathuar and J. F. Scott, Multiferroic and magnetoelectric materials, *Nature*, 2006, **442**, 759–765, DOI: 10.1038/nature05023.

97 S. K. Yadav, P. D. Prasad, A. Soosairaj, K. Divya, A. A. Arunmozhi, L. R. Asirvatham, V. S. Manikandan, M. Navaneethan and A. Thirumurugan, Study on the Structural, Magnetic, and Magnetodielectric Properties of M-type $BaFe_{12}O_{19}$ and $SrFe_{12}O_{19}$ Hexaferrite Nanoparticles, *Surf. Interfaces*, 2024, **52**, 104956, DOI: 10.1016/j.surfin.2024.104956.

98 S. K. Yadav, P. D. Prasad, A. Soosairaj, K. Divya, A. A. Arunmozhi, L. R. Asirvatham, V. S. Manikandan, M. Navaneethan and A. Thirumurugan, Investigation of Magnetocapacitance and Magnetoconductivity in Single-Phase Y-Type Hexaferrite $Ba_2Co_2Fe_{12}O_{22}$ Nanoparticles, *Surf. Interfaces*, 2024, **54**, 105162, DOI: 10.1016/j.surfin.2024.105162.

99 M. I. Bichurin and V. M. Petrov, Theory of low-frequency magnetoelectric coupling in magnetostrictive-piezoelectric bilayers, *Phys. Rev. B:Condens. Matter Mater. Phys.*, 2003, **68**, 054402, DOI: 10.1103/PhysRevB.68.054402.

100 G.-L. Yu, H.-W. Zhang, F.-M. Bai, Y.-X. Li and J. Li, Theoretical investigation of magnetoelectric effect in multilayer magnetoelectric composites, *Compos. Struct.*, 2015, **119**, 738–748, DOI: 10.1016/j.compstruct.2014.09.049.

101 I. A. Osaretin and R. G. Rojas, Theoretical model for the magnetoelectric effect in magnetostrictive/piezoelectric composites, *Phys. Rev. B:Condens. Matter Mater. Phys.*, 2010, **82**, 174415, DOI: 10.1103/PhysRevB.82.174415.

102 Y. Wang, D. Hasanyan, M. Li, J. Gao, J. Li, D. Viehland and H. Luo, Theoretical model for geometry-dependent magnetoelectric effect in magnetostrictive/piezoelectric composites, *J. Appl. Phys.*, 2012, **111**, 124513, DOI: 10.1063/1.4729832.

103 N. Pakam and A. Arockiarajan, An analytical model for predicting the effective properties of magneto-electro-elastic (MEE) composites, *Comput. Mater. Sci.*, 2012, **65**, 19–28, DOI: 10.1016/j.commatsci.2012.07.003.

104 H. Hong, K. Bi and Y. G. Wang, Magnetoelectric performance in Ni/Pb(Zr,Ti)$O_3$/FeCo trilayered cylindrical composites, *J. Alloys Compd.*, 2012, **545**, 182–185, DOI: 10.1016/j.jallcom.2012.08.048.

105 X. H. Ge, H. Ji, Y. Li, J. K. Chen and Y. G. Wang, Diameter and sequence effects on magnetoelectric effect in FeCo/Pb(Zr,Ti)$O_3$/Ni trilayered long cylindrical composite structures, *J. Alloys Compd.*, 2018, **752**, 303–307, DOI: 10.1016/j.jallcom.2018.04.153.

106 H. . Q. Shen, Y. G. Wang, D. Xie and J. H. Cheng, Magnetoelectric effect in FeCo/PMN-PT/FeCo trilayers prepared by electroless deposition of FeCo on PMN-PT crystals with various orientations, *J. Alloys Compd.*, 2014, **610**, 11–14, DOI: 10.1016/j.jallcom.2014.04.221.

107 J. Shi, M. Wu, W. Hu, C. Lu, X. Mu and J. Zhu, A study of high piezomagnetic (Fe-Ga/Fe-Ni) multilayers for magnetoelectric device, *J. Alloys Compd.*, 2019, **806**, 1465–1468, DOI: 10.1016/j.jallcom.2019.07.265.

108 S. U. Jen and Y. C. Chen, Field annealing effect on magnetostriction and sensitivity of the ferromagnetic $Fe_{60}Co_{18}Ga_{22}$/Si(100) film, *J. Magn. Magn. Mater.*, 2018, **466**, 55–59, DOI: 10.1016/j.jmmm.2018.05.092.

109 S. W. Meeks and J. C. Hill, Piezomagnetic and elastic properties of metallic glass alloys $Fe_{67}CO_{18}B_{14}Si_1$ and $Fe_{81}B_{13.5}Si_{3.5}C_2$, *J. Appl. Phys.*, 1983, **54**, 6584–6593, DOI: 10.1063/1.331893.

110 D. A. Petrov, V. S. Leontiev, G. A. Semenov, S. N. Ivanov, O. V. Sokolov, A. I. Kozonov, K. A. Syrovarova, K. V. Semenova and M. I. Bichurin, The study of the Metglas/GaAs/Metglas magnetostrictive-piezo-semiconductive structure for practical application, *J. Phys.: Conf. Ser.*, 2021, **2052**, 012032, DOI: 10.1088/1742-6596/2052/1/012032.

111 T. Deng, Z. Chen, W. Di, B. Fang and H. Luo, Enhancement magnetoelectric effect in Metglas-Fe by annealing, *Appl. Phys. A*, 2021, **127**, 899, DOI: 10.1007/s00339-021-05045-z.

112 D. Davino, A. Giustiniani and C. Visone, The piezomagnetic parameters of Terfenol-D: An experimental viewpoint, *Phys. B*, 2012, **407**, 1427–1432, DOI: 10.1016/j.physb.2011.05.059.

113 C.-hong Lin and Y.-Z. Lin, Analysis of nonlinear piezomagnetism for magnetostrictive terfenol-D composites, *J. Magn. Magn. Mater.*, 2021, **540**, 168490, DOI: 10.1016/j.jmmm.2021.168490.

114 Z. Chen, Y. Su and S. A. Meguid, The effect of field-orientation on the magnetoelectric coupling in Terfenol-D/PZT/Terfenol-D laminated structure, *J. Appl. Phys.*, 2014, **116**, 173910, DOI: 10.1063/1.4901069.

115 G. Jian, F. Xue, C. Zhang, C. Yan, N. Zhao and C. P. Wong, Orientation dependence of elastic and piezomagnetic properties in $NiFe_2O_4$, *J. Magn. Magn Mater.*, 2017, **442**, 141–144, DOI: 10.1016/j.jmmm.2017.06.103.

116 A. Aubert, V. Loyau, F. Mazaleyrat and M. LoBue, Investigation of Piezomagnetism in Nickel Ferrite, *IEEE Sens. J.*, 2023, **23**, 5660–5669, DOI: 10.1109/JSEN.2023.3237910.

117 A. D. Sheikh and V. L. Mathe, Effect of the piezomagnetic $NiFe_2O_4$ phase on the piezoelectric $Pb(Mg_{1/3}Nb_{2/3})_{0.67}Ti_{0.33}O_3$ phase in magnetoelectric composites, *Smart Mater. Struct.*, 2009, **18**, 065014, DOI: 10.1088/0964-1726/18/6/065014.

118 K. V. Siva, S. Sudersan and A. Arockiarajan, Bipolar magnetostriction in $CoFe_2O_4$: Effect of sintering, measurement temperature, and prestress, *J. Appl. Phys.*, 2020, **128**, 103904, DOI: 10.1063/5.0021796.

119 M. V. Reddy, A. Lisfi, S. Pokhare and D. Das, Colossal piezomagnetic response in magnetically pressed $Zr^{+4}$ substituted cobalt ferrites, *Sci. Rep.*, 2017, **7**, 7935, DOI: 10.1038/s41598-017-08160-1.

120 Z. Gubinyi, C. Batur, A. Sayir and F. Dynys, Electrical properties of PZT piezoelectric ceramic at high temperatures, *J. Electroceram.*, 2008, **20**, 95–105, DOI: 10.1007/s10832-007-9364-3.

121 N. Izyumskaya, Y.-I. Alivov, S.-J. Cho, H. Morko, H. Lee and Y. S. Kang, Processing, Structure, Properties, and Applications of PZT Thin Films, *Crit. Rev. Solid State Mater. Sci.*, 2007, **32**, 111–202, DOI: 10.1080/10408430701707347.

122 G. L. Smith, J. S. Pulskamp, L. M. Sanchez, D. M. Potrepka, R. M. Proie, T. G. Ivanov, R. Q. Rudy, W. D. Nothwang, S. S. Bedair, C. D. Meyer and R. G. Polcawich, PZT-Based Piezoelectric MEMS Technology, *J. Am. Ceram. Soc.*, 2012, **95**(6), 1777–1792, DOI: 10.1111/j.1551-2916.2012.05155.x.

123 J.-M. Kiat, Y. Uesu, B. Dkhil, M. Matsuda, C. Malibert and G. Calvarin, Monoclinic structure of unpoled morphotropic high piezoelectric PMN-PT and PZN-PT compounds, *Phys. Rev. B:Condens. Matter Mater. Phys.*, 2002, **65**, 064106, DOI: 10.1103/PhysRevB.65.064106.

124 S. Xu, Y.-W. Yeh, G. Poirier, M. C. McAlpine, R. A. Register and N. Yao, Flexible Piezoelectric PMN–PT Nanowire-Based Nanocomposite and Device, *Nano Lett.*, 2013, **13**(6), 2393–2398, DOI: 10.1021/nl400169t.

125 A. Hall, M. Allahverdi, E. K. Akdogan and A. Safari, Piezoelectric/electrostrictive multimaterial PMN-PT monomorph actuators, *J. Eur. Ceram. Soc.*, 2005, **25**(12), 2991–2997, DOI: 10.1016/j.jeurceramsoc.2005.03.196.

126 T. Kobayashi, M. Ichiki, R. Kondou, K. Nakamura and R. Maeda, Fabrication of piezoelectric microcantilevers using LaNiO3 buffered Pb(Zr,Ti)O3 thin film, *J. Manuf. Syst.*, 2018, **18**, 035007, DOI: 10.1088/0960-1317/18/3/035007.

127 P. W. Jaschin, R. Bhimireddi and K. B. R. Varma, Enhanced Dielectric Properties of $LaNiO_3/BaTiO_3$/PVDF: A Three-Phase Percolative Polymer Nanocrystal Composite, *ACS Appl. Mater. Interfaces*, 2018, **10**(32), 27278–27286, DOI: 10.1021/acsami.8b07786.

128 Y. Wang, H. Cheng, Y. Shi, T. Nishikado and I. Kanno, High performance $LaNiO_3$-buffered, (001)-oriented PZT piezoelectric films integrated on (111) Si, *Appl. Phys. Lett.*, 2022, **121**, 182902, DOI: 10.1063/5.0107526.

129 M. Acosta, N. Novak, V. Rojas, S. Patel, R. Vaish, J. Koruza, G. A. Rossetti, Jr. and J. Rödel, $BaTiO_3$-based piezoelectrics: Fundamentals, current status, and perspectives, *Appl. Phys. Rev.*, 2017, **4**, 041305, DOI: 10.1063/1.4990046.

130 D. Ghosh, A. Sakata, J. Carter, P. A. Thomas, H. Han, J. C. Nino and J. L. Jones, Domain Wall Displacement is the Origin of Superior Permittivity and Piezoelectricity in $BaTiO_3$ at Intermediate Grain Sizes, *Adv. Funct. Mater.*, 2014, **24**(7), 885–896, DOI: 10.1002/adfm.201301913.

131 A. Iqbal and F. M. -Yasin, Reactive Sputtering of Aluminum Nitride (002) Thin Films for Piezoelectric Applications: A Review, *Sensors*, 2018, **18**(6), 1797, DOI: 10.3390/s18061797.

132 C. M. Lueng, H. L. W. Chan, C. Surya and C. L. Choy, Piezoelectric coefficient of aluminum nitride and gallium nitride, *J. Appl. Phys.*, 2000, **88**, 5360–5363, DOI: 10.1063/1.1317244.

133 S. T. Haider, M. A. Shah, D.-G. Lee and S. Hur, A Review of the Recent Applications of Aluminum Nitride-Based Piezoelectric Devices, *IEEE Access*, 2023, **11**, 58779–58795, DOI: 10.1109/ACCESS.2023.3276716.

134 S. Mohammadpourfazeli, S. Arash, A. Ansari, S. Yang, K. Mallick and R. Bagherzadeh, Future prospects and recent developments of polyvinylidene fluoride (PVDF) piezoelectric polymer; fabrication methods, structure, and electro-mechanical properties, *RSC Adv.*, 2023, **13**, 370–387, DOI: 10.1039/D2RA06774A.

135 Z. Feng, Z. Zhao, Y. Liu, Y. Liu, X. Cao, D.-G. Yu and K. Wang, Piezoelectric Effect Polyvinylidene Fluoride (PVDF): From Energy Harvester to Smart Skin and Electronic Textiles, *Adv. Mater. Technol.*, 2023, **8**(11), 2300021, DOI: 10.1002/admt.202300021.

136 Y. Fu, E. C Harvey, M. K Ghantasala and G. M. Spinks, Design, fabrication and testing of piezoelectric polymer PVDF microactuators, *Smart Mater. Struct.*, 2006, **15**, S141, DOI: 10.1088/0964-1726/15/1/023.

137 D. P. Pabba, N. Ram, J. Kaarthik, V. R. Bhaviripudi, S. K. Yadav, A. Soosairaj, N. K. Pabba, V. Annapureddy, A. Thirumurugan, H. S. Panda and R. Aepuru, assessing mechanical and stray magnetic field energy harvesting

 

capabilities in lead-free PVDF/BCT-BZT composites integrated with Metglas, *Ceram. Int.*, 2024, **50**, 33009–33017, DOI: 10.1016/j.ceramint.2024.06.115.

138 D. Viehland, M. Wuttig, J. McCord and E. Quandt, Magnetoelectric magnetic field sensors, *MRS Bull.*, 2018, **43**, 834–840, DOI: 10.1557/mrs.2018.261.

139 D. Saveliev, D. Chashin, L. Fetisov, M. Shamonin and Y. Fetisov, Ceramic-Heterostructure-Based Magnetoelectric Voltage Transformer with an Adjustable Transformation Ratio, *Materials*, 2020, **13**(18), 3981, DOI: 10.3390/ma13183981.

140 F. Narita and M. Fox, A Review on Piezoelectric, Magnetostrictive, and Magnetoelectric Materials and Device Technologies for Energy Harvesting Applications, *Adv. Eng. Mater.*, 2018, **20**(5), 1700743, DOI: 10.1002/adem.201700743.

141 S. Dong, J. Zhai, Z. Xing, J.-F. Li and D. Viehland, Extremely low frequency response of magnetoelectric multilayer composites, *Appl. Phys. Lett.*, 2005, **86**, 102901–102905, DOI: 10.1063/1.1881784.

142 J. Zhai, Z. Xing, S. Dong, J. Li and D. Viehland, Detection of pico Tesla magnetic fields using magneto electric sensors at room temperature, *Appl. Phys. Lett.*, 2006, **88**, 062510–062520, DOI: 10.1063/1.2172706.

143 M. Li, A. Matyushov, C. Dong, H. Chen, H. Lin, T. Nan, Z. Qian, M. Rinaldi, Y. Lin and N. X. Sun, Ultra-sensitive NEMS magnetoelectric sensor for picotesla DC magnetic field detection, *Appl. Phys. Lett.*, 2017, **110**, 143510, DOI: 10.1063/1.4979694.

144 D. T. H. Giang and N. H. Duc, Magnetoelectric sensor for microtesla magnetic fields based on $(Fe_{80}Co_{20})_{78}Si_{12}B_{10}$/PZT laminates, *Sens. Actuators, A*, 2009, **149**, 229–232, DOI: 10.1016/j.sna.2008.12.003.

145 Z. Chu, C. Dong, C. Tu, X. Liang, H. Chen, C. Sun, Z. Yu, S. Dong and N.-X. Sun, A low power and high sensitivity magnetic field sensor based on converse magnetoelectric effect, *Appl. Phys. Lett.*, 2019, **115**, 162901–162910, DOI: 10.1063/1.5122774.

146 R. Carvalho, S. Lanceros-Mendez and P. Martins, Tailoring polymer-based magnetoelectrics for spintronics: Evaluating the converse effect, *Appl. Mater. Today*, 2024, **38**, 102216, DOI: 10.1016/j.apmt.2024.102216.

147 Y.-M. Jia, F.-F. Wang, X.-Y. Zhao, H.-S. Luo, S. W. Or and H. L. W. Chan, Converse magnetoelectric effects in piezoelectric–piezomagnetic layered composites, *Compos. Sci. Technol.*, 2008, **68**(6), 1440–1444, DOI: 10.1016/j.compscitech.2007.10.046.

148 G. Srinivasan and Y. K. Fetisov, Microwave Magnetoelectric Effects and Signal Processing Devices, *Integr. Ferroelectr.*, 2006, **83**, 89–98, DOI: 10.1080/10584580600949105.

149 W. Kleemann, Multiferroic and magnetoelectric nanocomposites for data processing, *J. Phys. D:Appl. Phys.*, 2017, **50**(9), 223001, DOI: 10.1088/1361-6463/aa6c04.

150 W. Yinan, E. Song, Y. Wang, D. Su, X. Guo and Z. Ma, Dual-drive DC magnetic sensor based on converse magnetoelectric coupling effect, *J. Appl. Phys.*, 2025, **137**, 124505, DOI: 10.1063/5.0260874.

151 Y. Chen, T. Fitchorov, A. L. Geiler, J. Gao, C. Vittoria and V. G. Harris, Dynamic response of converse magnetoelectric effect in a PMN-PT-based multiferroic heterostructure, *Appl. Phys. A*, 2010, **100**, 1149–1155, DOI: 10.1007/s00339-010-5726-9.

152 Y. Jia, S. W. Or, H. L. W. Chan, X. Zhao and H. Luo, Converse magnetoelectric effect in laminated composites of PMN–PT single crystal and Terfenol-D alloy, *Appl. Phys. Lett.*, 2006, **88**, 242902, DOI: 10.1063/1.2212054.

153 S. Wongprasod, N. Tanapongpisit, P. Laohana, T. M. Huyen Nguyen, H. Q. Van, S. Kim, S. Srikam, S. Sonsupap, N. Chanlek, M. Horprathum, A. Khamkongkaeo, S. Maensiri, W. Meevasana, C. Wung Bark and W. Saenrang, Porous Electrospun Carbon Nanofibers Bearing TiO2 Hollow Nanospheres for Supercapacitor Electrodes, *ACS Appl. Nano Mater.*, 2024, **7**(6), 6712–6721, DOI: 10.1021/acsanm.4c00922.

154 A. Mamun, M. Kiari and L. Sabantina, Recent Review of Electrospun Porous Carbon Nanofiber Mats for Energy Storage and Generation Applications, *Membranes*, 2023, **13**(10), 830, DOI: 10.3390/membranes13100830.

155 S. Shin, Y. Yoon, S. Park and M. W. Shin, Fabrication of core-shell structured cobalt nanoparticle/carbon nanofiber as a bifunctional catalyst for the oxygen reduction/evolution reactions, *J. Alloys Compd.*, 2023, **939**, 168731, DOI: 10.1016/j.jallcom.2023.168731.

156 J. Bai, D. Zhou, X. Zhu, N. Wang, R. Chen and B. Wang, New SOFC cathode: 3D Core–Shell-Structured La0.6Sr0.4Co0.2Fe0.8O3−δ@PrO2−δ Nanofibers Prepared by Coaxial Electrospinning, *ACS Appl. Energy Mater.*, 2022, **5**(9), 11178–11190, DOI: 10.1021/acsaem.2c01782.

157 M. Ghazalian, S. Afshar, A. Rostami, S. Rashedi and S. H. Bahrami, Fabrication and characterization of chitosan-polycaprolactone core-shell nanofibers containing tetracycline hydrochloride, *Colloids Surf., A*, 2022, **636**, 128163, DOI: 10.1016/j.colsurfa.2021.128163.

158 S. Rashedi, S. Afshar, A. Rostami, M. Ghazalian and H. Nazockdast, Co-electrospun poly(lactic acid)/gelatin nanofibrous scaffold prepared by a new solvent system: morphological, mechanical and *in vitro* degradability properties, *Int. J. Polym. Mater. Polym. Biomater.*, 2021, **70**(8), 545–553, DOI: 10.1080/00914037.2020.1740987.

159 E. Hajiani, S. Osfouri, R. Azin, S. Zaeri and A. Rostami, Sustained release of phenytoin from jellyfish collagen-based electrospun nanofibers: A wound dressing candidate with promising cell compatibility, *J. Drug Delivery Sci. Technol.*, 2025, **112**, 107183, DOI: 10.1016/j.jddst.2025.107183.

160 R. Ge, Y. Ji, Y. Ding, C. Huang, H. He and D.-G. Yu, Electrospun self-emulsifying core-shell nanofibers for effective delivery of paclitaxel, *Front. Bioeng. Biotechnol.*, 2023, **11**, DOI: 10.3389/fbioe.2023.1112338.

161 Y. Li, Du Jia, X. Sun, D. Lan, J. Cui, Hu Zhao, Y. Zhang and W. He, Preparation of TiO2/nitrogen-doped CNF composites as high-performance lithium-ion battery anodes by electrospinning, *J. Cryst. Growth*, 2023, **624**, 127417, DOI: 10.1016/j.jcrysgro.2023.127417.

162 A. Greiner and J. H. Wendorff, Electrospinning: A Fascinating Method for the Preparation of Ultrathin Fibers, *Angew. Chem., Int. Ed.*, 2007, **46**(30), 5670–5703, DOI: 10.1002/anie.200604646.

163 N. R. Tanha and M. Nouri, Core-shell Nanofibers of Silk Fibroin/Polycaprolactone-Clindamycin: Study on Nanofibers Structure and Controlled Release Behavior, *Polym. Sci., Ser. A*, 2019, **61**, 85–95, DOI: 10.1134/S0965545X19010085.

164 C. Jiang, J. Nie and G. Ma, A polymer/metal core–shell nanofiber membrane by electrospinning with an electric field, and its application for catalyst support, *RSC Adv.*, 2016, **6**, 22996, DOI: 10.1039/c5ra27687j.

165 P. Moradipour, M. Limoee, S. Janfaza and L. Behbood, Core-Shell Nanofibers Based on Polycaprolactone/Polyvinyl Alcohol and Polycaprolactone/Collagen for Biomedical Applications, *J. Pharm. Innovation*, 2022, **17**, 911–920, DOI: 10.1007/s12247-021-09568-z.

166 Y. Liu, P. Zhou, B. Ge, J. Liu, J. Zhang, W. Zhang, T. Zhang and G. Srinivasan, Strain-Mediated Magneto-Electric Effects in Coaxial Nanofibers of Y/W-Type Hexagonal Ferrites and Ferroelectrics, *J. Compos. Sci.*, 2021, **5**, 268, DOI: 10.3390/jcs5100268.

167 M. Abasalta, A. Asefnejad, M. T. Khorasani, A. R. Saadatabadi and M. Irani, Adsorption and sustained release of doxorubicin from N-carboxymethyl chitosan/polyvinyl alcohol/poly(ε-caprolactone) composite and core-shell nanofibers, *J. Drug Delivery Sci. Technol.*, 2022, **67**, 102937, DOI: 10.1016/j.jddst.2021.102937.

168 E. Korina, O. Stoilova, N. Manolova and I. Rashkov, Polymer fibers with magnetic core decorated with titanium dioxide prospective for photocatalytic water treatment, *J. Environ. Chem. Eng.*, 2018, **6**(2), 2075–2084, DOI: 10.1016/j.jece.2018.03.016.

169 J. K. Park, O.-V. P. -Nguyen and H. S. Yoo, Coaxial Electrospun Nanofibers with Different Shell Contents to Control Cell Adhesion and Viability, *ACS Omega*, 2020, **5**(43), 28178–28185, DOI: 10.1021/acsomega.0c03902.

170 M. Zhang, C. Liu, B. Li, Y. Shen, H. Wang, K. Ji, X. Mao, L. Wei, R. Sun and F. Zhou, Electrospun PVDF-based piezoelectric nanofibers: materials, structures, and applications, *Nanoscale Adv.*, 2023, **5**, 1043–1059, DOI: 10.1039/D2NA00773H.

171 R. Singh, F. Ahmed, P. Polley and J. Giri, Fabrication and Characterization of Core–Shell Nanofibers Using a Next-Generation Airbrush for Biomedical Applications, *ACS Appl. Mater. Interfaces*, 2018, **10**(49), 41924–41934, DOI: 10.1021/acsami.8b13809.

172 M.-R. Norouzi, L. G. Mobarakeh, F. Itel, J. Schoeller, H. Fashandi, A. Borzi, A. Neels, G. Fortunato and R. M. Rossi, Emulsion electrospinning of sodium alginate/poly(ε-caprolactone) core/shell nanofibers for biomedical applications, *Nanoscale Adv.*, 2022, **4**, 2929–2941, DOI: 10.1039/D2NA00201A.

173 M. Naeimirad, A. Zadhoush, R. Kotek, R. E. Neisiany, S. N. Khorasani and S. Ramakrishna, Recent advances in core/shell bicomponent fibers and nanofibers: A review, *J. Appl. Polym. Sci.*, 2018, **135**, 46265, DOI: 10.1002/app.46265.

174 K. Jalaja, D. Naskar, S. C. Kundu and N. R. James, Potential of electrospun core–shell structured gelatin–chitosan nanofibers for biomedical applications, *Carbohydr. Polym.*, 2016, **136**, 1098–1107, DOI: 10.1016/j.carbpol.2015.10.014.

175 A. L. Yarin, Coaxial electrospinning and emulsion electrospinning of core–shell fibers, *Polym. Adv. Technol.*, 2011, **22**, 310–317, DOI: 10.1002/pat.1781.

176 B. Abadi, N. Goshtasbi, S. Bolouria, J. Tahsili, M. A. -Sardou and H. Forootanfar, Electrospun hybrid nanofibers: Fabrication, characterization, and biomedical applications, *Front. Bioeng. Biotechnol.*, 2022, **10**, DOI: 10.3389/fbioe.2022.986975.

177 B. Rezaei, M. Ghani, M. Askari, A. M. Shoushtari and R. M. A. Malek, Fabrication of Thermal Intelligent Core/Shell Nanofibers by the Solution Coaxial Electrospinning Process, *Adv. Polym. Technol.*, 2015, DOI: 10.1002/adv.21534.

178 S. N. Reznik, A. L. Yarin, E. Zussman and L. Bercovici, Evolution of a compound droplet attached to a core-shell nozzle under the action of a strong electric field, *Phys. Fluids*, 2006, **18**, 062101, DOI: 10.1063/1.2206747.

179 A. K. Moghe and B. S. Gupta, Co-axial Electrospinning for Nanofiber Structures: Preparation and Applications, *Polym. Rev.*, 2008, **48**, 353–377, DOI: 10.1080/15583720802022257.

180 N. E. Zander, Hierarchically Structured Electrospun Fibers, *Polymers*, 2013, **5**(1), 19–44, DOI: 10.3390/polym5010019.

181 D. Han and A. J. Steckl, Coaxial Electrospinning Formation of Complex Polymer Fibers and their Applications, *ChemPlusChem*, 2019, **84**(10), 1453–1497, DOI: 10.1002/cplu.201900281.

182 N. R. Tanha and M. Nouri, An experimental study on the coaxial electrospinning of silk fibroin/poly(vinyl alcohol)–salicylic acid core-shell nanofibers and process optimization using response surface methodology, *J. Ind. Textil.*, 2017, **48**(5), 884–903, DOI: 10.1177/1528083717747334.

183 A. S. Motamedi, H. Mirzadeh, F. Hajiesmaeilbaigi, S. B. Khoulenjani and M. Al. Shokrgozar, Effect of electrospinning parameters on morphological properties of PVDF nanofibrous scaffolds, *Prog. Biomater.*, 2017, **6**, 113–123, DOI: 10.1007/s40204-017-0071-0.

184 M. Kashif, S. Rasul, M. M. Mohideen and Y. Liu, Advancing Electrochemical Energy Storage: A Review of Electrospinning Factors and Their Impact, *Energies*, 2025, **18**(9), 2399, DOI: 10.3390/en18092399.

185 C. Li, Q. Li, X. Ni, G. Liu, W. Cheng and G. Han, Coaxial Electrospinning and Characterization of Core-Shell Structured Cellulose Nanocrystal Reinforced PMMA/PAN Composite Fibers, *Materials*, 2017, **10**(6), 572, DOI: 10.3390/ma10060572.

186 G. I. Taylor, Electrically driven jets, *Proc. A*, 1969, **313**(1515), 453–475, DOI: 10.1098/rspa.1969.0205.

 

187 W. E. Teo and S. Ramakrishna, A review on electrospinning design and nanofibre assemblies, *Nanotechnology*, 2006, **17**, R89, DOI: 10.1088/0957-4484/17/14/R01.
188 P. Koushki, S. H. Bahrami and M. R. Mohammadi, Coaxial nanofibers from poly(caprolactone)/poly(vinyl alcohol)/Thyme and their antibacterial properties, *J. Ind. Textil.*, 2016, **47**(5), 834–852, DOI: 10.1177/1528083716674906.
189 J. Hu, S. Zhang and B. Tang, Rational design of nanomaterials for high energy density dielectric capacitors *via* electrospinning, *Energy Storage Mater.*, 2021, **37**, 530–555, DOI: 10.1016/j.ensm.2021.02.035.
190 H. Fong, I. Chun and D. H. Reneker, Beaded nanofibers formed during electrospinning, *Polymer*, 1999, **40**, 4585–4592, DOI: 10.1016/S0032-3861(99)00068-3.
191 O. O. Dosunmu, G. G. Chase, W. Kataphinan and D. H. Reneker, Electrospinning of polymer nanofibres from multiple jets on a porous tubular surface, *Nanotechnology*, 2006, **17**, 1123, DOI: 10.1088/0957-4484/17/4/046.
192 T. Subbiah, G. S. Bhat, R. W. Tock, S. Parameswaran and S. S. Ramkumar, Electrospinning of nanofibers, *J. Appl. Polym. Sci.*, 2005, **96**(2), 557–569, DOI: 10.1002/app.21481.
193 Z.-M. Huang, Y.-Z. Zhang, M. Kotaki and S. Ramakrishna, A review on polymer nanofibers by electrospinning and their applications in nanocomposites, *Compos. Sci. Technol.*, 2003, **63**(15), 2223–2253, DOI: 10.1016/S0266-3538(03)00178-7.
194 D. H. Reneker and A. L. Yarin, Electrospinning jets and polymer nanofibers, *Polymer*, 2008, **49**(10), 2387–2425, DOI: 10.1016/j.polymer.2008.02.002.
195 D. Li and Y. Xia, Electrospinning of Nanofibers: Reinventing the Wheel?, *Adv. Mater.*, 2004, **16**(14), 1151–1170, DOI: 10.1002/adma.200400719.
196 W. E. Teo, M. Kotaki, X. M. Mo and S. Ramakrishna, Porous tubular structures with controlled fibre orientation using a modified electrospinning method, *Nanotechnology*, 2005, **16**, 918, DOI: 10.1088/0957-4484/16/6/049.
197 A. Khalf and S. V. Madihally, Recent advances in multiaxial electrospinning for drug delivery, *Eur. J. Pharm. Biopharm.*, 2017, **112**, 1–17, DOI: 10.1016/j.ejpb.2016.11.010.
198 A. Mickova, M. Buzgo, O. Benada, M. Rampichova, Z. Fisar, E. Filova, M. Tesarova, D. Lukas and E. Amler, Core/Shell Nanofibers with Embedded Liposomes as a Drug Delivery System, *Biomacromolecules*, 2012, **13**(4), 952–962, DOI: 10.1021/bm2018118.
199 Y. Lu, J. Huang, G. Yu, R. Cardenas, S. Wei, E. K. Wujcik and Z. Guo, Coaxial electrospun fibers: applications in drug delivery and tissue engineering, *Wiley Interdiscip. Rev.:Nanomed. Nanobiotechnol.*, 2016, **8**, 654–677, DOI: 10.1002/wnan.1391.
200 M. Liu, X. Hao, Y. Wang, Z. Jiang and H. Zhang, A biodegradable core-sheath nanofibrous 3D hierarchy prepared by emulsion electrospinning for sustained drug release, *J. Mater. Sci.*, 2020, **55**, 16730–16743, DOI: 10.1007/s10853-020-05205-1.
201 X. Xu, X. Zhuang, X. Chen, X. Wang, L. Yang and X. Jing, Preparation of Core-Sheath Composite Nanofibers by Emulsion Electrospinning, *Macromol. Rapid Commun.*, 2006, **27**(19), 1637–1642, DOI: 10.1002/marc.200600384.
202 G. F. Elfawal, A. O. Šišková and A. E. Andicsová, Electrospinning: A Game-Changer in Fiber Production and Practical Applications, *Fibers Polym.*, 2025, **26**, 4133–4160, DOI: 10.1007/s12221-025-01105-w.
203 N. Nikmarama, S. Roohinejad, S. Hashemic, M. Koubaa, F. J. Barba, A. Abbaspourrad and R. Greiner, Emulsion-based systems for fabrication of electrospun nanofibers: food, pharmaceutical and biomedical applications, *RSC Adv.*, 2017, **7**, 28951–28964, DOI: 10.1039/C7RA00179G.
204 C. Zhang, F. Feng and H. Zhang, Emulsion electrospinning: Fundamentals, food applications and prospects, *Trends Food Sci. Technol.*, 2018, **80**, 175–186, DOI: 10.1016/j.tifs.2018.08.005.
205 H. Cheng, X. Yang, X. Che, M. Yang and G. Zhai, Biomedical application and controlled drug release of electrospun fibrous materials, *Mater. Sci. Eng., C*, 2018, **90**, 750–763, DOI: 10.1016/j.msec.2018.05.007.
206 M. F. Abdullah, T. Nuge, A. Andriyana, B. C. Ang and F. Muhamad, Core–Shell Fibers: Design, Roles, and Controllable Release Strategies in Tissue Engineering and Drug Delivery, *Polymers*, 2019, **11**(12), 2008, DOI: 10.3390/polym11122008.
207 Y. Wang, D. -Guang Yu, Y. Liu and Y. -Nan Liu, Progress of Electrospun Nanofibrous Carriers for Modifications to Drug Release Profiles, *J. Funct. Biomater.*, 2022, **13**(4), 289, DOI: 10.3390/jfb13040289.
208 Š. Zupančič, Core-shell nanofibers as drug delivery systems, *Acta Pharm.*, 2019, **69**, 131–153, DOI: 10.2478/acph-2019-0014.
209 S. Ghosh, A. K. Yadav, P. M. Gurave and R. K. Srivastava, Unique Fiber Morphologies from Emulsion Electrospinning—A Case Study of Poly(ε-caprolactone) and Its Applications, *Colloids Interfaces*, 2023, **7**(1), 19, DOI: 10.3390/colloids7010019.
210 Y. Cho, J. W. Baek, M. Sagong, S. l. Ahn and J. S. Nam, Il-Doo Kim, Electrospinning and Nanofiber Technology: Fundamentals, Innovations, and Applications, *Adv. Mater.*, 2025, **37**(28), 2500162, DOI: 10.1002/adma.202500162.
211 J. Hu, M. P. Prabhakaran, X. Ding and S. Ramalrishna, Emulsion electrospinning of polycaprolactone: influence of surfactant type towards the scaffold properties, *J. Biomater. Sci., Polym.*, 2015, **26**, 57–75, DOI: 10.1080/09205063.2014.982241.
212 D. Liu, Q. Shi, S. Jin, Y. Shao and J. Huang, Self-assembled core-shell structured organic nanofibers fabricated by single-nozzle electrospinning for highly sensitive ammonia sensors, *InfoMat*, 2019, **1**, 525–532, DOI: 10.1002/inf2.12036.
213 S. Sanwaria, S. Singh, A. Horechyy, P. Formanek, M. Stamm, R. Srivastavaa and B. Nandan, Multifunctional core–shell polymer–inorganic hybrid nanofibers prepared *via* block copolymer self-assembly, *RSC Adv.*, 2015, **5**, 89861, DOI: 10.1039/c5ra17161j.

214 T. Khudiyev, O. Tobail and M. Bayindir, Tailoring self-organized nanostructured morphologies in kilometer-long polymer fiber, *Sci. Rep.*, 2014, **4**, 4864, DOI: 10.1038/srep04864.

215 S. Saha, S. Acharya, Y. Liu, P. Zhou, M. R. Page and G. Srinivasan, Review of Magnetoelectric Effects on Coaxial Fibers of Ferrites and Ferroelectrics, *Appl. Sci.*, 2025, **15**, 5162, DOI: 10.3390/app15095162.

216 S. Xie, F. Ma, Y. Liu and J. Li, Multiferroic $CoFe_2O_4$–$Pb(Zr_{0.52}Ti_{0.48})O_3$ core-shell nanofibers and their magnetoelectric coupling, *Nanoscale*, 2011, **3**, 3152, DOI: 10.1039/C1NR10288E.

217 G. Sreenivasulu, J. Zhang, R. Zhang, M. Popov, V. Petrov and G. Srinivasan, Multiferroic Core-Shell Nanofibers, Assembly in a Magnetic Field, and Studies on Magneto-Electric Interactions, *Materials*, 2018, **11**, 18, DOI: 10.3390/ma11010018.

218 V. M. Petrov, J. Zhang, H. Qu, P. Zhou, T. Zhang and G. Srinivasan, Theory of magnetoelectric effects in multiferroic core–shell nanofibers of hexagonal ferrites and ferroelectrics, *J. Phys. D: Appl. Phys.*, 2018, **51**, 284004, DOI: 10.1088/1361-6463/aac56f.

219 Y. Liu, G. Sreenivasulu, P. Zhou, J. Fu, D. Filippov, W. Zhang, T. Zhou, T. Zhang, P. Shah, M. R. Page, G. Srinivasan, S. Berweger, T. M. Wallis and P. Kabos, Converse magneto-electric effects in a core–shell multiferroic nanofiber by electric field tuning of ferromagnetic resonance, *Sci. Rep.*, 2020, **10**, 20170, DOI: 10.1038/s41598-020-77041-x.

220 K. Shahzad, M. A. Abbasi, M. H. Rafe, A. Pestereva, F. Ullah, M. Zaman, M. Irfan, M. Afzal and A. Orlova, Doxorubicin-loaded core@shell cobalt ferrite-barium titanate magnetoelectric nanofibers for improved anticancer activity, *Biomed. Mater.*, 2025, **20**, 015021, DOI: 10.1088/1748-605X/ad971e.

221 B. Ge, J. Zhang, S. Saha, S. Acharya, C. Kshirsagar, S. Menon, M. Jain, M. R. Page and G. Srinivasan, Evidence for a Giant Magneto-Electric Coupling in Bulk Composites with Coaxial Fibers of Nickel–Zinc Ferrite and PZT, *J. Compos. Sci.*, 2024, **8**, 309, DOI: 10.3390/jcs8080309.

222 S. K. Yadav and J. Hemalatha, Electrospinning, and characterization of magnetoelectric $NdFeO_3$–$PbZr_{0.52}Ti_{0.48}O_3$ Core–Shell nanofibers, *Ceram. Int.*, 2022, **48**, 18415–18424, DOI: 10.1016/j.ceramint.2022.03.110.

223 S. K. Yadav and J. Hemalatha, Direct magnetoelectric and magnetodielectric studies of electrospun $Ba_2Ni_2Fe_{12}O_{22}$–$Pb(Zr_{0.52}Ti_{0.48})O_3$ core–shell nanofibers, *J. Magn. Magn. Mater.*, 2022, **564**, 170174, DOI: 10.1016/j.jmmm.2022.170174.

224 Y. Hadouch, D. Mezzane, M. Amjoud, V. Laguta, K. Hoummada, V. O. Dolocan, M. Jouiad, M. Lahcini, H. Uršič, V. Fišinger, N. Novak, Z. Kutnjak, Y. Gagou, I. Lukyanchuk and M. E. Marssi, Multiferroic $CoFe_2O_4$–$Ba_{0.95}Ca_{0.05}Ti_{0.89}Sn_{0.11}O_3$ Core–Shell Nanofibers for Magnetic Field Sensor Applications, *ACS Appl. Nano Mater.*, 2023, **12**(6), 10236–10245, DOI: 10.1021/acsanm.3c01101.

225 S. K. Yadav and J. Hemalatha, Synthesis and characterization of magnetoelectric $Ba_2Zn_2Fe_{12}O_{22}$–$PbZr_{0.52}Ti_{0.48}O_3$ electrospun core–shell nanofibers for the AC/DC magnetic field sensor application, *Appl. Phys. A*, 2024, **130**, 67, DOI: 10.1007/s00339-023-07158-z.

226 B. Iskandarani, N. R. Mojarrad, A. Yürüm, S. A. Gürsel and B. Y. Kaplan, Electrospun Nanofiber Electrodes for Boosted Performance and Durability at Lower Humidity Operation of PEM Fuel Cells, *Energy Fuels*, 2022, **36**, 9282–9294, DOI: 10.1021/acs.energyfuels.2c01595.

227 S. Kabir, T. V. Cleve, S. K. Khandavalli, S. Medina, S. Pylypenko, S. Mauger, M. Ulsh and K. C. Neyerlin, Toward Optimizing Electrospun Nanofiber Fuel Cell Catalyst Layers: Microstructure and Pt Accessibility, *ACS Appl. Energy Mater.*, 2021, **4**, 3341–3351, DOI: 10.1021/acsaem.0c03073.

228 S. K. Khandavalli, N. S.- Nene, S. Kabir, S. Sur, J. P. Rothstein, K. C. Neyerlin, S. A. Mauger and M. Ulsh, Toward Optimizing Electrospun Nanofiber Fuel Cell Catalyst Layers: Polymer−Particle Interactions and Spinnability, *ACS Appl. Polym. Mater.*, 2021, **3**, 2374–2384, DOI: 10.1021/acsapm.0c01354.

229 N. Liu, S. Bi, Y. Zhang, Y. Ou, C. Gong, J. Ran, Y. Chen and Y. Yang, Nanofiber-based polymer electrolyte membranes for fuel cells, *Carbon Energy*, 2025, **7**(7), e677, DOI: 10.1002/cey2.677.

230 V. Kallina, F. Hasché and M. Oezaslan, Advanced design of electrospun nanofiber cathode catalyst layers for PEM fuel cells at low humidity, *Curr. Opin. Electrochem.*, 2024, **47**, 101559, DOI: 10.1016/j.coelec.2024.101559.

231 W. Li, Y. Bai, F. Li, C. Liu, K. -Yu Chan, X. Feng and X. Lu, Core–shell TiO2/C nanofibers as supports for electrocatalytic and synergistic photo electrocatalytic oxidation of methanol, *J. Mater. Chem.*, 2012, **22**, 4025, DOI: 10.1039/c2jm14847a.

232 B. Singh and E. Dempsey, Exceptional Pt nanoparticle decoration of functionalised carbon nanofibers: a strategy to improve the utility of Pt and support material for direct methanol fuel cell applications, *RSC Adv.*, 2013, **3**, 2279, DOI: 10.1039/c2ra21862c.

233 M. Karuppannan, Y. Kim, S. Gok, E. Lee, J. Y. Hwang, J.-H. Jang, Y.-H. Cho, T. Lim, Y.-E. Sung and O. J. Kwon, A highly durable carbon-nanofiber-supported Pt–C core–shell cathode catalyst for ultra-low Pt loading proton exchange membrane fuel cells: facile carbon encapsulation, *Energy Environ. Sci.*, 2019, **12**, 2820, DOI: 10.1039/c9ee01000a.

234 N. Senthilkumar, G. G. kumar and A. Manthiram, 3D Hierarchical Core–Shell Nanostructured Arrays on Carbon Fibers as Catalysts for Direct Urea Fuel Cells, *Adv. Energy Mater.*, 2018, **8**(8), 1702207, DOI: 10.1002/aenm.201702207.

235 H. F. Lee, P. Chin Wang and Y. W. C.- Yang, An electrospun hygroscopic and electron-conductive core-shell silica@carbon nanofiber for microporous layer in proton-

 

exchange membrane fuel cell, *J. Solid State Electrochem.*, 2019, **23**, 971–984, DOI: 10.1007/s10008-019-04198-5.

236 Y. Choi, H. Jin Cho, J. Kim, J.-Y. Kang, J. Seo, J. H. Kim, S. J. Jeong, D.-K. Lim, Il-doo Kim and W. Jung, Nanofiber Composites as Highly Active and Robust Anodes for Direct-Hydrocarbon Solid Oxide Fuel Cells, *ACS Nano*, 2022, **16**, 14517–14526, DOI: 10.1021/acsnano.2c04927.

237 J. Yang, J. Wang, L. Fu, K. Wu, Z. Liu, K. Wu and J. Zhou, Electrospun Core−Shell Fibers for High-Efficient Composite Cathode-Based Solid Oxide Fuel Cells, *Energy Fuels*, 2021, **35**, 1768–1778, DOI: 10.1021/acs.energyfuels.0c02953.

238 D. Lee, S. Gok, Y. Kim, Y.-E. Sung, E. Lee, J.-H. Jang, J. Y. Hwang, O. J. Kwon and T. Lim, Methanol Tolerant Pt−C Core−Shell Cathode Catalyst for Direct Methanol Fuel Cells, *ACS Appl. Mater. Interfaces*, 2020, **12**, 44588–44596, DOI: 10.1021/acsami.0c07812.

239 O. Delikaya, N. Bevilacqua, L. Eifert, U. Kunz, R. Zeis and C. Roth, Porous electrospun carbon nanofibers network as an integrated electrode@gas diffusion layer for high temperature polymer electrolyte membrane fuel cells, *Electrochim. Acta*, 2020, **345**, 136192, DOI: 10.1016/j.electacta.2020.136192.

240 A. Symillidis, S. Georgiadou and W.-F. Lin, Conductive core/shell polymer nanofibres as anode materials for direct ethanol fuel cells, *Adv. Sens. Energy Mater.*, 2023, **2**, 100070, DOI: 10.1016/j.asems.2023.100070.

241 C. Sanna, P. Costamagna and P. Holtappels, Electrochemical Impedance Spectroscopy of Core-Shell Nanofiber Cathodes, with $Ce_{0.9}Gd_{0.1}O_{1.95}$ (Core) and Cu-Doped $La_{0.6}Sr_{0.4}MnO_3$ (Shell), for Application in Solid Oxide Fuel Cells, *ChemElectroChem*, 2023, **10**, e202300101, DOI: 10.1002/celc.202300101.

242 H. Jiang, Y. Hu, P. Zhao, Y. Li and K. Zhu, Modulation of protein release from biodegradable core–shell structured fibers prepared by coaxial electrospinning, *J. Biomed. Mater. Res., Part B*, 2006, **79B**(1), 50–57, DOI: 10.1002/jbm.b.30510.

243 M. Maleki, M. Latifi, M. A. Tehran and S. Mathur, Electrospun core–shell nanofibers for drug encapsulation and sustained release, *Polym. Eng. Sci.*, 2013, **53**(8), 1770–1779, DOI: 10.1002/pen.23426.

244 K. Kalwar, W.-X. Sun, D. Li, X. -Ji Zhang and D. Shan, Coaxial electrospinning of polycaprolactone@chitosan: Characterization and silver nanoparticles incorporation for antibacterial activity, *React. Funct. Polym.*, 2016, **107**, 87–92, DOI: 10.1016/j.reactfunctpolym.2016.08.010.

245 M. Oviedo, Y. Montoya, W. Agudelo, A. G. -García and J. Bustamante, Effect of Molecular Weight and Nanoarchitecture of Chitosan and Polycaprolactone Electrospun Membranes on Physicochemical and Hemocompatible Properties for Possible Wound Dressing, *Polymers*, 2021, **13**, 4320, DOI: 10.3390/polym13244320.

246 B. Pant, M. Park and S.-J. Park, Drug Delivery Applications of Core-Sheath Nanofibers Prepared by Coaxial Electrospinning: A Review, *Pharmaceutics*, 2019, **11**(7), 305, DOI: 10.3390/pharmaceutics11070305.

247 J. Li, Y. Liu and H. E. Abdelhakim, Drug Delivery Applications of Coaxial Electrospun Nanofibres in Cancer Therapy, *Molecules*, 2022, **27**, 1803, DOI: 10.3390/molecules27061803.

248 N. Rajabifar, A. Rostami, S. Afshar, P. Mosallanezhad, P. Zarrintaj, M. Shahrousvand and H. Nazockdast, Wound Dressing with Electrospun Core-Shell Nanofibers: From Material Selection to Synthesis, *Polymers*, 2024, **16**, 2526, DOI: 10.3390/polym16172526.

249 L. Hou, X. Zhang, P. E. Mikael, L. Lin, W. Dong, Y. Zheng, T. J. Simmons, F. Zhang and R. J. Linhardt, Biodegradable and Bioactive PCL−PGS Core−Shell Fibers for Tissue Engineering, *ACS Omega*, 2017, **2**(10), 6321–6328, DOI: 10.1021/acsomega.7b00460.

250 J. C. Silva, R. N. Udangawa, J. Chen, C. D. Mancinelli, F. F. F. Garrudo, P. E. Mikael, J. M. S. Cabral, F. C. Ferreira and R. J. Linhardt, Kartogenin-loaded coaxial PGS/PCL aligned nanofibers for cartilage tissue engineering, *Mater. Sci. Eng., C*, 2020, **107**, 110291, DOI: 10.1016/j.msec.2019.110291.

251 M. A. Al Fahad, H.-Y. Lee, S. Park, M. Choi, P. C. Shanto, M. Park, S. H. Bae and B.-T. Lee, Small-diameter vascular graft composing of core-shell structured micro-nanofibers loaded with heparin and VEGF for endothelialization and prevention of neointimal hyperplasia, *Biomaterials*, 2024, **306**, 122507, DOI: 10.1016/j.biomaterials.2024.122507.

252 D. Kharaghani, P. Gitigard, H. Ohtani, K. Oh Kim, S. Ullah, Y. Saito, M. Qamar Khan and I. S. Kim, Design and characterization of dual drug delivery based on in-situ assembled PVA/PAN core-shell nanofibers for wound dressing application, *Sci. Rep.*, 2019, **9**, 12640, DOI: 10.1038/s41598-019-49132-x.

253 J. Li, T. Zhang, M. Pan, F. Xue, F. Lv, Q. Ke and H. Xu, Nanofiber/hydrogel core–shell scaffolds with three-dimensional multilayer patterned structure for accelerating diabetic wound healing, *J. Nanobiotechnol.*, 2022, **20**, 28, DOI: 10.1186/s12951-021-01208-5.

254 J. Guo, T. Wang, Z. Yan, D. Ji, J. Li and H. Pan, Preparation and evaluation of dual drug-loaded nanofiber membranes based on coaxial electrostatic spinning technology, *Int. J. Pharm.*, 2022, **629**, 122410, DOI: 10.1016/j.ijpharm.2022.122410.

255 A. J.-N. Abadi, H. P. Toroudi, M. Hadjianfar, Z. Mirjafary, R. F. -Majidi and A. Akbarzadeh, Core–shell nanofibers for localized melanoma therapy delivering Pioglitazone nanoemulsions and gemcitabine dual loaded system, *Sci. Rep.*, 2025, **15**, 28401, DOI: 10.1038/s41598-025-14483-1.

256 P. Mosallanezhad, N. Rajabifar, A. Rostami, Z. Ahmadi, R. Taghdimi and H. Nazockdast, Preparation and structural analyses of antimicrobial core-shell chitosan-polycaprolactone nanofibers for controlled curcumin release, *Colloids Surf., A*, 2025, **716**, 136736, DOI: 10.1016/j.colsurfa.2025.136736.